FLORIDA INTERNATIONAL UNIVERSITY

Miami, Florida

THE CYCLODEXTRIN-PERFLUORINATED SURFACTANT HOST-GUEST COMPLEX: FUNDAMENTAL STUDIES FOR POTENTIAL ENVIRONMENTAL REMEDIATION AND THERAPEUTIC APPLICATIONS

A dissertation submitted in partial fulfillment of

the requirements for the degree of

DOCTOR OF PHILOSOPHY

in

CHEMISTRY

by

Mary Joelle Errico

2018

To: Dean Michael R. Heithaus
College of Arts, Sciences and Education

This dissertation, written by Mary Joelle Errico, and entitled The Cyclodextrin-Perfluorinated Surfactant Host-Guest Complex: Fundamental Studies for Potential Environmental Remediation and Therapeutic Applications, having been approved in respect to style and intellectual content, is referred to you for judgment.

We have read this dissertation and recommend that it be approved.

_____
Piero R. Gardinali

_____
Watson J. Lees

_____
Joong Ho Moon

_____
Gary M. Rand

_____
Kevin E. O'Shea, Major Professor

Date of Defense: May 22, 2018

The dissertation of Mary Joelle Errico is approved.

_____
Dean Michael R. Heithaus
College of Arts, Sciences and Education

_____
Andrés G. Gil
Vice President for Research and Economic Development
and Dean of the University Graduate School

Florida International University, 2018

DEDICATION

To my husband, Michael.

Without your love and support, I would have never made it this far.

“I don’t have all the answers yet, but I’m getting closer.” – Billy Joel

ACKNOWLEDGMENTS

I would like to thank Dr. Kevin O'Shea for his excellent mentorship. His guidance, advice, and support were critical to my success in graduate school and my journey from chemistry student to chemist. I thank him for providing me the right mixture of direction and freedom, and for helping me realize my passion in host-guest chemistry and NMR spectroscopy. I also thank him for encouraging collaboration with other professors and researchers, which helped both my dissertation and my training as a scientist. Most of all, I thank him for being understanding and kind, and for always believing in me and my work.

I would like to thank my committee: Dr. Piero Gardinali, Dr. Watson Lees, Dr. Joong Ho Moon, Dr. Gary Rand, and Dr. Angel Kaifer. Their advice and guidance throughout graduate school helped shape and refine my dissertation projects.

I would like to thank my collaborators: Dr. John Berry, Dr. Jaroslava Miksovska, and Dr. Ion Ghiviriga. I learned so much from them and loved working with them.

I would like to thank my previous mentors: Dr. Christian Wolf, Dr. Rachel Noble, Dr. Keith Bentley, and Dr. Brett Froelich. Their mentorship during my undergraduate years prepared me well for graduate school, and I thank them for their continued support throughout my graduate education. I would especially like to thank Dr. Bentley and Dr. Froelich for teaching me good lab techniques and introducing me to scientific research.

I would like to thank Dr. O'Shea's research group, both new and old, for always being a great group of people to work with. I would especially like to thank the four group members I spent the majority of my graduate experience with: Mamun Rashid, Danni Cui, A.M. Abdullah, and Marcela Jaramillo. When experiments failed, or when

papers were published, through the good and bad, they were always there to commiserate or celebrate with, and they will always be some of my best friends.

Finally, I would like to thank my family: my husband Michael, for helping me stay strong; my sister Babs, for cheering me up; and especially my parents, for all their love, support, and encouragement. They always knew I would finish, and their belief in me motivated me more than they know.

The Presidential Fellowship, Doctoral Evidence Acquisition (DEA) Fellowship, and Dissertation Year Fellowship (DYF) were supported by FIU's University Graduate School. The experiments in Chapter 4 were supported by the National Science Foundation (Grant No. 1748752). Conference travel funding was provided by the College of Arts, Sciences & Education, the Graduate and Professional Student Committee, and the South Florida ACS Local Section. The PFECA samples from SynQuest in Chapters 3 and 4 were provided by Dr. Detlef Knappe. The zebrafish embryos in Chapter 6 were provided by Dr. Pat Gibbs.

Chapter 2 and portions of Chapter 1 were reprinted with permission from Weiss-Errico, M.J.; O'Shea, K.E. Detailed NMR investigation of cyclodextrin-perfluorinated surfactant interactions in aqueous media. J. Hazard. Mater. 2017, 329, 57-65. Copyright 2017 Elsevier.

Chapter 3 and portions of Chapter 1 were reprinted with permission from Weiss-Errico, M.J.; Ghiviriga, I.; O'Shea, K.E. ^{19}F NMR characterization of the encapsulation of emerging perfluoroethercarboxylic acids by cyclodextrins. J. Phys. Chem. B 2017, 121, 8359-8366. Copyright 2017 American Chemical Society.

Chapter 5 and portions of Chapter 1 were reprinted with permission from Weiss-Errico, M.J.; Miksovska, J.; O'Shea, K.E. β-Cyclodextrin reverses binding of perfluorooctanoic acid to human serum albumin. Chem. Res. Toxicol. 2018, 31, 277-284. Copyright 2018 American Chemical Society.

Chapter 6 and portions of Chapter 1 were reprinted with permission from Weiss-Errico, M.J.; Berry, J.P.; O'Shea, K.E. β-Cyclodextrin attenuates perfluorooctanoic acid toxicity in the zebrafish embryo model. Toxics 2017, 5, 31. Copyright 2017 MDPI.

ABSTRACT OF THE DISSERTATION

THE CYCLODEXTRIN-PERFLUORINATED SURFACTANT HOST-GUEST COMPLEX: FUNDAMENTAL STUDIES FOR POTENTIAL ENVIRONMENTAL REMEDIATION AND THERAPEUTIC APPLICATIONS

by

Mary Joelle Errico

Florida International University, 2018

Miami, Florida

Professor Kevin E. O'Shea, Major Professor

Perfluoroalkyl substances (PFASs) are contaminants of emerging concern, and have been detected in drinking water, wildlife, humans, and the environment. Cyclodextrins (CDs), cyclic sugars composed of glucose monomers, are proposed as a potential remediation strategy. CDs can form host-guest complexes with hydrophobic molecules; this complexation could be capitalized on for PFAS removal and sequestration. These dissertation projects aim to study the fundamental host-guest interactions between a variety of PFASs and CDs for eventual applications in environmental and biological remediation. 1D and 2D Nuclear magnetic resonance (NMR) spectroscopic methods were employed to determine the strength, dynamics, and structure of the CD:PFAS host-guest complexes. Legacy and emerging PFASs were studied with the three native CDs (α-, β-, and γ-CDs) as well as β-CD derivatives. β-CD and its derivatives exhibit the strongest complexation with all studied PFASs, with association constants of 10^2-10^5 M^{-1}, depending on PFAS chain length, functional groups, and branching. The host-guest complex was not significantly disturbed under different

environmental conditions, such as changing pH, ionic strength, and in the presence of humic acid. A competition study between perfluorooctanoic acid (PFOA), β-CD, and human serum albumin (HSA), the most abundant protein in blood serum, was then conducted using NMR, circular dichroism, and fluorescence spectroscopies. Excess β-CD was able to totally reverse all PFOA binding to HSA. Finally, the host-guest complex was studied within a biological organism to test its viability as a remediation strategy. The attenuation of the toxicity of PFOA in zebrafish embryos, a model organism for toxicology studies, was tested with β-CD. Excess β-CD increased the LC_{50} (lethal concentration for 50 % of the population) of PFOA compared to PFOA in the absence of β-CD ($p < 0.0001$). These dissertation projects suggest that the encapsulation of PFASs by CDs has potential in PFAS remediation strategies.

TABLE OF CONTENTS

LIST OF TABLES

TABLE PAGE

LIST OF FIGURES

FIGURE PAGE

ABBREVIATIONS AND ACRONYMS

(2-Hydroxy-3-*N*,*N*,*N*-trimethylamino)propyl-β-cyclodextrin	QACD
1*H*,1*H*,2*H*,2*H*-Perfluorooctanesulfonic acid (6:2 fluorotelomer sulfonate)	6:2 FTS
6-Monodeoxy-6-monoamino-β-cyclodextrin	Mono-am-β-CD
8-Anilinonaphthalene-1-sulfonic acid	1,8-ANS
Adamantane-carboxylic acid	Ada-COOH
Cyclodextrin	CD
Heptakis(6-deoxy-6-amino)-β-cyclodextrin	Hepta-am-β-CD
Heteronuclear Overhauser effect spectroscopy	HOESY
Human serum albumin	HSA
Lethal concentration for 50 % of the population	LC_{50}
Maximum wavelength	λ_{max}
Nuclear magnetic resonance	NMR
Nuclear Overhauser effect	NOE
Perfluoro(2-methyl-3-oxahexanoic) acid	PFPrOPrA (GenX)
Perfluoro(3,6,9-trioxadecanoic) acid	PFO3DA
Perfluoro(3,6,9-trioxatridecanoic) acid	PFO3TDA
Perfluoro(3,6-dioxadecanoic) acid	PFO2DA
Perfluoro(3,6-dioxheptanoic) acid	PFO2HpA
Perfluoro(3-oxabutanoic) acid	PFMOPrA
Perfluoro(4-oxapentanoic) acid	PFMOBA
Perfluoro(5-oxa-6-dimethylhexanoic) acid	PFDMMOBA

Perfluoroalkyl substance	PFAS
Perfluorobutanoic acid	PFBA
Perfluorocarboxylic acid	PFCA
Perfluorodecanoic acid	PFDA
Perfluoroethercarboxylic acid	PFECA
Perfluoroheptanoic acid	PFHpA
Perfluorohexanoic acid	PFHxA
Perfluorononanoic acid	PFNA
Perfluorooctanesulfonamide	PFOSA
Perfluorooctanesulfonate	PFOS
Perfluorooctanoic acid	PFOA
Perfluoropentanoic acid	PFPA
Sulfobutylated β-cyclodextrin	SBECD
α-Cyclodextrin	α-CD
β-Cyclodextrin	β-CD
γ-Cyclodextrin	γ-CD

CHAPTER 1

Introduction

1.1 Perfluorinated Surfactants

Perfluorinated surfactants, or perfluoroalkyl substances (PFASs), are emerging contaminants of concern and problematic persistent organic pollutants. Their extreme persistence in the environment has posed many challenges to their remediation.

1.1.1 Structure and Function

The unique properties of PFASs arise from their molecular structure. PFASs generally are surfactant-like in nature, with a hydrophobic tail and a hydrophilic head group (Prevedourous et al. 2006, Jensen and Leffers 2008, Buck et al. 2011, Wang et al. 2017). The hydrophobic tail is either per- or poly-fluorinated, and head groups include carboxylates, sulfonates, sulfonamides, and phosphonates, among others (Wang et al. 2017). Their dual nature renders them both hydrophobic and lipophobic (Prevedourous et al. 2006, Jensen and Leffers 2008, Buck et al. 2011, Wang et al. 2017). The pK_a of the polar head groups are less than that of the corresponding hydrogenated surfactants; for example, hydrogenated carboxylic acids have a pK_a of about 4, whereas perfluorinated carboxylic acids have a $pK_a \sim 0$, meaning PFASs have a negative charge in most environmentally relevant pH (Goss 2008). The numerous carbon-fluorine bonds in the perfluorinated backbone, furthermore, give the structure extreme chemical and thermal stability (Prevedourous et al. 2006, Jensen and Leffers 2008, Buck et al. 2011, Wang et al. 2017). Finally, they are relatively soluble in water, depending on chain length of the perfluorinated backbone (with longer chain PFASs less soluble than shorter chain) (Prevedourous et al. 2006, Cousins et al. 2011, Wang et al. 2017). Chain length is typically between four and twelve carbons. Historically, the most widely produced and

used PFASs have eight carbons in their backbone, including perfluorooctanoic acid (PFOA) and perfluorooctanesulfonic acid (PFOS), shown in Figure 1.1 (Prevedouros et al. 2006, Wang et al. 2017).

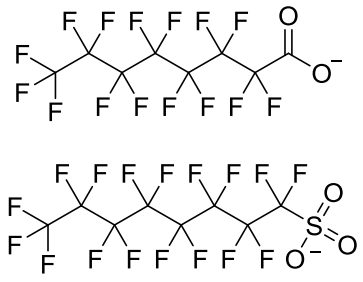

Figure 1.1: Structures of two legacy PFASs. Above: Perfluorooctanoic acid (PFOA); Below: Perfluorooctanesulfonic acid (PFOS).

The molecular structure gives PFASs properties desirable to various industries. PFASs have been traditionally used in three applications. The first application is as processing aids in fluoropolymer (including PTFE, DuPont/Chemours brand name Teflon) synthesis (Prevedourous et al. 2006). PFASs aid solvation of tetrafluoroethylene monomers and PTFE itself so that emulsion polymerization can occur. The second application is as surfactants in aqueous film-forming foams (AFFF) (Prevedouros et al. 2006, Barzen-Hanson et al. 2017, Wang et al. 2017). AFFF are used to stop hydrocarbon fires, by coating the surface of the hydrocarbon with PFASs to prevent oxygen from reacting with the hydrocarbon. AFFF have been extensively used by the military, especially in air craft hangers and air craft carriers, though they are also used in commercial airports (Barzen-Hanson et al. 2017). The third application of PFASs is in various consumer products with water-, grease-, or stain-repellant properties

(Prevedouros et al. 2006, D'Hollander et al. 2010, Schaider et al. 2017). Examples include food packaging (especially fast food, microwave popcorn bags, and pizza boxes), stain removers, and water-proof clothing (Prevedouros et al. 2006, D'Hollander et al. 2010, Schaider et al. 2017).

The widespread use of PFASs, coupled with their water solubility and incredible stability under environmental conditions, has led to their occurrence in humans, wildlife, and the environment (Prevedouros et al. 2006, Houde et al. 2006, Jensen and Leffers 2008, Kannan 2011, Hu et al. 2016, Strynar et al. 2015, Sun et al. 2016, Glassmeyer et al. 2017, Barzen-Hanson et al. 2017, Wang et al. 2017). They have been detected around the globe, even in remote regions, in water, soil, and the atmosphere (Prevedouros et al. 2006, Cousins et al. 2011, Gebbink et al. 2016). Furthermore, they are bioaccumulative, leading to high concentrations in top predators (Houde et al. 2006, Prevedouros et al. 2006). They are of special concern because of their toxicity in animals and exposed human populations.

1.1.2 Health Effects and Exposure

PFASs, especially long chain PFASs, have been linked to adverse health effects. The best known case of general population exposure to PFASs was the contamination of the Ohio River by DuPont's Washington Works plant (Frisbee et al. 2009). This plant was a major producer of Teflon, and used PFOA as the processing aid in the polymerization reaction. PFOA from the plant was released into the adjacent Ohio River. The first indicator of this release was the death of a herd of cattle owned by a nearby rancher. Eventually, the case became a class action lawsuit, as an unusually high number

of people in the surrounding towns had cancer and other ailments (Frisbee et al. 2009). Part of the settlement was for DuPont to pay for research into the effects of PFOA exposure, leading to the "C8 Project" (Frisbee et al. 2009). The researchers found six probable links to PFOA exposure: kidney cancer, testicular cancer, ulcerative colitis, thyroid disease, hypercholesterolemia (high cholesterol), and pregnancy-induced hypertension (Frisbee et al. 2009, Lopez-Espinosa et al. 2012, Barry et al. 2013, Vieira et al. 2013). PFOA exposure has also been linked to liver cancer, bladder cancer, infertility, and developmental delays in other studies (Betts 2007, Jensen and Leffers 2008, Kannan 2011). Other PFASs show similar health effects (Jensen and Leffers 2008). The greatest exposure route of PFASs is through drinking water, though exposure can also occur when using consumer products containing PFASs (Hu et al. 2016, Schaider et al. 2017, D'Hollander et al. 2010). Due to recent contamination of PFOA and PFOS in Hoosick Falls, New York, the United States Environmental Protection Agency (EPA) has issued a lifetime advisory limit of 70 parts per trillion (ppt) for PFOA and PFOS combined (*EPA 800-F-16-003*).

Unlike other persistent organic pollutants, PFASs do not accumulate in fat tissue. Instead, they predominantly reside in blood serum, though they will later accumulate in bone and organs such as the brain, liver, bladder, and kidneys (Olsen et al. 2007, Jensen and Leffers 2008, Kannan 2011, Pérez et al. 2013). PFASs have relatively long half-lives (time in which half of the original concentration is eliminated from the body) in the body considering that they do not accumulate in fat: PFOA has a half-life of about 3.8 years, and PFOS has a half-life of about 5.4 years (Olsen et al. 2007). Over 99% of the United States population has measurable levels, with an average of 2 parts per billion (ppb), of

PFOA and PFOS in their blood (Calafat et al. 2007). Those exposed to higher concentrations of PFASs, such as those studied in the C8 Project, have 20-200 ppb in their blood, whereas factory workers in PFAS manufacturing plants have upwards of 1000 ppb (or 1 parts per million, ppm) in their blood (Olsen et al. 2007, Frisbee et al. 2009).

PFOA is also known to bind to human serum albumin (HSA), the most abundant protein in human blood serum (Han et al. 2003, Jensen and Leffers 2008, Wu et al. 2009). The interaction between PFOA and HSA has been investigated by a variety of methods, including nuclear magnetic resonance (NMR), fluorescence, infrared, and circular dichroism spectroscopies, equilibrium dialysis, isothermal titration calorimetry (ITC), and molecular modeling (Han et al. 2003, Wu et al. 2009, Chen and Guo 2009, Salvalaglio et al. 2010, MacManus-Spencer et al. 2010, Bischel et al. 2010, Hebert and MacManus-Spencer 2010). The binding of PFOA to HSA has been reported to occur at multiple sites (up to 13) (Han et al. 2003, Wu et al. 2009, Salvalaglio et al. 2010), primarily to hydrophobic pockets known to interact with fatty acids, hormones, and hydrophobic drugs, with the strongest binding constant on the order of 10^5 M^{-1} (Han et al. 2003, Wu et al. 2009, Chen and Guo 2009, Salvalaglio et al. 2010, MacManus-Spencer et al. 2010, Bischel et al. 2010).

The toxicological effects of PFOA have also been studied on a variety of organisms, such as zebrafish. Zebrafish, particularly embryonic and larval stages, have emerged as an important model system in a wide range of fields including assessment of chemical toxicity (Yang et al. 2009, Planchart et al. 2016). Practical advantages of the zebrafish embryo system include ease of rearing and a high fecundity, as well as small

(~1 mm) and nearly transparent embryos, rapid (≤5–7 day) embryo development, and a fully sequenced genome. As such, the zebrafish embryo has been employed to look at a wide range of environmental contaminants in terms of acute and chronic toxicity (Hinton et al. 2005, Scholz et al. 2008, Sarmah and Marrs 2016). Acute toxicological endpoints (e.g., embryotoxicity, teratogenicity, neurotoxicity), which are readily accessible in the zebrafish embryo model, are aligned with the reported health concerns associated with PFOA, and the system has been used to evaluate toxicity of PFOA and related PFASs (Hagenaars et al. 2011, Zheng et al. 2011, Hagenaars et al. 2013, Ding et al. 2013, Ulhaq et al. 2015, Jantzen et al. 2016a, Jantzen et al. 2016b, Jantzen et al. 2017, Rainieri et al. 2017).

1.1.3 Current Remediation Techniques

Although PFOA and PFOS have been phased out of production in the United States and Europe, they are still detected in the environment due to their persistence (Hu et al. 2016, Glassmeyer et al. 2017, Wang et al. 2017). In fact, a joint study by the EPA and United States Geological Survery (USGS) found that every water treatment plant they tested had measurable levels of PFASs in the water supply, with many of the water supplies having levels above the EPA lifetime advisory limit of 70 ppt (Glassmeyer et al. 2017). Furthermore, they found that the PFASs were not significantly removed during water treatment (Glassmeyer et al. 2017). An estimated six million Americans drink water exceeding the EPA limit (Hu et al. 2016).

Compounding the problem is the development of “emerging” PFASs by industries to replace “legacy” PFASs (such as PFOA and PFOS) (Wang et al. 2017). One of the

major types of emerging PFASs is perfluoroethercarboxylic acids, or PFECAs (Wang et al. 2013, Wang et al. 2017). PFECAs have an analogous structure to perfluorocarboxylic acids (PFCAs) like PFOA, except oxygen atoms are inserted into the carbon backbone to create ether functionalities. The presence of ether oxygens was expected to aid degradation of these compounds in the environment (Wang et al. 2013, Wang et al. 2015). Recent studies, however, have suggested that PFECAs have similar persistence and potential for transport in the environment as legacy PFASs (Wang et al. 2015, Gomis et al. 2015), and preliminary studies indicate that they may, in fact, be more toxic than legacy PFASs (Gomis et al. 2018, Sheng et al. 2018). An investigation near a PFECA manufacturer in North Carolina, furthermore, revealed that PFECAs are not susceptible to advanced processes in water treatment facilities (Strynar et al. 2015, Sun et al. 2016). Thus, both the remaining legacy PFASs and the currently manufactured emerging PFASs are threats to environmental and human health.

Many remediation strategies for PFAS removal from the environment have been previously studied. Examples of these include: adsorption by activated carbon or mineral materials; nanofiltration and reverse osmosis; and advanced oxidation processes, ultrasonic degradation, and reduction (Arvaniti and Stasinakis 2015, Merino et al. 2016). Oxidative and reductive technologies are effective only under extreme conditions, such as high pressure, high temperature, very acidic or alkaline pH, and with high concentrations of PFASs, and thus are inefficient for remediation in environmentally relevant conditions at low PFAS concentrations (Arvaniti and Stasinakis 2015, Merino et al. 2016). Adsorption processes are much more promising, with rapid removal of PFASs using activated carbon; however, this process is fouled by natural organic matter such as humic

acid, and so is much less effective in environmental conditions (Arvaniti and Staskinakis 2015, Dudley et al. 2015, Merino et al. 2016). Furthermore, activated carbon adsorption is not effective for removal of short chain PFASs currently being produced due to phasing out of long chain PFAS production (Dudley et al. 2015, Merino et al. 2016). New remediation strategies are greatly needed.

1.2 Cyclodextrins

Cyclodextrins (CDs) are cyclic sugar oligomers composed of glucose monomers. They have previously been proposed as a remediation strategy for environmental pollutants.

1.2.1 Structure and Function

Cyclodextrins are non-toxic, water soluble, and inexpensive. CDs were first isolated during bacterial transformation of potato starch in 1891 (Szejtli 1998). They are now readily synthesized by adding cyclodextrin glycosyltransferase (CGTase) to starch (Szejtli 1998). Three CDs are widely produced: α-, β-, and γ-CDs, composed of six, seven, and eight glucose monomers, respectively. The glucose monomers are joined by α-1,4-glucosidic linkages, forming the CD into a truncated cone shape, with a larger side and smaller side. The larger side is lined with 12-16 secondary hydroxyl groups and the smaller side is lined with 6-8 primary hydroxyl groups, depending on the size of the CD, making the exterior relatively hydrophilic. The interior of the cavity, however, is lined with C-H bonds, rendering it relatively hydrophobic (Szejtli 1998). The glucose monomer and the side view of the toroid structure of β-cyclodextrin are pictured in

Figure 1.2. H1, H2, and H4 face towards the exterior, whereas H3 and H5 face towards the interior. H6 are the methylene protons adjacent to the primary hydroxyl groups, which have free rotation.

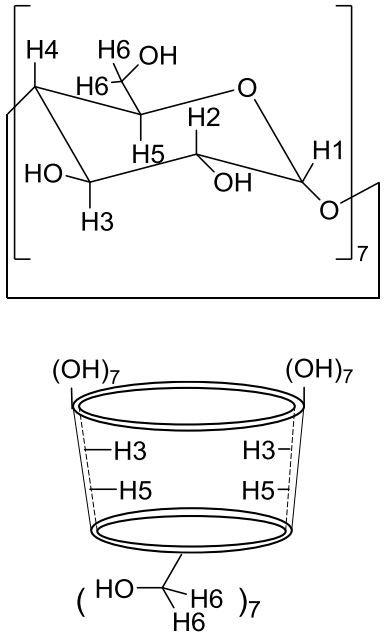

Figure 1.2: Structure of β-CD. Above: The glucose monomer with labeled protons. Below: Side view of the toroid structure, showing the interior protons (H3 and H5), the secondary hydroxyl groups on the large end, and the primary hydroxyl groups (next to H6) on the small end.

The dual hydrophobic-hydrophilic nature of CDs makes them well-suited for host-guest chemistry of hydrophobic molecules in aqueous solution (Martin Del Valle 2004). Host-guest chemistry involves a guest molecule associating with the interior of a host molecule. A hydrophobic molecule will readily complex with the hydrophobic CD cavity instead of remaining in the aqueous solution (Rekharsky and Inoue 1998). Furthermore, polar functionalities on the guest can hydrogen-bond with the hydroxyl groups lining the CD cavity perimeter to strengthen the interactions (Saenger and Steiner

1998, Lipkowitz 1998, Takahashi 1998, Wagner 2012). CDs can also be modified with charged functional groups, such as positively charged amino groups or negatively charged sulfonate groups, in place of the hydroxyl groups, facilitating electrostatic attraction between the cyclodextrin and an oppositely charged guest (Ito et al. 1996, Kitae et al. 1998, Szente and Szejtli 1999, Wenz et al. 2008). The host-guest inclusion complex is very favorable depending on the molecular size of the guest, the type of CD, and the ability for strong van der Waals interactions, H-bonding, or ionic bonding to occur (Rekharsky and Inoue 1998).

1.2.2 Nuclear Magnetic Resonance Spectroscopy to Measure Host-Guest Interactions

Host-guest interactions have been measured by a variety of techniques. Some of these techniques include: NMR, fluorescence, UV-vis, infrared, and circular dichroism spectroscopies; mass spectrometry; X-ray crystallography; ITC; capillary electrophoresis; and conductivity measurements (Valente and Söderman 2014). NMR spectroscopy has been widely used to measure the strength of the host-guest association, as well as determine the structure and dynamics of the complex (Schneider et al. 1998, Pessine et al. 2012, Valente and Söderman 2014). NMR is ideal for systems where the guest protons do not overlap with the CD protons, or the guest molecule has no or few protons in its structure.

NMR signals are not only dependent on the structure of the molecule: they are also, to a lesser extent, influenced by the environment surrounding the molecule. When a guest molecule is in solution, it will have one set of chemical shifts corresponding to each NMR-active nucleus; when it is inside a host molecule, the NMR signals will shift to

reflect the change in environment (whether more shielded or less shielded). This change in chemical shift can be measured in order to determine the strength of association between the host and guest (Schneider et al. 1998, Valente and Söderman 2014). If the equilibrium exchange is faster than the NMR time scale, then only one set of peaks will be observed (Schneider et al. 1998). This set of peaks will be the average between the fraction of free guest and the fraction of complexed guest:

$$\delta_{obs} = \chi_G \delta_G + \chi_{H:G} \delta_{H:G} \quad (1.1)$$

$$\Delta\delta_{obs} = \delta_{obs} - \delta_G \quad (1.2)$$

$$\Delta\delta_{H:G} = \delta_{H:G} - \delta_G \quad (1.3)$$

The observed chemical shift, δ_{obs}, is dependent upon the fraction of guest molecules in the uncomplexed state, χ_G, (free guest, [G]) and complexed state, $\chi_{H:G}$, (guest in host, [H:G]), and their respective chemical shifts, δ_G and $\delta_{H:G}$. The change in observed chemical shift, $\Delta\delta_{obs}$, is the observed chemical shift less the free guest chemical shift. The change in the complexed species' chemical shift, $\Delta\delta_{H:G}$, is the difference between $\delta_{H:G}$ and δ_G. Rearrangement of these equations yields:

$$\Delta\delta_{obs} = \chi_{H:G} \Delta\delta_{H:G} \quad (1.4)$$

The change in observed chemical shift is thus related to the mole fraction of the complexed species and the change in the complexed species' chemical shift compared to the uncomplexed species' chemical shift. The association constant for the 1:1 host:guest interaction, $K_{1:1}$, is related to the concentration of the complexed and free guest.

$$G + H \rightleftarrows H{:}G \tag{1.5}$$

$$K_{1:1} = \frac{[H{:}G]}{[H][G]} \tag{1.6}$$

$$GT = [G] + [H{:}G] \tag{1.7}$$

$$HT = [H] + [H{:}G] \tag{1.8}$$

The concentration of guest in solution, *GT* (or guest total), is equal to both free and complexed concentrations. The concentration of host in solution, *HT* (or host total), is likewise equal to both free and complexed concentrations. Combining all these equations yields

$$\Delta\delta_{obs} = \frac{\Delta\delta_{H:G}}{2GT}\{GT + HT + \frac{1}{K_{1:1}} - \left(\left(GT + HT + \frac{1}{K_{1:1}}\right)^2 - 4GTHT\right)^{\frac{1}{2}}\} \tag{1.9}$$

This gives the change in observed chemical shift as a function of total host concentration when the guest concentration is held constant. For the 2:1 host:guest association constant, $K_{2:1}$, the equation is:

$$G + 2H \rightleftarrows 2H{:}G \tag{1.10}$$

$$K_{2:1} = \frac{[2H{:}G]}{[G][H]^2} \tag{1.11}$$

$$GT = [G] + [2H{:}G] \tag{1.12}$$

$$HT = [H] + [2H{:}G] \tag{1.13}$$

$$\Delta\delta_{obs} = \frac{\Delta\delta_{2H:G}}{4HT(HT+GT)}\left\{4GTHT + HT^2 + \frac{1}{K_{2:1}} - \left(\left(4GTHT + HT^2 + \frac{1}{K_{2:1}}\right)^2 - 16GTHT^2(HT+GT)\right)^{\frac{1}{2}}\right\} \quad (1.14)$$

For host-guest interactions exhibiting both 1:1 and 2:1 interactions:

$$\Delta\delta_{obs} = \frac{\Delta\delta_{H:G}}{2GT}\left\{GT + HT + \frac{1}{K_{1:1}} - \left(\left(GT + HT + \frac{1}{K_{1:1}}\right)^2 - 4GTHT\right)^{\frac{1}{2}}\right\} + \frac{\Delta\delta_{2H:G}}{4HT(HT+GT)}\left\{4GTHT + HT^2 + \frac{1}{K_{2:1}} - \left(\left(4GTHT + HT^2 + \frac{1}{K_{2:1}}\right)^2 - 16GTHT^2(HT+GT)\right)^{\frac{1}{2}}\right\} \quad (1.15)$$

The change in observed chemical shift as a function of total host concentration can be modeled by these equations to yield accurate association constants (Schneider et al. 1998, Ramos Cabrer et al. 1999, Valente and Söderman 2014).

Competition experiments can be conducted to qualitatively compare the strength of host complexation between two molecules. For these experiments, the NMR spectra of the first complex and second complex are taken separately, and then both guest molecules are added to different concentrations of the host molecule and compared to the original

spectra. Whichever guest molecule has a stronger association constant with the host will determine which NMR spectrum the mixture resembles. For example, if the first guest molecule has a stronger association constant with the host than the second molecule, then the spectrum of the mixture will resemble the spectrum of the first molecule and host alone. Competition studies are useful to determine which host-guest complex will be formed in set conditions.

Another NMR experiment to study host-guest interactions is nuclear Overhauser effect (NOE) spectroscopy. NOE experiments examine the proximity of nuclei through-space, rather than through-bond (Overhauser 1953, Solomon 1955). Two nuclei that are close in three dimensional space will therefore have a crosspeak in a two-dimensional (2D) NOE NMR spectrum. NOE experiments have been used previously to determine how the guest molecule is oriented inside the host molecule, as well as confirm the inclusion complex, by examining which host protons show crosspeaks with which guest nuclei (whether protons or heteronuclei) (Schneider et al. 1998).

1.2.3 Applications and Previous Studies

Cyclodextrins have been used in various industries, including pharmaceuticals and drug delivery, food additives, odor elimination, nanotechnology, and chromatography (Szejtli 1998, Arun et al. 2008, Frömming and Szejtli 2013). These industries capitalize on the host-guest interactions CDs can display with a variety of hydrophobic guests. An emerging industry for CDs is environmental remediation of pollutants (Crini and Morcellet 2002, Crini 2005, Morin-Crini and Crini 2013, Nagy et al. 2014, Moulahcene et al. 2015). CDs have the potential to encapsulate a variety of

pollutants in water and soil, such as organic contaminants and heavy metals. Polymeric or solid-support materials based on CDs have been proposed as remediation strategies (Crini and Morcellet 2002, Crini 2005, Morin-Crini and Crini 2013, Nagy et al. 2014, Moulahcene et al. 2015).

CDs have previously been show to exhibit host-guest interactions with perfluorocarboxylic acids (PFCAs) of various chain lengths (Palepu and Reinsborough 1989, Palepu and Richardson 1989, Guo et al. 1992, Wilson and Verrall 1998a, Lima et al. 2007, Karoyo et al. 2011, Karoyo et al. 2013, Karoyo et al. 2015). Previously ^{19}F NMR spectroscopy has been used to study the change in chemical shifts of each fluorine peak on the PFAS backbone in order to calculate the strength of complexation (Guo et al. 1992, Wilson and Verrall 1998a, Karoyo et al. 2011, Karoyo et al. 2013, Karoyo et al. 2015). β-CD, the mid-sized CD, is the most promising for complexation of PFCAs, and exhibits both 1:1 and 2:1 complexes with PFCAs (Guo et al. 1992, Wilson and Verrall 1998a). Several β-CD polymeric materials have also been developed to remove PFOA and PFOS from water (Karoyo and Wilson 2013, Karoyo and Wilson 2015, Karoyo and Wilson 2016, Xiao et al. 2017). The fundamental host-guest interactions between PFASs and CDs, however, are not fully understood, and other PFASs, such as perfluorosulfonate derivatives and emerging PFECAs, have not been studied. Most importantly, the structure and dynamics of the host-guest complex between PFASs and CDs have not been determined. This structural information is necessary in understanding why the interactions between PFASs and CDs are favorable, and how these interactions can be utilized to create effective CD-based environmental or biological removal technologies for PFASs, especially emerging PFASs, and improve upon the previously tested

polymeric materials (Karoyo and Wilson 2013, Karoyo and Wilson 2015, Karoyo and Wilson 2016, Xiao et al. 2017). Furthermore, therapeutic or biological applications of the CD:PFAS host-guest interactions have not been explored.

1.3 General Objectives of the Dissertation Projects

These dissertation projects aim to study the fundamental host-guest interactions between a variety of PFASs and CDs for eventual applications in environmental and biological remediation. 1D and 2D NMR spectroscopic methods were employed to determine the strength, dynamics and structure of the host-guest complexes. Legacy (Chapter 2) and emerging (Chapter 3) PFASs were studied with the three native CDs as well as CD derivatives (Chapter 4). A competition study using β-CD to reverse the binding of PFOA to HSA was conducted with NMR, circular dichroism, and fluorescence spectroscopies to further understand the nature of the host-guest complex (Chapter 5). Finally, the attenuation of the toxicity of PFOA in zebrafish embryos was tested with β-CD to examine if the host-guest complex is a viable remediation strategy (Chapter 6).

CHAPTER 2

Host-Guest Interactions between Cyclodextrins and Legacy Perfluoroalkyl Substances

2.1 Abstract

Perfluoroalkyl substances (PFASs) are contaminants of serious concern because of their toxicological properties, widespread presence in drinking water sources, and incredible stability in the environment. To assess the potential application of cyclodextrins (CDs) for PFAS remediation, we investigated their complexation with linear fluorinated carboxylic acids, sulfonates, and a sulfonamide with carbon backbones ranging from C4-C9. ^{19}F Nuclear Magnetic Resonance (NMR) spectroscopy studies demonstrated β-CD formed the strongest complexes with these PFASs. The polar head group had a modest influence, but for PFASs with backbones longer than six carbons, strong association constants are observed for 1:1 ($K_{1:1} \sim 10^5\ M^{-1}$) and 2:1 ($K_{2:1} \sim 10^3\ M^{-1}$) β-CD:PFAS complexes. Excess β-CD can be used to complex 99.5% of the longer chain PFASs. Competition studies with adamantane-carboxylic acid and phenol confirmed the nature and persistence of the β-CD:PFAS complex. Detailed analyses of the individual NMR chemical shifts and Job plots indicate the favored positions of β-CD along the PFAS chain. Solution pH, ionic strength, and the presence of humic acid have modest influence on the β-CD:PFAS complex. The strong encapsulation of PFASs by β-CD under a variety of water quality conditions demonstrates the tremendous potential of CD-based materials for the environmental remediation of PFASs.

2.2 Introduction

Reported herein are detailed NMR studies of eight PFASs with different polar head groups and varying chain lengths. Adamantane-carboxylic acid, a powerful β-CD inclusion guest, and phenol, a model environmental pollutant, were used to confirm the strength and nature of the β-CD:PFOA complex. The complex is robust under a variety of water quality conditions, including a range of ionic strength and solution pH values, and in the presence of humic acid. The results demonstrate the promise of CD-based materials for the environmental remediation of a variety of fluorinated surfactants in a wide range of water quality conditions.

2.3 Experimental Methods

Perfluorobutanoic acid (PFBA), perfluoropentanoic acid (PFPA), perfluoroheptanoic acid (PFHpA), perfluorooctanoic acid (PFOA), perfluorononanoic acid (PFNA), hexafluorobenzene, adamantane-carboxylic acid, phenol, and humic acid were purchased from Sigma-Aldrich. Potassium perfluorooctanesulfonate (PFOS), perfluorooctanesulfonamide (PFOSA), and 1*H*,1*H*,2*H*,2*H*-perfluorooctanesulfonic acid (6:2 fluorotelomer sulfonate, 6:2 FTS) were purchased from SynQuest Labs. α-, β-, and γ-Cyclodextrin were purchased from Acros Organics. Deuterium oxide (99.9% D) was purchased from Sigma-Aldrich and stored at 4 °C. All chemicals were used without further purification. Structures and abbreviations can be found in Appendix 1.

2.3.1 Sample Preparation

Solutions of 2.42×10^{-3} M perfluorocarboyxlic acids and 6.05×10^{-4} M perfluorosulfonates/sulfonamide were prepared in 50% D_2O and 50% DI H_2O, adjusted with 0.036 M NaOH to solution pH 7. Hexafluorobenzene (0.17 μL, 1.44×10^{-3} M) was added as an internal standard. Various cyclodextrins were added in different stoichiometric ratios. Solutions were sonicated in a cleaning bath for five minutes to ensure dissolution of substrates.

2.3.2 Environmental Conditions and Competition Studies

The competition studies were performed with PFOA, β-CD, and adamantane-carboxylic acid or phenol. The studies on the effects of environmental conditions on the complex were performed with PFOA and β-CD. For the ionic strength experiments, NaCl at 0.01, 0.1, and 1.0 M was added to samples of PFOA and β-CD. For the pH experiments, pH was adjusted to 2, 4 and 10 using 0.1 M solutions of NaOH and HCl. For the humic acid experiments, 0.5 mg/mL of humic acid (Sigma-Aldrich H16752, Lot# STBC5468V) was added to each sample.

2.3.3 NMR Spectroscopy

^{19}F and ^{1}H NMR spectroscopy was performed with a 400 MHz Bruker instrument with a quad probe. The hexafluorobenzene peak was used as an internal standard at -164.9 ppm for ^{19}F NMR and DSS was used as an internal standard at 0 ppm for ^{1}H NMR. The chemical shift of the internal standards did not change in the presence of the CD. The chemical shift of each peak was recorded. Representative spectra taken at

different times were unchanged over a one-week time window. Assignment of the fluorine and carbon positions was previously reported (Guo et al. 1992, Wilson and Verrall 1998a, Wilson 1998). The association constants for $K_{1:1}$ (1:1 CD:PFAS) and $K_{2:1}$ (2:1 CD:PFAS) were determined using a method described by Ramos Cabrer, et al. (1999) (Chapter 1). Nonlinear least-squares regression analysis was performed in GraphPad Prism (version 5.03, La Jolla, CA) and Mathworks Matlab (version R2013b, Natick, MA) to determine the individual association constants.

2.4 Results and Discussion

The PFASs and CDs were dissolved in 1 mL (50% D_2O and 50% H_2O) at the desired CD:PFAS ratios over a wide range from 1:5 to 6:1 PFAS:CD ratios. ^{19}F NMR spectra were obtained at specific ratios and the chemical shifts compared (for individual NMR data, see Appendix 1). As the ratio of CD increases, there are distinct changes in the chemical shifts and shape of the ^{19}F NMR peaks. Peak broadening is assigned to a more rigid structure of the guest when within the host (Karoyo et al. 2011, Karoyo et al. 2013, Karoyo et al. 2015). Based on the results herein as well as the numerous previous studies, we focused on the β-CD:PFAS complexes (Guo et al. 1992, Wilson and Verrall 1998a, Karoyo et al. 2011, Karoyo et al. 2013, Karoyo et al. 2015). Figure 2.1 shows representative ^{19}F NMR spectra of perfluorooctanoic acid (PFOA) and β-cyclodextrin (β-CD) at various ratios. The PFOA peaks are labeled by their position; for example, “F2” refers to the fluorine atoms attached to the second carbon (with the carboxylate carbon assigned position number one according to the IUPAC nomenclature rules). As the cyclodextrin concentration increased, the chemical shift of the fluorine atoms changed, in

some cases dramatically. The observed change in chemical shift becomes obvious as the β-CD:PFOA ratio approaches a 1:1 ratio. With the addition of more than one equivalent of β-CD, the chemical shift gradually decreases indicating a second feature: 2:1 β-CD:PFOA complexation.

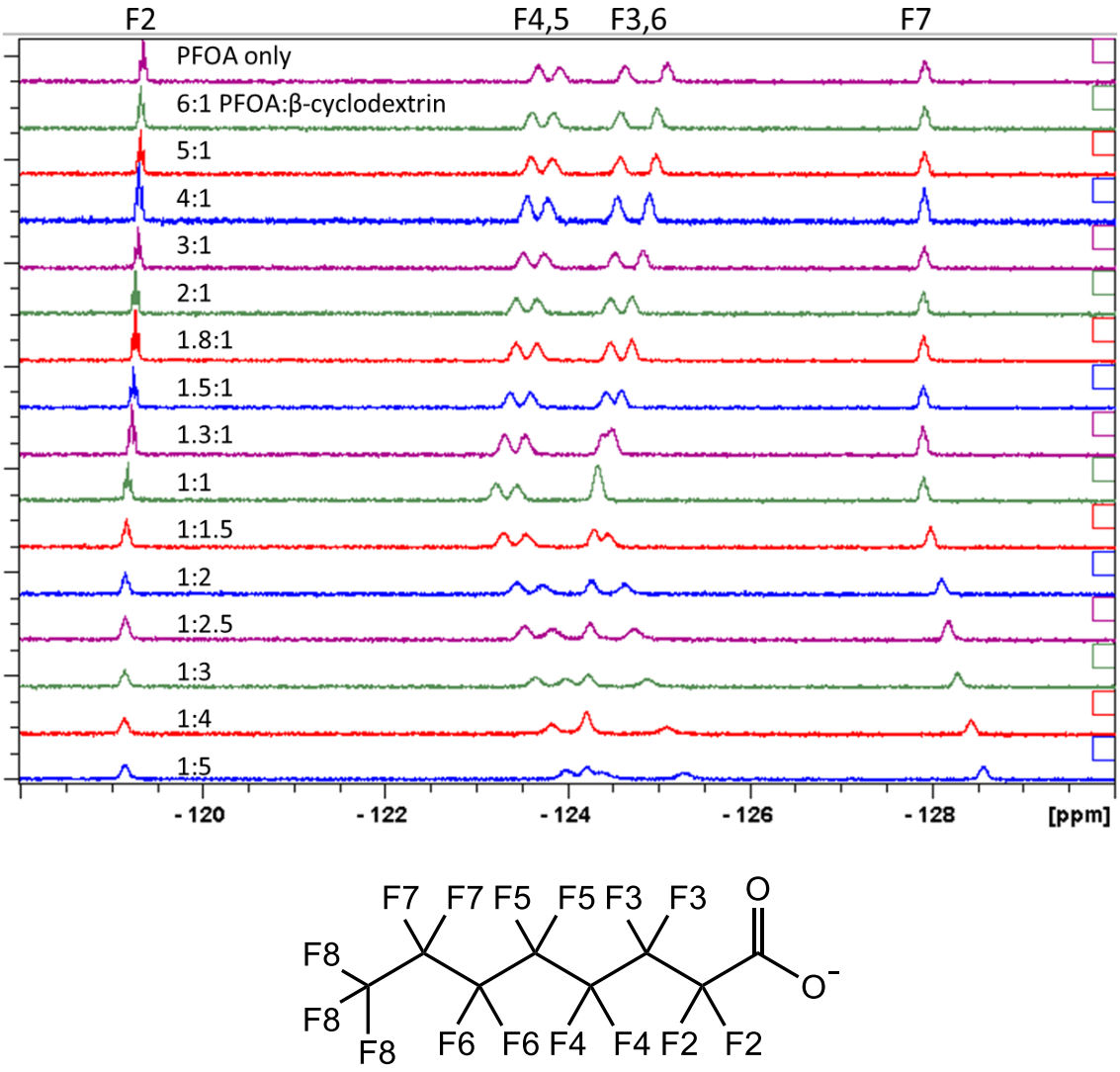

Figure 2.1: ^{19}F NMR spectra of PFOA-β-CD complex. Above: Representative ^{19}F NMR spectra of PFOA (0.00242 M) with β-CD at various ratios, abbreviated to fluorines F2-F7 (F8 and hexafluorobenzene peaks not pictured), 50% D_2O/50% H_2O. Below: PFOA numbering scheme.

To probe the nature of the β-CD:PFOA complex, competition experiments were run using adamantane-carboxylic acid (Ada-COOH). Ada-COOH is a cage-shaped hydrocarbon known to strongly complex to the interior of β-CD with a $K_{1:1} = 2.0 \times 10^5$ M^{-1} (Eftink et al. 1989, Kwak and Gomez 1996). The ^1H NMR spectra of 1:1 β-CD:PFOA and 1:1 β-CD:Ada-COOH complexes were run to establish the chemical shifts of the β-CD protons in the individual complexes. The exterior protons (H1, H2, and H4) are unaffected by the presence of these guests, while the interior protons (H3 and H5) and the primary hydroxyl group (H6 of the methylene) undergo notable shifts in the presence of PFOA and Ada-COOH, as shown in Figure 2.2 (for Ada-COOH protons see Appendix 1). The addition of PFOA to the robust β-CD:Ada-COOH complex results in changes in the chemical shifts of the protons of β-CD. The chemical shift of H3, when both guests are present, is most similar to a 1:1 β-CD:PFOA complex, whereas the chemical shift of H5 appears to be an average of the 1:1 β-CD:PFOA and 1:1 β-CD:Ada-COOH complexes. To further probe the complexation, the host-guest ratio was varied and ^{19}F NMR spectra taken (Appendix 1). At a 1:1:0.5 β-CD:Ada-COOH:PFOA ratio, the ^{19}F NMR spectrum indicates a 1:1 complex between PFOA and β-CD with no evidence of free PFOA. The results demonstrate PFOA readily replaces Ada-COOH within β-CD. With addition of PFOA beyond the 0.5 equivalents, the ^{19}F NMR spectra show presence of free PFOA, indicating a robust competition between PFOA and Ada-COOH for β-CD complexation, consistent with their strong association constants ~ 10^5 M^{-1} (Eftink et al. 1989, Guo et al. 1992, Kwak and Gomez 1996, Wilson and Verrall 1998a, Wilson 1998). The Ada-COOH competitive binding experiments establish encapsulation of PFOA within the β-CD cavity and demonstrate the persistence of the β-CD:PFOA complex.

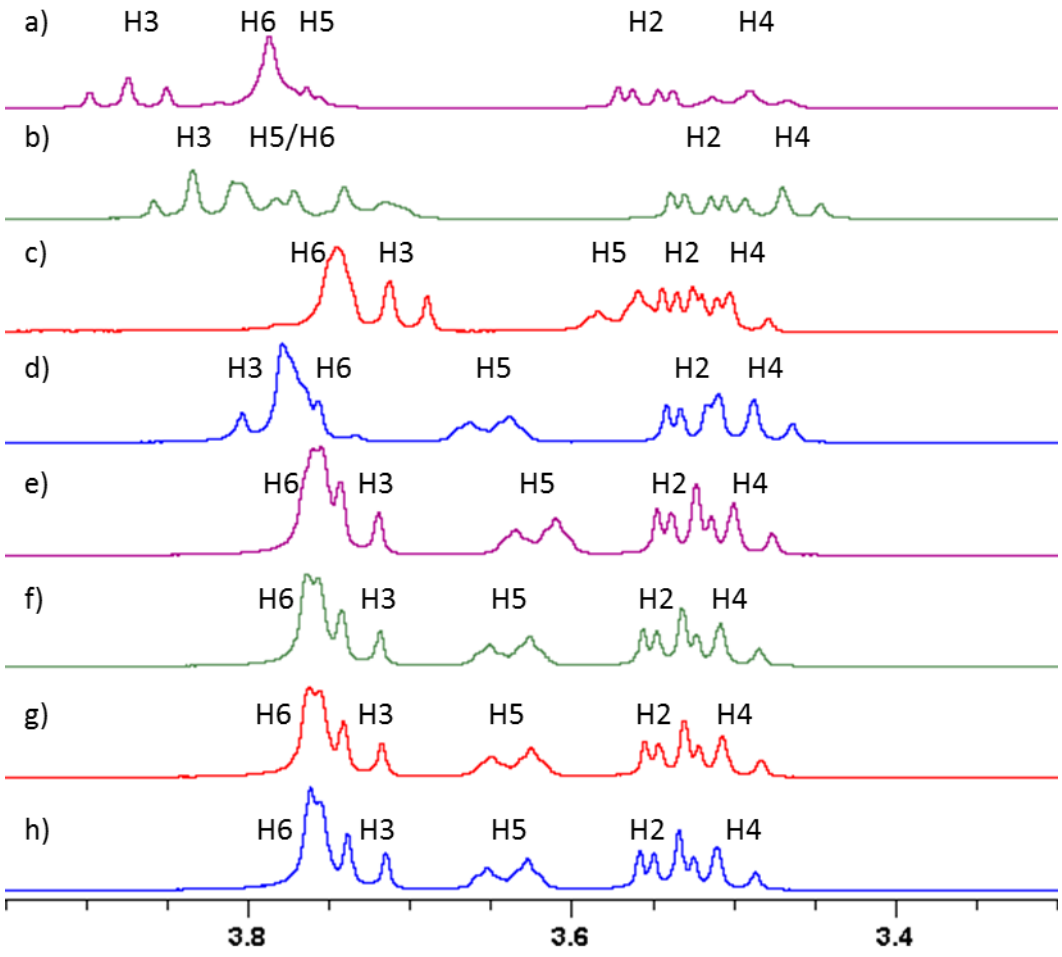

Figure 2.2: PFOA-Ada-COOH competition study. ^{1}H NMR spectra of β-CD (0.00242 M), D_2O. a) β-CD only; b) 1:1 β-CD:Ada-COOH; c) 1:1 β-CD:PFOA; d) 1:1:0.5 β-CD:Ada-COOH:PFOA; e) 1:1:0.75 β-CD:Ada-COOH:PFOA; f) 1:1:1 β-CD:Ada-COOH:PFOA; g) 1:1:1.5 β-CD:Ada-COOH:PFOA; h) 1:1:2 β-CD:Ada-COOH:PFOA.

An analogous competition experiment was conducted between phenol and PFOA. Phenol is reported to have an equilibrium constant with β-CD on the order of ~ 10^2 M^{-1} (Rekharsky and Inoue 1998, Le Saux et al. 2006, Lo Meo et al. 2007). The proton spectrum of a 1:1 β-CD:phenol mixture indicates formation of a host-guest complex, as shown in Figure 2.3 (for the individual spectra, see Appendix 1). When PFOA is added to a 1:1 solution of β-CD:phenol, the chemical shifts of β-CD protons H3 and H5 mirror

that of a solution with only PFOA and β-CD, without phenol, indicating only PFOA is interacting with β-CD, with either no or minimal interaction between phenol and β-CD. Furthermore, the chemical shifts of the ^{19}F NMR peaks suggest that at low PFOA ratios (1:1:0.5 and 1:1:0.75 β-CD:phenol:PFOA), 2:1 β-CD:PFOA complexes are formed in addition to the 1:1 complex. Hence the 2:1 β-CD:PFOA complex is favored over the β-CD:phenol complex.

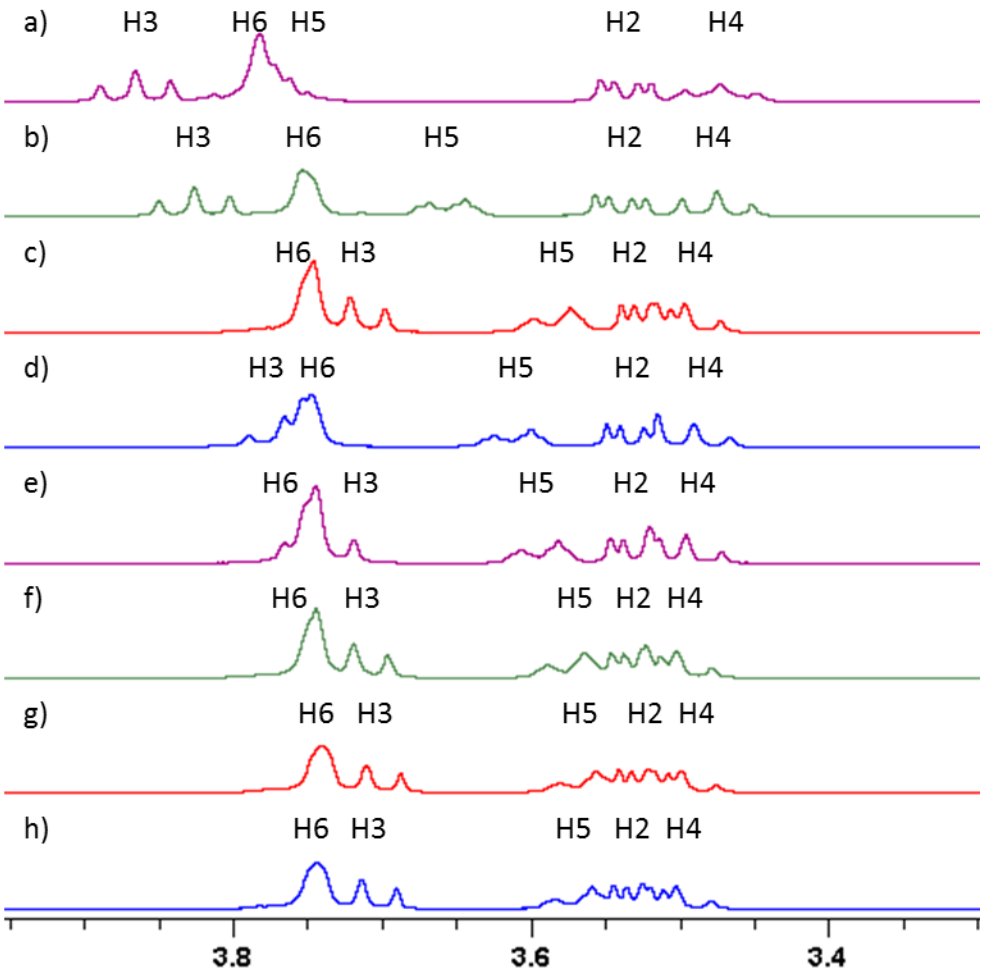

Figure 2.3: PFOA-Phenol competition study. ^{1}H NMR spectra of β-CD (0.00242 M), D_2O. a) β-CD only; b) 1:1 β-CD:Phenol; c) 1:1 β-CD:PFOA; d) 1:1:0.5 β-CD:Phenol:PFOA; e) 1:1:0.75 β-CD:Phenol:PFOA; f) 1:1:1 β-CD:Phenol:PFOA; g) 1:1:1.5 β-CD:Phenol:PFOA; h) 1:1:2 β-CD:Phenol:PFOA.

The competition studies demonstrate β-CD can selectively complex PFOA in the presence of other substrates, such as phenol. Previous studies demonstrated non-fluorinated carboxylic acids also do not disrupt the formation of the 1:1 β-CD:PFOA complex (Xing et al. 2007). Ada-COOH is unique in the strength of its β-CD complexation, but such structures are not expected to be present in the environment. PFOA and other perfluorinated surfactants with strong β-CD association constants are thus expected to be the only contaminants in environmental samples with such powerful complexation to β-CD. The stability of the β-CD:PFAS complex in the presence of the model pollutant phenol indicates promise for applications of β-CD for environmental PFAS remediation.

Monitoring chemical shifts with the titration of guest over a range of host concentrations has been extensively used to assess host-guest interactions (Guo et al. 1992, Wilson and Verrall 1998a, Wilson and Verrall 1998b, Wilson 1998, Ramos Cabrer et al. 1999, Lima et al. 2007, Karoyo et al. 2011, Pessine et al. 2012, Karoyo et al. 2013, Valente and Söderman 2014, Karoyo et al. 2015). Detailed analyses of the changes in chemical shifts of individual fluorine atoms upon complexation with β-CD can provide structural information about the complex. The chemical shifts of individual fluorine atoms were evaluated to assess the favored position of β-CD and dynamics of the host-guest complex. Representative plots of the changes in chemical shift against β-CD concentration for the fluorine atoms at the individual positions F2, F5, and F8 of PFOA are illustrated in Figure 2.4. The magnitude of the change in chemical shift within the same PFOA molecule varied significantly with the addition of β-CD depending on the position along the backbone. For fluorine atoms F2 and F3 adjacent to the polar head

group, the change in chemical shift increases with increasing β-CD concentration. The chemical shifts of F2 and F3 do not change significantly with the addition of excess β-CD, consistent with previous reports of F2 and F3 residing outside the β-CD cavity (Karoyo et al. 2015). The changes in chemical shifts of F4, F5, and F6 (F4-6) increase incrementally with β-CD concentration until the 1:1 stoichiometric ratio, indicating one β-CD complexes one PFOA. The changes in chemical shifts are greater for F4-6 compared to F2 and F3, (ex. $\Delta\delta_{F5}$: 0.46 ppm, $\Delta\delta_{F2}$: 0.20 ppm). These observations suggest the β-CD molecule interacts to a much greater extent with the middle of the PFOA molecule, as illustrated in Figure 2.5. Above the 1:1 β-CD:PFOA ratio, the changes in chemical shift of F4-6 decrease with β-CD concentration, suggesting higher- or mixed-order complexes (Wilson and Verrall 1998a, Wilson 1998, Karoyo et al. 2011, Karoyo et al. 2013, Karoyo et al. 2015). The mathematical description of mixed host-guest complexes is well established (Chapter 1). The experimental data for the β-CD:PFOA complex are best fit by a model that takes into account 1:1 and 2:1 CD:PFAS complexes, as previously reported (Wilson and Verrall 1998a, Wilson 1998, Karoyo et al. 2011, Karoyo et al. 2013, Karoyo et al. 2015). The second stage of the change in the chemical shift signifies the second β-CD capping the tail of the PFOA chain. For F7 and F8, the minimal change in chemical shift for the initial equivalent of β-CD suggests the host-guest interactions are mainly with the middle of the chain F4-6. Under such conditions the environment of F7 and F8 is not changed because the PFOA tail is outside the CD cavity. However, a change in chemical shifts for F7 and F8 are observed with the addition of a second equivalent of β-CD, consistent with a 2:1 complex, as illustrated in Figure 2.5. The relatively larger change in chemical shift for F7 and F8 above the 1:1

host-guest ratio compared to F4-6 further supports the conclusion of a second β-CD capping the tail end of the PFOA chain (ex. $\Delta\delta_{F8}$: -0.65 ppm; $\Delta\delta_{F5}$: -0.46 ppm).

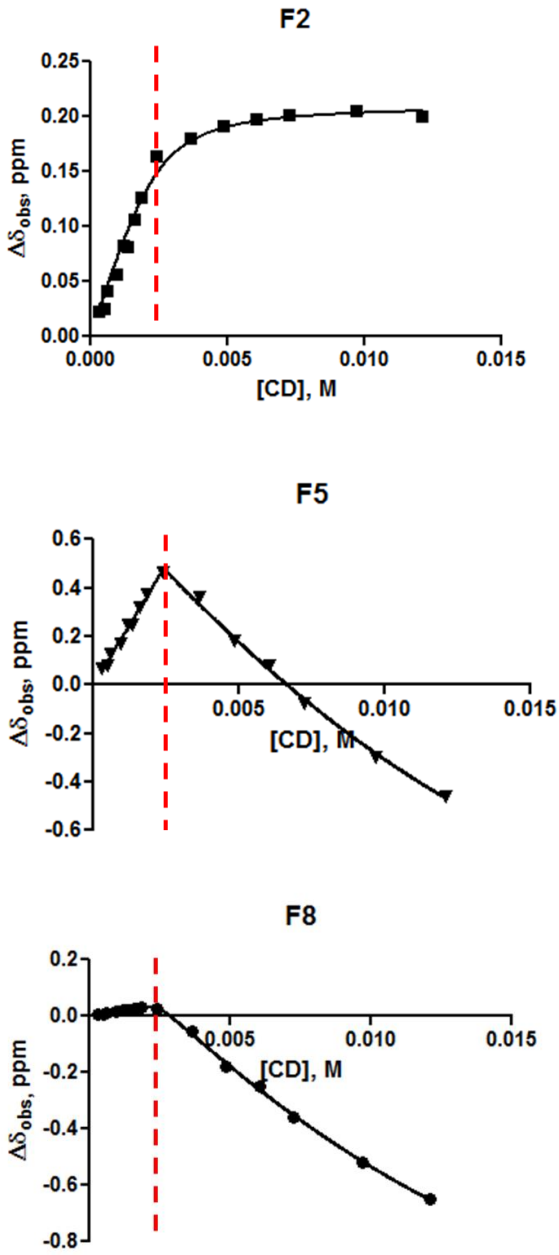

Figure 2.4: Representative graphs of change in observed chemical shift dependent on β-CD concentration for F2, F5, and F8 of PFOA fit by Equations 1.9 or 1.15 (Chapter 1). Dotted line represents 1:1 β-CD:PFOA ratio.

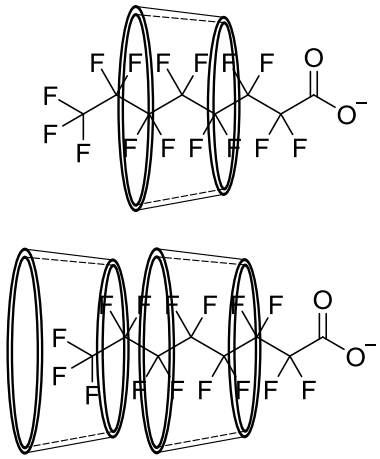

Figure 2.5: 1:1 and 2:1 β-CD:PFOA complexes.

Job analyses were conducted for PFOA and β-CD to further elucidate the stoichiometry of the complex (Job 1928). The concentrations and ratios employed to construct the Job plots can be found in Appendix 1. Representative plots for F2, F5, and F8 are shown in Figure 2.6. For F2 and F3, the maxima are at the mole fraction of 0.5 (corresponding to a 1:1 ratio). The maximum peak is rounded suggesting a 1:1 complex is formed but with a weaker equilibrium constant (~ 10^2-10^3 M^{-1}). In contrast, the Job plots for F4-6 have sharp maxima at 0.5 mole fraction, suggesting a 1:1 complex with a stronger equilibrium constant (~ 10^5 M^{-1}). For F7 and F8, however, a minimum is shown at 0.2 and a maximum at 0.5 mole fraction. Ulatowski, et al. have cited the limited applicability of Job plots when multiple complexes are formed, and that Job plots with minimums and maximums do not indicate the stoichiometry of the complex (2016). Since F7 and F8 are not influenced appreciably until the 2:1 complex is formed, the Job plot is not reliable.

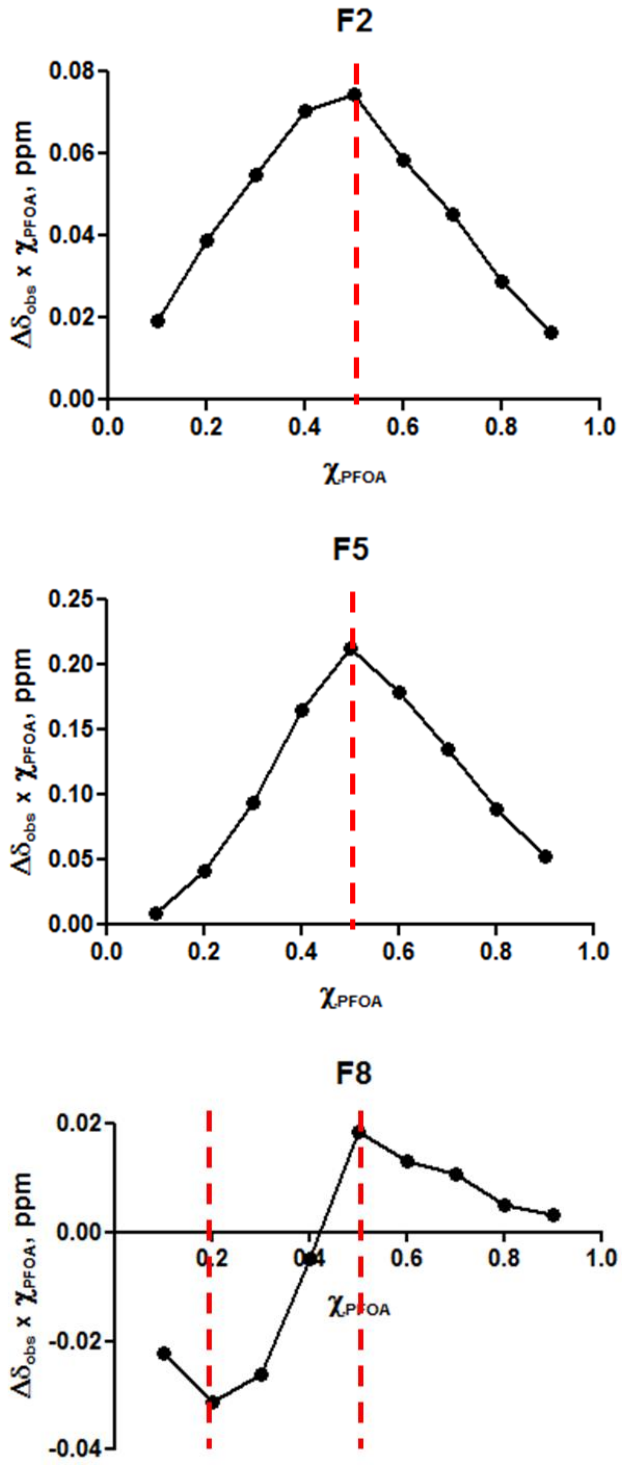

Figure 2.6: Representative Job plots for β-CD interaction with F2, F5, and F8 of PFOA. Solid line used as a guide (not a fit). Dotted line represents maximum and minimum (if applicable) of plot.

Although the changes in the chemical shifts will differ based on the specific location of the CD and the dynamics of the complex, only one equilibrium constant is reported for each host-guest complex. Chemical shifts are influenced by a number of factors (Wilson and Verrall 1998a, Karoyo et al. 2015), but the change from a polar environment (solvent water) to a non-polar environment (within CD) and the shielding effects of the CD typically lead to the most pronounced changes in chemical shifts for the specific atoms of the guest contained within the CD host, with smaller changes for guest atoms outside the CD. This phenomenon leads to stronger equilibrium constants when using NMR peaks that have larger shifts than peaks with smaller shifts. The calculated equilibrium constants for each NMR peak for PFOA complexed with β-CD are shown in Table 2.1 (for other compounds, see Appendix 1). F2 and F3 have 1:1 equilibrium constants ($K_{1:1}$) on the order of 10^3 M^{-1}, with no values for the 2:1 equilibrium constant ($K_{2:1}$). F4-F6 have $K_{1:1}$ values on the order of ~ 10^5 M^{-1}, with $K_{2:1}$ on the order of 10^3 M^{-1}. F7 and F8 exhibit $K_{1:1}$ values ~ 10^4 M^{-1}, and $K_{2:1}$ ~ 10^3 M^{-1}. Based on these results and previous reports, β-CD may move along the PFAS chain, but it predominantly resides at the middle of the chain (F4-6) with the second β-CD complexing with the end of the chain (F7 and F8).

Table 2.1: Association constants for β-CD:PFOA complex
400 MHz ^{19}F NMR at room temperature; values and uncertainty calculated in Prism and Matlab

Fluorine	$K_{1:1}$, M^{-1}	$K_{2:1}$, M^{-1}	$\Delta\delta_{cd\text{-}F}$, ppm	$\Delta\delta_{2cd\text{-}F}$, ppm	R^2
2	$3.27 \pm 0.94 \times 10^3$	Not observed	0.212 ± 0.006	Not observed	0.987
3	$1.73 \pm 0.28 \times 10^3$	Not observed	0.448 ± 0.011	Not observed	0.993
4	$6.77 \pm 0.39 \times 10^5$	$1.01 \pm 0.35 \times 10^3$	0.729 ± 0.027	-21.8 ± 5.8	0.997
5	$4.04 \pm 0.87 \times 10^5$	$1.30 \pm 0.42 \times 10^3$	0.815 ± 0.028	-22.1 ± 7.2	0.997
6	$1.36 \pm 0.14 \times 10^6$	$1.18 \pm 0.53 \times 10^3$	1.08 ± 0.05	-23.6 ± 7.9	0.993
7	$2.27 \pm 0.83 \times 10^4$	$1.32 \pm 0.98 \times 10^3$	0.302 ± 0.110	-16.1 ± 8.0	0.988
8	$6.07 \pm 0.73 \times 10^4$	$1.17 \pm 0.21 \times 10^3$	0.281 ± 0.020	-17.5 ± 2.3	0.999

$K_{1:1}$: 1:1 CD:PFAS association constant
$K_{2:1}$: 2:1 CD:PFAS association constant
$\Delta\delta_{cd\text{-}F}$: Maximum change in chemical shift of the 1:1 CD:PFAS complex
$\Delta\delta_{2cd\text{-}F}$: Maximum change in chemical shift of the 2:1 CD:PFAS complex

These conclusions are further supported by the molecular sizes of these compounds. The cross-section size of the β-CD cavity is 30.2 $Å^2$, compared to the cross section of PFASs, which is 28.3 $Å^2$ (Lo Nostro et al. 2003). In comparison, the cross-section of the α-CD cavity is 18.9 $Å^2$ and the γ-CD cavity is 49.0 $Å^2$ (Lo Nostro et al. 2003). The model molecular fragment C_3F_6 (PFAS chain with three carbons) has a cross section and volume that matches the cavity of β-CD (Appendix 1, Lo Nostro et al. 2003), thus three carbons can reside within the cyclodextrin cavity (F4-6 in the case of PFOA). The second β-CD interacts with F7-8, leaving some remaining room in the second CD cavity for a water molecule as proposed by Karoyo, et al. (2015).

To extend our study, we measured the association constants for β-CD with a series of perfluorinated carboxylic acids as well as sulfonates and a sulfonamide (previously not

reported). A summary of the measured association constants for the series of compounds is provided in Table 2.2 (for detailed analyses of all three CDs, see Appendix 1). The β-CD:PFAS complexes for the long chain PFASs are strong (10^4-10^5 M^{-1}), corresponding to less than 5% free PFAS at a 1:1 β-CD:PFAS ratio. The short chain PFASs (C<6) exhibit $K_{1:1} \sim 10^2$ M^{-1}. The head group of the surfactant had a modest effect on the equilibrium constants and a 2:1 CD:PFAS interaction was also observed for all long chain PFASs (C>6). The strength of the equilibrium constants $K_{1:1}$ for PFASs with an eight carbon backbone and different head groups is as follows: PFOS (sulfonate) > PFOA (carboxylate) > PFOSA (sulfonamide) ~ FTS (sulfonate + $-CH_2CH_2-$). The sulfonate and carboxylate groups possess formal negative charge capable of forming strong hydrogen-bonding interactions with hydroxyl groups on β-CD. For the sulfonate of PFOS there are three hydrogen bonding sites, whereas there are only two for the carboxylate in PFOA, which may be responsible for the slightly weaker $K_{1:1}$ for PFOA. PFOSA is neutral thus will have weaker hydrogen bonding, while FTS has an $-CH_2CH_2-$ group adjacent to the sulfonate which is solvated better by water, leading to the relatively weaker $K_{1:1}$ observed. Hydrocarbon chains also have much smaller cross sections than fluorocarbons, causing weaker host-guest interactions with β-CD (Wilson and Verrall 1998b, Lo Nostro et al. 2003).

Table 2.2: Association constants for 1:1 and 2:1 complexes of β-cyclodextrin with PFASs in aqueous media at room temperature

PFAS	PFBA	PFPA	PFHpA	PFOA	PFNA	PFOS*	PFOSA	6:2 FTS
$K_{1:1}$, M^{-1}	$2.90 \pm 0.24 \times 10^2$	$7.60 \pm 0.44 \times 10^2$	$4.30 \pm 0.85 \times 10^5$	$5.00 \pm 0.10 \times 10^5$	$3.37 \pm 0.35 \times 10^5$	$6.96 \pm 0.79 \times 10^5$	$1.02 \pm 0.16 \times 10^5$	$8.99 \pm 0.36 \times 10^4$
$K_{2:1}$, M^{-1}	-	-	$2.30 \pm 0.27 \times 10^3$	$1.20 \pm 0.50 \times 10^3$	$7.80 \pm 0.66 \times 10^3$	$5.95 \pm 1.70 \times 10^4$	$2.70 \pm 0.57 \times 10^4$	$1.35 \pm 0.38 \times 10^3$

**Reported % linear isomer is 75.4% (Herrera 2008)*

To expand the study to address concerns for environmental applications, the β-CD:PFOA complex was further studied under different water quality conditions, including pH (2, 4, 7, 10), ionic strengths (0.01 M, 0.1 M, and 1.0 M NaCl), and in the presence of humic acid (refer to Appendix 1 for details). Solution pH did not have a significant effect on 1:1 interactions. Increased pH, however, was correlated to a 50 % increase in $K_{2:1}$. In acidic pH, the solution has a greater percentage of positive ions, whereas in alkaline pH, the solution has a greater percentage of negative ions. The pK_a of PFOA is approximately 0, and thus PFOA is expected to be predominantly anionic in all pHs studied (Goss 2008). When the solution is acidic, PFOA could be more solvated due to the favored interactions between the anionic head and the cations and/or protonation in solution. Thus the formation of the 2:1 complex is less favored. In alkaline solution, however, PFOA could be less solvated due to the repulsive interactions between the anionic head and the anions in solution. The formation of the 2:1 complex would in this case be favored. However, the 1:1 complex is unaffected, indicating that the first association constant is dominated by the hydrophobic interactions between the CD cavity

and the PFOA chain. The association of a second β-CD onto the tail, however, is influenced by solution pH by changing the solvation of PFOA.

Ionic strength had a modest effect on the 1:1 interactions but did not exhibit a measureable effect on the 2:1 interactions. For F2 and F3 of PFOA, the individually calculated $K_{1:1}$ decreased with increasing ionic strength; for F4-6, ionic strength did not have significant effects on $K_{1:1}$; and for F7 and F8, $K_{1:1}$ increased with increasing ionic strength, indicating that the favored population structure shifted towards the end of the chain (closer to F7 and F8 and further from F2 and F3). Ionic strength can influence the solvation of a compound in solution. In a previous study, Moulachene, et al. found that increasing ionic strength increased the association between β-CD and progesterone (2015). As the ionic strength of the solution increased, the solvation of the progesterone (a relatively hydrophobic compound) decreased, increasing the thermodynamic favorability of the van der Waals interactions between host and guest. PFOA, however, has a dual hydrophobic and hydrophilic nature. Since PFOA is anionic in these samples, increasing ionic strength enhances the partitioning of the carboxylate group of PFOA to the bulk aqueous media, as it can interact with the positive sodium ions. Such interactions can affect the environments of F2 and F3, enhancing their solvation because of their proximity to the carboxylate group. Thus, this portion of the PFOA molecule acts more ionic in nature and thus can interact with the salt ions in solution. On the other hand, the tail of PFOA does not favorably interact with the ionic solution, much like the progesterone in the previous study, and so it is more favorable for it to interact with the CD cavity. The tail of the PFOA is dominated by its hydrophobic character and thus will be less solvated in the ionic solution. The 2:1 interaction is not affected by ionic strength,

implying that the hydrophobic character of the PFOA molecule dominates and will overcome the ionic interactions near the head group. Previous studies with surfactants have found that increased ionic strength can lower the critical micelle concentration (cmc) (Choppinet et al. 1999), though this is not indicated under our conditions.

Humic acid is a component of natural organic matter rich in carboxylic acid and phenol functionalities. Previous studies have suggested that CDs can interact with humic acid but PFOA does not have significant association with humic acid (Liu et al. 2004, Li et al. 2012). For the 1:1 interactions, presence of humic acid (0.5 g/L) decreased the individually calculated $K_{1:1}$ of F2 and F3, did not affect $K_{1:1}$ for F4-6, and increased $K_{1:1}$ of F7 and F8. This result suggests that humic acid promotes a shift in in the favored positions of β-CD along the backbone of PFOA. For the 2:1 interactions, the presence of humic acid decreased $K_{2:1}$ by 50 % or more for each fluorine atom. Since humic acid-CD interactions have been reported, the results suggest that the humic acid is also interacting with β-CD. The humic acid in this study is isolated from crude lignite, which contains many carboxylic acid and hydroxyl groups. These functional groups could hydrogen-bond with the hydroxyl groups on the CD perimeter. β-CD thus could be encapsulating the end of the PFOA chain, while also interacting via hydrogen-bonding with the humic acid. This structure would inhibit a second CD from interacting with the PFOA chain (the humic acid effectively acting as a cap to the CD cavity). Thus, the presence of humic acid affects the position of β-CD, and only allows one β-CD to interact strongly with the PFOA chain.

2.5 Conclusions

Our studies demonstrate β-CD is an outstanding complexing agent for PFHpA, PFOA, PFNA, PFOS, PFOSA, and 6:2 FTS, with association constants of ~10^5 M^{-1}. The longer chain PFASs form 1:1 and 2:1 complexes with β-CD. The strength of the 1:1 equilibrium constants for PFASs with an eight carbon backbone and different head groups with β-CD is as follows: PFOS (sulfonate) > PFOA (carboxylate) > PFOSA (sulfonamide) ~ FTS (sulfonate + $-CH_2CH_2-$). The addition of excess β-CD can dramatically reduce the amount of free (uncomplexed) PFAS in aqueous media to ~ 0.5%. The β-CD:PFAS complexes for longer chain PFASs are robust, with the middle section of the PFASs contained inside the CD cavity as evidenced by the change in chemical shift data and Job plot. The cross sectional areas and molecular volumes of the PFAS chain and the interior of β-CD appear to be ideal for facilitating strong attractive van der Waals interactions, resulting in the powerful host-guest complexation observed. While the β-CD:PFAS interactions are influenced by ionic strength, pH, and presence of humic acid, the changes are relatively small and the 1:1 β-CD:PFAS complex remains very strong. The strong β-CD:PFAS complexes are persistent in the presence of completing inclusion guests phenol and Ada-COOH. Our results demonstrate β-CD is a powerful complexing agent of PFASs under a variety of environmental conditions. β-CD can be readily attached to a number of solid and polymeric supports (Crini and Morcellet 2002, Martin Del Valle 2004, Crini 2005, Faraji et al. 2011, Nagy et al. 2014, Wang et al. 2014, Liu et al. 2014, Moulahcene et al. 2015, Karoyo and Wilson 2013, Karoyo and Wilson 2015, Karoyo and Wilson 2016, Xiao et al. 2017). With further development, the

practical application of host-guest chemistry using β-CD-based materials may play a critical role for the removal and/or separation science of PFASs.

CHAPTER 3

Host-Guest Interactions between Cyclodextrins and Emerging Perfluoroalkyl Substances

3.1 Abstract

Legacy perfluoroalkyl substances (PFASs) are known environmental pollutants with serious adverse health effects. Perfluoroethercarboxylic acids (PFECAs), emerging PFASs now being substituted for legacy PFASs, have recently been detected in the environment. Cyclodextrins (CDs) have been proposed as agents for the remediation of problematic pollutants, including legacy PFASs. The current study uses ^{19}F NMR spectroscopy to measure the complexation of mono-, di-, and triether PFECAs by CDs for eventual environmental applications. Eight PFECAs were characterized by ^{19}F and ^{13}C NMR. The change in chemical shift of individual fluorines upon complexation of CDs at various stoichiometric ratios was used to determine the host-guest association constants. All studied PFECAs were most strongly encapsulated by β-CD, with association constants from 10^2-10^5 M^{-1} depending on chain length and number of ether functionalities. ^{19}F-^{1}H Heteronuclear Overhauser Effect Spectroscopy (HOESY) NMR experiments were performed for the β-CD complexes of two branched monoethers, PFPrOPrA ("GenX") and PFDMMOBA, to elucidate the structural details of the complexes, determine the specific orientation and position of β-CD along the PFAS chain, and assess the roles of hydrogen-bonding and PFECA branching on the host-guest interactions. The results give new understanding into the fundamental nature of the host-guest complex between cyclodextrins and perfluorinated surfactants.

3.2 Introduction

The association constants between the three cyclodextrins and eight commercially available PFECAs (including mono-, di-, and triethers) were determined by ^{19}F NMR spectroscopy. The fundamental host-guest interactions between PFASs and CDs were further characterized by extended analyses of two branched monoethers with β-CD. ^{19}F-^{1}H Heteronuclear Overhauser Effect Spectroscopy (HOESY) NMR experiments of the branched ethers at 1:1 and 2:1 β-CD:PFECA ratios were conducted to determine the proximity of the fluorines of the PFECA (guest molecule) and protons of the CD (host molecule) in the complex. Furthermore, the HOESY experiment was used to elucidate the orientation of β-CD, which has a smaller side with primary hydroxyl groups and a larger side with secondary hydroxyl groups, along the PFAS backbone in the CD:PFAS complexes. The present study gives valuable information for the design of CD-based remediation strategies for legacy and emerging PFASs, as well as fundamental structural information and insight into the formation and nature of the host-guest complex.

3.3 Experimental Methods

Perfluoro(3-oxabutanoic) acid (PFMOPrA), perfluoro(4-oxapentanoic) acid (PFMOBA), perfluoro(5-oxa-6-dimethylhexanoic) acid (PFDMMOBA), perfluoro(3,6-dioxaheptanoic) acid (PFO2HpA), perfluoro(3,6-dioxadecanoic) acid (PFO2DA), perfluoro(3,6,9-trioxadecanoic) acid (PFO3DA), and perfluoro(3,6,9-trioxatridecanoic) acid (PFO3TDA) were purchased from SynQuest Labs. Perfluoro(2-methyl-3-oxahexanoic) acid (PFPrOPrA, "GenX") was purchased from Alfa Aesar. Hexafluorobenzene was purchased from Sigma-Aldrich. α-, β-, and γ-Cyclodextrins were

purchased from Acros Organics. Deuterium oxide (99.9% D) was purchased from Sigma-Aldrich and stored at 4 °C. Sodium deuteroxide (99.5% D, 30% in D_2O) was purchased from Cambridge Isotope Labs. All chemicals were used without further purification. For abbreviations and structures, refer to Appendix 2.

3.3.1 Sample Preparation

For the titration experiments, samples were prepared as previously described (Chapter 2). The concentration of each PFECA was 2.42×10^{-3} M, except for PFO3TDA which had a concentration of 6.05×10^{-4} M because of possible micelle formation at higher concentrations. The solution consisted of 50 % D_2O and 50 % DI H_2O, adjusted to pH 7 with 0.036 M NaOH. Hexafluorobenzene (1.44×10^{-3} M) was added as an internal standard. Each cyclodextrin (α-, β-, γ-) was added at various stoichiometric ratios and the solution was sonicated until dissolution of the CD was achieved. For the ^{19}F-^{13}C gHMBC experiments, 18 μL of each PFECA was dissolved in 700 μL of $CDCl_3$. For the ^{19}F-^{1}H HOESY experiments, samples were prepared of 0.100 M β-CD in D_2O with NaOD added to aid dissolution. Either PFDMMOBA or PFPrOPrA (0.100 or 0.050 M) was added to make the 1:1 and 2:1 β-CD:PFECA ratios.

3.3.2 ^{19}F and ^{13}C NMR Spectroscopy

^{19}F NMR spectroscopy was performed with a 400 MHz Bruker instrument with a quad probe (operating at 376.498 MHz for ^{19}F). Hexafluorobenzene was used as the internal standard with a chemical shift of -164.9 ppm. For the titration experiments, the chemical shift of each peak was recorded, and the 1:1 and 2:1 association constants were

calculated in GraphPad Prism (version 5.03, La Jolla, CA) and Mathworks Matlab (version R2013b, Natick, MA) by Ramos Cabrer, et al.'s method (Chapter 1) (1999).

^{19}F-^{13}C gradient Heteronuclear Multiple Bond Coherence (gHMBC) NMR spectroscopy was performed on a 500 MHz Varian Inova spectrometer equipped with a 3 r.f. channel console. 1D ^{13}C NMR spectra of PFASs would require application of ^{19}F decoupling over a large frequency band (about 70 ppm, or 33 kHz). Instead, the ^{13}C NMR chemical shifts were obtained using 2D ^{19}F-^{13}C gHMBC experiments as an indirect method, which require less decoupling as well as providing a 27-fold increase in signal to noise compared to conventional ^{13}C NMR spectra. ^{19}F-^{13}C gHMBC spectra were recorded in less than an hour. The ^{19}F spectra were run on a spectral window from -40 to -140 ppm, in 4 transients, with a 90 ° pulse (5.3 μs), a relaxation delay of 1 s and an acquisition time of 3 s. The gHMBC spectrum was run on a minimal spectral window in *f2* in 8k points. The spectral window in *f1* was from 90 to 170 ppm, and 256 increments were used, each in 4 transients and with a relaxation delay of 1 s. The FIDs were weighted in *f2* with a Gaussian function of 0.1 s shifted 0.08 s and in *f1* with a Gaussian of 0.1 s. The polarization transfer delay was 16.7 ms, corresponding to a coupling constant of 30 Hz, which yielded cross-peaks for couplings over one bond (easily identified by their splitting of ~ 280 Hz) and couplings over two bonds.

3.3.3 ^{19}F-^{1}H HOESY NMR Spectroscopy

The NMR spectra for the HOESY experiments were run on a Varian Inova spectrometer, operating at 500 MHz for ^{1}H, equipped with a 3 r.f. channel console, at 25 °C. The probe was a 5 mm probe with two channels, ^{1}H and ^{19}F, connected to channels 1

and 3 in the console, correspondingly. ^{1}H and ^{19}F chemical shifts were referenced on the TMS and $CFCl_3$ scales.

The ^{1}H NMR spectra were run on a spectral window from -0.5 to 9.5 ppm, in 1 transient, with a 90 ° pulse (19 μs), a relaxation delay of 1 s and an acquisition time of 3.2 s. The ^{19}F spectra were run on a spectral window from -60 to -170 ppm, in 16 transients, with a 90 ° pulse (12 μs), a relaxation delay of 1 s and an acquisition time of 0.63 s. The HOESY spectrum was run with observation of ^{19}F and a mixing time of 50 ms for PFDMMOBA and 100 ms for PFPrOPrA, on a spectral window from -170 to -60 ppm and 16k points in *f2*. The spectral window in *f1* was from 3 to 5 ppm for PFDMMOBA and 3 to 4 ppm for PFPrOPrA, and 128 increments were used, with a total experiment time of 20 hrs for the 2:1 ratios and 5 hrs for the 1:1 ratios.

3.4 Results and Discussion

The PFECA structures were numbered according to the position of the fluorine atoms (see Appendix 2), with "F2" referring to the fluorines on the carbon next to the carboxylate head group. Chain length is defined as the longest continuous chain of carbons and oxygens starting at the carbonyl carbon (does not include branching). The PFECAs are divided into short chain (chain length < 7) and long chain (chain length ≥ 7). In this report we will refer to PFECAs with "high oxygen content" (HOC) and "low oxygen content" (LOC). These designations refer to the ratio of oxygen atoms to chain length. An HOC PFECA is defined as an PFECA with a oxygen:chain length ratio of 0.5 or greater (including the carboxylate oxygens), and a LOC PFECA has an oxygen:chain length ratio less than 0.5 (for HOC and LOC designations, refer to Appendix 2).

3.4.1 Assignment of the PFECA ^{19}F NMR Spectra

Assignments of individual fluorine peaks of the eight studied PFECAs, as shown in Figure 3.1, were determined by chemical shift, splitting pattern, integration, peak broadening, and comparison with ^{19}F NMR spectra of legacy PFASs. Assignments were confirmed by the ^{19}F-^{13}C gHMBC experiments. ^{19}F and ^{13}C NMR chemical shifts are displayed in Figure 3.1 (for detailed coupling constants and splitting patterns of ^{19}F NMR peaks, refer to Appendix 2). Seven general types of fluorine peaks were observed and assigned to specific structures, with consistent chemical shifts regardless of chain length and number of oxygens, as shown in Table 3.1. The fluorine peaks shifted more downfield when adjacent to an oxygen atom and more upfield when surrounded by fluoromethylene subunits (with similar chemical shifts to legacy PFASs) (Guo et al. 1992, Wilson and Verrall 1998a). Downfield chemical shifts are correlated to decreased shielding, whereas upfield chemical shifts are correlated to increased shielding. The presence of the ether oxygen leads to deshielding of the adjacent fluorines, causing their chemical shift to be shifted downfield compared to what is expected from a legacy PFAS. The splitting patterns were also examined. Through-space coupling, instead of through-bond coupling, is characteristic for saturated perfluorinated molecules (Petrakis and Sederholm 1961). Fluorines that are four bonds apart are closer in space than fluorines three bonds apart in PFAS structures (refer to the structures included in Figure 3.1). Thus, in general, four bond coupling constants were observed ($^4J_{F\text{-}F} \approx$ 8-11 Hz), but not three bond coupling constants ($^3J_{F\text{-}F} \approx$ 0-3 Hz). The HOC PFECAs generally had sharper peaks and a more defined splitting pattern than LOC PFECAs due to the oxygen linkages extending the distance between fluorine atoms, and thus decreasing the amount and

strength of coupling interactions along the fluorinated backbone. Peak broadening was observed for longer chain PFECAs, especially LOC PFECAs, in the middle of the chain, due to the complex splitting pattern arising from the number and variety of other fluorines within coupling proximity.

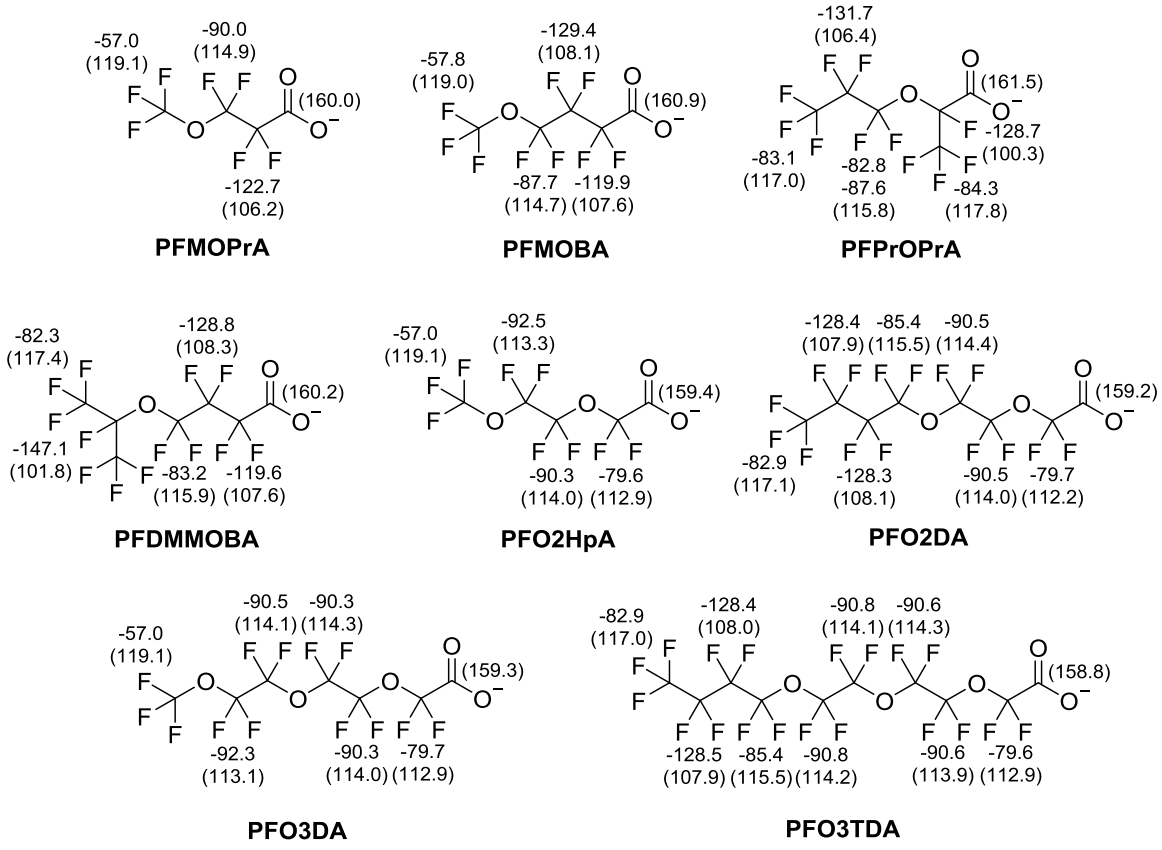

Figure 3.1: ^{19}F and ^{13}C NMR chemical shifts of the studied PFECAs. The ^{19}F NMR chemical shifts (in D_2O; referenced to hexafluorobenzene) are listed first; the ^{13}C NMR chemical shifts (in $CDCl_3$; referenced to $CDCl_3$) are listed second in parentheses.

Table 3.1: Chemical shifts of PFECA ^{19}F NMR peaks[a]

Structure (peak in bold)	Chemical shift, ppm
$^{-}OOC\text{-}C\mathbf{F_2}\text{-}O\text{-}$	-79
$^{-}OOC\text{-}C\mathbf{F_2}\text{-}CF_2\text{-}$	-119 – -122
$\text{-}O\text{-}C\mathbf{F_2}\text{-}C\mathbf{F_2}\text{-}O\text{-}$	-90 – -92
$\text{-}O\text{-}C\mathbf{F_2}\text{-}CF_2\text{-}CF_2\text{-}$	-83 – -87
$\text{-}O\text{-}CF_2\text{-}C\mathbf{F_2}\text{-}CF_2\text{-}$	-128 – -129
$\text{-}CF_2\text{-}O\text{-}C\mathbf{F_3}$	-57
$\text{-}CF_2\text{-}CF_2\text{-}C\mathbf{F_3}$	-82 – -83

[a] *Referenced to hexafluorobenzene (-164.9 ppm)*

3.4.2 Association Constants of PFECAs with α-, β-, and γ-Cyclodextrin

The ^{19}F NMR spectrum of each PFECA was monitored as a function of CD concentration. The individual CD:PFECA association constants were determined via non-linear least-squares regression analysis of the change in observed chemical shift (Ramos Cabrer et al. 1999). The association constants determined for individual fluorines were then averaged to find the average association constant for each PFECA with each CD. The results are shown in Table 3.2 (for ^{19}F NMR spectra, non-linear regression plots, and individual association constants, see Appendix 2).

Table 3.2: Average association constants of emerging PFASs with α-, β-, and γ-CDs

PFAS (chain length), oxygen content	α-CD (M^{-1})	β-CD (M^{-1})	γ-CD (M^{-1})
PFMOPrA (5), HOC	$2.60 \pm 1.14 \times 10^1$	$1.54 \pm 0.52 \times 10^2$	no significant association
PFMOBA (6), HOC	$3.37 \pm 1.40 \times 10^1$	$1.48 \pm 0.36 \times 10^3$	no significant association
PFPrOPrA (6), HOC	$2.36 \pm 1.10 \times 10^2$	$7.45 \pm 4.27 \times 10^2$	no significant association
PFDMMOBA (7), LOC	no significant association	$2.66 \pm 0.61 \times 10^4$	$6.85 \pm 1.82 \times 10^2$
PFO2HpA (7), HOC	$5.34 \pm 0.48 \times 10^1$	$4.74 \pm 2.04 \times 10^2$ (1:1) $3.87 \pm 1.40 \times 10^2$ (2:1)	$8.43 \pm 3.24 \times 10^1$
PFO2DA (10), LOC	no significant association	$1.38 \pm 0.40 \times 10^4$ (1:1) $7.72 \pm 2.43 \times 10^3$ (2:1)	$1.39 \pm 0.38 \times 10^3$
PFO3DA (10), HOC	$9.28 \pm 2.80 \times 10^1$	$3.03 \pm 1.09 \times 10^3$ (1:1) $4.12 \pm 1.08 \times 10^3$ (2:1)	$7.60 \pm 2.10 \times 10^2$
PFO3TDA (13), LOC	no significant association	$5.93 \pm 1.20 \times 10^5$ (1:1) $1.36 \pm 0.28 \times 10^5$ (2:1)	$3.48 \pm 1.50 \times 10^3$

The CD association constants with PFECAs did not have a direct relationship with chain length as observed with legacy PFASs (Chapter 2, Wilson and Verrall 1998a). Instead, the magnitude of association appears to depend on a number of factors, including oxygen content and branching. For α-CD, weak association constants are observed for the short chain PFECAs (chain length < 7). For long chain PFECAs (chain length ≥ 7), HOC PFO2HpA and PFO3DA show association with α-CD at the terminal $–CF_2OCF_3$ group, whereas the long chain LOC PFECAs, with a continuous chain of perfluorinated carbons

at the tail, exhibited no significant association with α-CD. The cross-sectional area of the α-CD cavity cannot fit the PFAS chain (cross-section of 18.9 $Å^2$ for α-CD cavity and 28.3 $Å^2$ for PFASs) (Lo Nostro et al. 2003), leading to the weak or non-existent complexation (on the order of 10^1-10^2 M^{-1}) with the studied PFECAs that may be attributed to association besides host-guest (i.e., aggregate formation). For γ-CD, moderate association constants (on the order of 10^2-10^3 M^{-1}) were observed for the long chain PFECAs. LOC PFECAs had stronger association with γ-CD when compared to HOC PFECAs of the same chain length (for example, PFO2DA vs. PFO3DA). The cross-section size of γ-CD (49.0 $Å^2$) is larger than necessary to accommodate PFASs, resulting in weaker host-guest interactions (Lo Nostro et al. 2003). Since $–CF_2–$ groups have a larger van der Waals radius than oxygen, the PFECAs with more fluorinated carbons (LOC) will have more favorable interactions with the γ-CD cavity than HOC PFECAs. Short chain PFECAs are too small in comparison to the γ-CD cavity to exhibit attractive molecular interactions leading to relatively insignificant host-guest interactions observed.

β-CD exhibited the strongest interactions with all studied PFECAs. Stronger association constants were observed for longer chain PFECAs and LOC PFECAs when compared with shorter chain PFECAs and HOC PFECAs respectively. β-CD has the ideal cavity cross-section (30.2 $Å^2$) to accommodate linear perfluorinated carbon chains as guests, resulting in strong van der Waals interactions between the fluorinated chain and β-CD cavity (Lo Nostro et al. 2003). Oxygen, which has a smaller van der Waals radius than $–CF_2–$, does not fit tightly within the β-CD cavity, thus weakening the interactions promoting complexation between the PFECA and β-CD. The 1:1 β-CD:PFECA association constants are affected by chain length and oxygen content. Long

chain PFECAs (except PFDMMOBA) also form stable 2:1 β-CD:PFECA complexes, like those described for legacy PFASs (Chapter 2, Wilson and Verrall 1998a). The 2:1 β-CD:PFECA association constants increase with chain length with the strongest association observed for the longest chain PFECA (PFO3TDA), suggesting that chain length is the most important factor in determining the strength of the 2:1 CD:PFAS complex.

The β-CD:PFECA and β-CD:legacy perfluorocarboxylic acid association constants are compared in Table 3.3. The comparison was made between compounds with the same chain length, defined as the longest continuous chain of atoms from the head group, not number of carbons. The PFECAs have weaker complexation with β-CD than the corresponding legacy PFAS (including perfluoropentanoic acid, PFPA; perfluorohexanoic acid, PFHxA; perfluoroheptanoic acid, PFHpA; and perfluorodecanoic acid, PFDA) of the same chain length. Generally, for each ether oxygen substituted for carbon in the PFAS chain, the association constant decreased by an order of magnitude. These results demonstrate that ether functionalities have weaker complexation with β-CD than the fluorinated carbon chain, and thus weaken the overall association. The interior of the cyclodextrin cavity is hydrophobic, and thus strongly associates with the hydrophobic fluorinated chain while having weak or nonexistent interactions with the smaller, more polar oxygens in the ether functionalities. LOC PFECAs not only have fewer ether oxygens per chain length, but also have longer sections of a continuous fluorinated carbon chain, facilitating strong association of β-CD with the fluorine-rich section of the chain.

Table 3.3: β-CD:PFECA association constants compared with β-CD:legacy PFASs

Chain length	Legacy PFAS	Association constant (M^{-1})	Emerging PFAS	Association constant (M^{-1})	Decrease (1:1)
5	PFPA[a]	7.60 +/- 0.44 x 10^2	PFMOPrA	1.54 +/- 0.52 x 10^2	< 10
6	PFHxA[b]	2.35 +/- 0.46 x 10^4	PFMOBA	1.48 +/- 0.36 x 10^3	~10
			PFPrOPrA	7.45 +/- 4.27 x 10^2	~100
7	PFHpA[a]	4.30 +/- 0.85 x 10^5 (1:1) 2.30 +/- 0.27 x 10^3 (2:1)	PFDMMOBA	2.66 +/- 0.61 x 10^4	~10
			PFO2HpA	4.74 +/- 2.04 x 10^2 (1:1) 3.87 +/- 1.40 x 10^2 (2:1)	~1000
10	PFDA[c]	~10^5 (1:1) ~10^3 (2:1)	PFO2DA	1.38 +/- 0.40 x 10^4 (1:1) 7.72 +/- 2.43 x 10^3 (2:1)	~10
			PFO3DA	3.03 +/- 1.09 x 10^3 (1:1) 4.12 +/- 1.08 x 10^3 (2:1)	~100

Legacy PFAS association constants from: [a] Chapter 2, [b] Wilson and Verrall 1998a, and [c] estimated based on association constants from PFOA and PFNA in Chapter 2

The effects of branching on the association constants were investigated in more detail with two branched monoethers, PFPrOPrA and PFDMMOBA. Both have segments of three fluorinated carbons, which should lead to favorable CD encapsulation (Chapter 2). For PFPrOPrA, branching occurs adjacent to the carboxylate head group, whereas for

PFDMMOBA, branching occurs after the ether near the tail (forming a fluorinated isopropyl group tail). β-CD displays much stronger complexation (~ 40 ×) with PFDMMOBA than PFPrOPrA. The position of branching has a dramatic effect on the strength of β-CD encapsulation, with branching near the tail leading to stronger host-guest complexation than branching near the head.

This result can be explained when taking into account the association constant of β-CD with linear PFMOBA. PFMOBA, with K = 1.48×10^3 M^{-1}, has a $–CF_2CF_2CF_2–$ segment attached to the carboxylate group and a perfluoromethyl ether as the tail section, an analogous structure to PFDMMOBA. In comparison, PFPrOPrA has an association constant of 7.45×10^2 M^{-1}, and PFDMMOBA has an association constant of 2.66×10^4 M^{-1}, with β-CD. All three compounds contain a $–CF_2CF_2CF_2–$ segment, and they are pictured in Figure 3.2 along with their 1:1 β-CD:PFECA association constants. From our previous work we have found that β-CD has a strong preference for association with the $–CF_2CF_2CF_2–$ segment, due to van der Waals interactions between the guest molecule and host cavity, and the molecular sizes of the PFASs and β-CD (Chapter 2). The measured association constants of the three ether compounds, however, indicate that other factors are also important in the host-guest interactions.

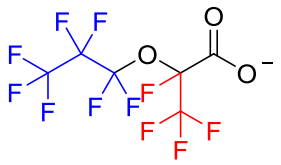

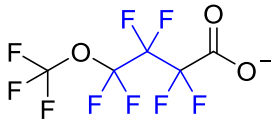

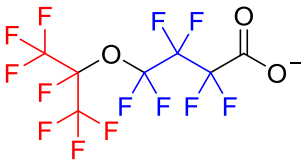

Figure 3.2: Structures of PFPrOPrA, PFMOBA, and PFDMMOBA, along with the 1:1 β-CD:PFECA association constants. Blue highlights the linear three carbon segment ideal for β-CD:PFAS interactions; red highlights branched portions of the molecule.

One major difference between these three compounds is the presence and placement of branched structures. The trifluoromethyl group ($–CF_3$) has an effective size between that of a hydrogenated isopropyl and *tert*-butyl group; thus, a fluorinated isopropyl group would be larger than a hydrogenated *tert*-butyl group (approximately the size of $–CBr_3$) (Dawson et al. 1980, Hughes et al. 2000, Krafft et al. 2009). Since the linear PFAS has a virtually perfect fit with the β-CD cavity, and the effective sizes of fluorinated functional groups are larger than their hydrocarbon counterparts, branching renders fluorocarbons too large to fit within the cavity. With this in mind, β-CD can only encapsulate the linear perfluorinated carbon chains and cannot accommodate the branched portion of the PFAS within the β-CD cavity. β-CD can thread over the tail, but not the branched head, of PFPrOPrA; the tail or the head of PFMOBA; and the head, but not the branched tail, of PFDMMOBA.

In addition to the effect of branching on encapsulation within the CD cavity, branching can also influence hydrogen-bonding between the host and guest. The carboxylate of linear perfluorocarboxylic acids, similar to other guest molecules containing a carboxylate, can hydrogen-bond to the hydroxyl groups lining the perimeter of the β-CD cavity (Saenger and Steiner 1998, Lipkowitz 1998, Takahashi 1998, Wagner 2012). The β-CD hydroxyls can be within a favorable distance for hydrogen-bonding to the carboxylate of both PFMOBA and PFDMMOBA, as the $–CF_2CF_2CF_2–$ segment that the CD will encapsulate is next to the carboxylate group. The branched portion of PFPrOPrA, however, prevents β-CD from moving along the fluorinated chain to be close enough to interact with the carboxylate head group. In contrast, the branched portion of PFDMMOBA prevents β-CD from sliding towards the tail end of the fluorinated chain, keeping the CD close enough to hydrogen-bond with the carboxylate. PFMOBA had no branching, and so although it can hydrogen-bond with β-CD, β-CD can still freely move along the PFMOBA chain, decreasing the chances of the hydrogen-bonding interactions.

The association constant of PFMOBA is greater than PFPrOPrA due to hydrogen-bonding, and the association constant of PFDMMOBA is greater than PFMOBA due to hindered movement of the CD along the tail end of chain. From these results it appears that the strength of CD:PFAS interactions is determined not only by hydrophobic interactions between the fluorinated chain and CD cavity, but also by hydrogen-bonding between the PFAS carboxylate and the hydroxyl groups along the CD perimeter. Branching close to the polar head group inhibits this hydrogen-bonding, while branching at the tail enhances association by stabilizing the complex. These results suggest that it is favorable for the carboxylate to thread through the CD cavity (as would be necessary in

the case of PFDMMOBA), even though this would cause the hydrophilic and anionic carboxylate to be in close proximity to the hydrophobic CD cavity and removed from the bulk aqueous solution. Previous studies of carboxylate-CD interactions, however, support our conclusions, by providing evidence of carboxylate inclusion in the CD cavity (Bergeron et al. 1977, Bergeron et al. 1978, Simova and Schneider 2000, Liu et al. 2001, Wang and Chen 2011, Saha et al. 2016). For example, α,ω-alkyl dicarboxylates have similar association constants with α-CD as their corresponding monocarboxylates (Watanbe et al. 1992, Wilson and Verrall 1998b, Wilson and Verrall 2000), suggesting that other factors, such as van der Waals interactions between the CD cavity and hydrophobic chain (either hydrogenated or fluorinated), are more important than the inclusion or threading of the hydrophilic moiety in or through the CD cavity for favorable host-guest complexation. The measured association constants of the PFECAs suggest that the carboxylate threading through the CD cavity has little effect on the host-guest complexation (as evidenced by the strong association between β-CD and PFDMMOBA, where this threading is required for inclusion). Instead, van der Waals interactions, hydrogen-bonding, and physical structure (branching vs. linear) of the PFECA are critical factors for strong encapsulation.

3.4.3 Structural Characterization of the CD:PFAS Complex

To further probe the structural details of the β-CD:PFECA complexes, and PFASs in general, ^{19}F-^{1}H Heteronuclear Overhauser Effect Spectroscopy (HOESY) NMR experiments were conducted (Battiste 2006). In HOESY NMR experiments, through-space nuclear Overhauser effects (NOEs) are observed between different nuclei. HOESY

signals are observed as a function of the distance between the nuclear spins of the fluorines on the PFAS (guest) and the protons on the CD (host). The intensity of the HOESY signal increases non-linearly with decreasing distance ($1/r^6$) between individual fluorines and protons. ^{19}F-^{1}H HOESY experiments were conducted on the β-CD:PFECA mixtures to determine the relative positon of fluorine atoms on the PFECA guest to the protons on the β-CD host.

The structure of β-CD is shown in Chapter 1 (Figure 1.2). H1, H2, and H4 extend to the outside of the CD, whereas H3 and H5 point towards the interior of the CD cavity. H6 are the methylene protons attached to the primary hydroxyl groups lining the smaller opening of the CD. Thus, NOEs between interior protons H3 and H5 and the perimeter protons H6 with the fluorines on the PFECA backbone contained within the CD interior are expected to be observed for the host-guest inclusion complex. The exterior protons (H1, H2, and H4) are not expected to exhibit any NOE with the PFECA fluorines. Furthermore, cyclodextrins are not cylinders, but truncated cones, having a smaller end and a larger end. The smaller side is lined with seven primary hydroxyl groups and the larger side is lined with fourteen secondary hydroxyl groups. H6 and H5 are closer to the smaller opening and H3 is closer to the larger opening. Thus, the orientation of the CD in the host-guest complex can be elucidated from the HOESY signals or crosspeaks of the fluorines along the backbone with H3, H5, and H6. The specific orientation of the CD relative to the head and tail of PFASs in solution has previously not been confirmed (Guo et al. 1992, Wilson and Verrall 1998a, Karoyo et al. 2011, Karoyo et al. 2013, Karoyo et al. 2015). The ^{19}F-^{1}H HOESY spectra of both 1:1 and 2:1 β-CD:PFECA ratios of PFDMMOBA and PFPrOPrA were analyzed.

The HOESY results are visualized by the proton slices across *f1* at the *f2* frequencies of the fluorine signals. For the β-CD:PFDMMOBA complex, all fluorines display crosspeaks with H3, H5 and H6 of the cyclodextrin, confirming the existence of the host-guest inclusion complex, as shown in Figure 3.3. No NOEs were observed between any of the fluorines and H1, H2, or H4. The intensities of the proton crosspeaks vary depending on the position of the fluorines, indicating relative distances. For the spectral slice of the 2D crosspeaks at F2, F3, and F4, H5 and H6 are dominant, whereas for the crosspeaks at F6 and F7, H3 is most intense. These results clearly show that the smaller opening of the cyclodextrin, with the primary hydroxyl groups, is facing the carboxylate head of PFDMMOBA, while the larger opening of the cyclodextrin, with the secondary hydroxyl groups, is facing the tail end of the PFECA, as shown in Figure 3.3. The NOE patterns for the 1:1 and 2:1 β-CD:PFDMMOBA ratios are the same, confirming that only a 1:1 complex is formed as concluded from the titration studies.

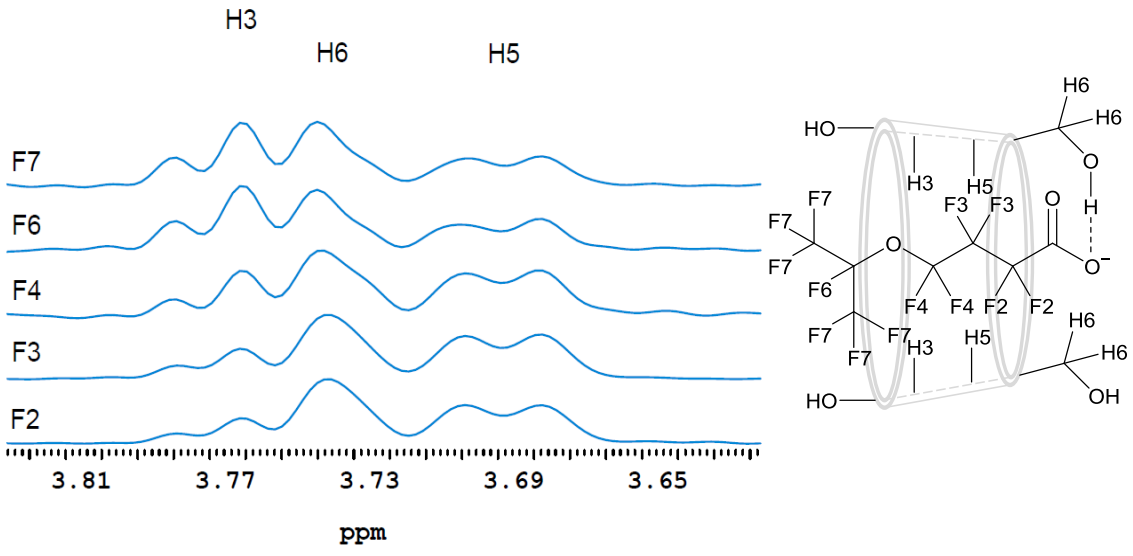

Figure 3.3: ^{19}F-^{1}H HOESY of β-CD:PFDMMOBA complex. The proton slices for each fluorine peak are shown. The host-guest structure is elucidated from the NOEs observed between each fluorine and proton. H3 is a triplet; H5 is a doublet; H6 is a broad singlet.

Likewise, all the fluorines of PFPrOPrA display crosspeaks with H3, H5, and H6 in the β-CD:PFPrOPrA complex, as pictured in Figure 3.4. Again, no crosspeaks were observed between any fluorine and H1, H2, or H4. For the slices at F2 and F3, H5 and H6 are dominant; for F5, H5 is most intense; and for F6 and F7, H3 is dominant. Again, the cyclodextrin is oriented with the primary hydroxyl groups facing the carboxylate, pictured in Figure 3.4. Only a 1:1 complex appears to be formed due to the same NOE pattern for both the 1:1 and 2:1 β-CD:PFPrOPrA ratios, confirming the results from the titration experiments.

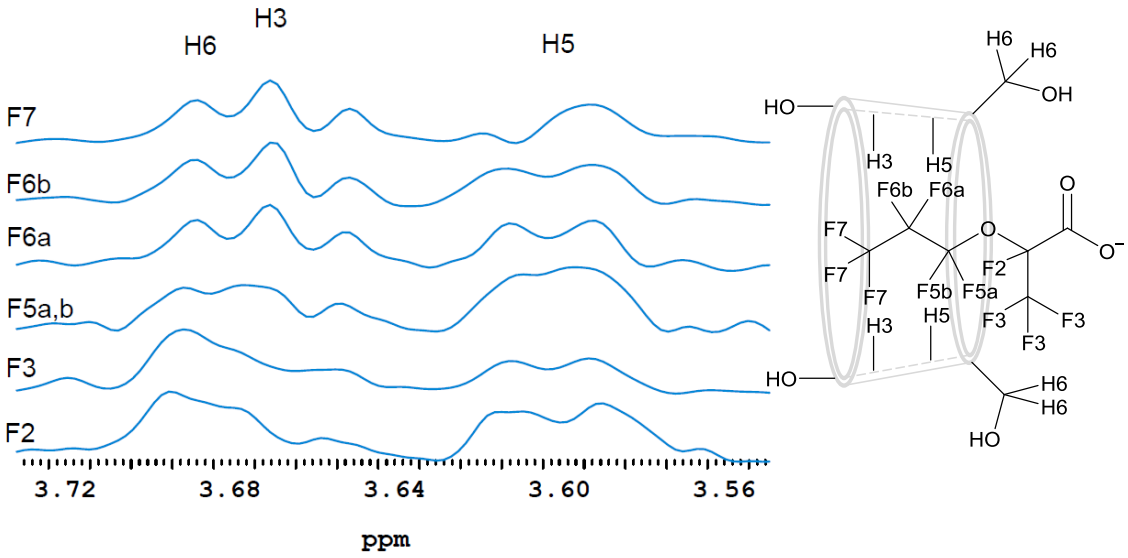

Figure 3.4: ^{19}F-^{1}H HOESY of β-CD:PFPrOPrA complex. The proton slices for each fluorine peak are shown. The host-guest structure is elucidated from the NOEs observed between each fluorine and proton. H3 is a triplet; H5 is a doublet; H6 is a broad singlet.

It is clear from the HOESY spectra that the primary hydroxyl groups are oriented towards the PFAS carboxylate in the CD:PFAS host-guest complex, regardless of branching, suggesting an optimal geometry for the CD:PFAS complex. The primary

hydroxyl groups are less sterically hindered and have more freedom of rotation than the secondary hydroxyl groups, which may make it more favorable for hydrogen-bonding between the primary hydroxyl groups of the CD and the carboxylate of the PFAS. Furthermore, the primary hydroxyl groups are further away from the bulk of the CD cavity, which would allow adequate separation of the PFAS chain-CD cavity interactions and the PFAS carboxylate-CD hydroxyl group interactions. These results support the conclusion that PFPrOPrA forms a weaker host-guest complex than PFDMMOBA with β-CD because of hindered hydrogen-bonding with the carboxylate due to the branched structure. Threading of the carboxylate through the CD cavity is also supported by the confirmed inclusion of PFDMMOBA by β-CD. Finally, the molecular sizes of PFASs, combined with the HOESY results, suggest that PFASs can enter the β-CD cavity by both the head and tail ends, as long as the primary hydroxyl side is facing the head group.

3.5 Conclusions

The host-guest inclusion complexes between three cyclodextrins and eight emerging perfluoroethercarboxylic acids were examined via 1D and 2D ^{19}F NMR spectroscopy. β-CD formed the strongest complexes with all studied PFECAs, while moderate interactions with γ-CD and weak interactions with α-CD were observed depending on PFECA chain length and the number of oxygens. Increasing number of ether oxygens per chain length lead to decreased 1:1 association constants with β-CD, with each additional oxygen corresponding to an order of magnitude decrease in association constant compared with legacy PFASs. 2:1 β-CD:PFECA association constants, however, appear to be mainly dependent on chain length. ^{19}F-^{1}H HOESY

NMR experiments of two branched monoethers gave two insights into the structure of the host-guest complex: 1) the small side of the CD (primary hydroxyl) faces the carboxylate in perfluorocarboxylic acids and 2) hydrogen-bonding plays an important role in the strength of the CD:PFAS host-guest interactions. Thus, 1:1 β-CD:PFAS association is affected by hydrophobic (van der Waals interactions between perfluorinated chain and CD cavity) and hydrophilic interactions (hydrogen-bonding between PFAS polar head group and CD primary hydroxyl groups), while 2:1 association is only dependent on hydrophobic interactions (chain length). Knowing the orientation of the CD in the complex as well as the intermolecular forces responsible for 1:1 and 2:1 β-CD:PFAS host-guest interactions will allow for the design of CD-based polymers or solid-support materials that are well-suited for CD:PFAS complexation.

CHAPTER 4

Host-Guest Interactions between β-Cyclodextrin Derivatives and Short Chain Perfluoroalkyl Substances

4.1 Abstract

Short chain perfluoroalkyl substances (PFASs) are being more widely used due to known negative health and environmental effects of long chain legacy PFASs such as perfluorooctanoic acid (PFOA) and perfluorooctanesulfonate (PFOS). However, the transport and persistence of short chain PFASs (whether fully fluorinated or with an ether functionality) is on par with legacy long chain PFASs, and preliminary tests suggest they have similar toxic effects. Previous tests with cyclodextrins (CDs) have been mixed, with association constants on the order of $10^1 – 10^3$ M^{-1} with β-CD (compared with PFOA and PFOS with association constants on the order of 10^5 M^{-1}). These association constants are on the same order of magnitude as most other organic pollutants, making β-CD not selective enough for emerging short chain PFASs to be useful for remediation purposes. Modifications to β-CD could increase this selectivity by increasing the association constant. In this study we have conducted ^{19}F NMR titration experiments to determine the association constants of various β-CD derivatives with short chain PFASs. Positively charged β-CD derivatives were chosen for their potential ionic interactions with negatively charged PFASs as well as their commercial availability. A negatively charged derivative was also chosen for comparison. Addition of positively charged groups on β-CD generally increased the association constants compared to the complex formed with native β-CD. The results give further understanding to the nature of the CD:PFAS host-guest complex and the various intermolecular forces that drive encapsulation.

4.2 Introduction

In this study, NMR titration experiments have been conducted to determine the association constants of various β-CD derivatives with short chain PFASs, as well as to further elucidate the nature of the host-guest complex. Positively charged β-CD derivatives have been chosen for their potential ionic interactions with negatively charged PFASs. A negatively charged β-CD derivative has also been chosen for comparison.

4.3 Experimental Methods

Perfluorobutanoic acid (PFBA), perfluoropentanoic acid (PFPA), and hexafluorobenzene were purchased from Sigma-Aldrich. Perfluoro(3-oxabutanoic) acid (PFMOPrA), perfluoro(4-oxapentanoic) acid (PFMOBA), and perfluoro(5-oxa-6-dimethylhexanoic) acid (PFDMMOBA) were purchased from SynQuest Labs. Perfluoro(2-methyl-3-oxahexanoic) acid (PFPrOPrA, "GenX") was purchased from Alfa Aesar. 6-Monodeoxy-6-monoamino-β-cyclodextrin hydrochloride (mono-am-β-CD), heptakis(6-deoxy-6-amino)-β-cyclodextrin heptahydrochloride (hepta-am-β-CD), (2-hydroxy-3-*N*,*N*,*N*-trimethylamino)propyl-β-cyclodextrin chloride (QACD; degree of substitution ~ 3-4), and sulfobutylated β-cyclodextrin sodium salt (SBECD; degree of substitution ~ 6.5) were purchased from Cyclolab Ltd (see Appendix 3 for structures). Deuterium oxide (99.9% D) was purchased from Sigma-Aldrich and stored at 4 °C. All chemicals were used without further purification.

4.3.1 Sample Preparation

For the titration experiments, samples were prepared as previously described (Chapter 2). The concentration of each PFAS was 2.42×10^{-3} M. The solution consisted of 50 % D_2O and 50 % DI H_2O, adjusted to pH 7 with 0.036 M NaOH. Hexafluorobenzene (1.44×10^{-3} M) was added as an internal standard. Each cyclodextrin was added at various stoichiometric ratios and the solution was sonicated for one minute to ensure dissolution of the compounds.

4.3.2 ^{19}F NMR Spectroscopy

^{19}F NMR spectroscopy was performed with a 400 MHz Bruker instrument with a quad probe (operating at 376.498 MHz for ^{19}F). Hexafluorobenzene was used as the internal standard with a chemical shift of -164.9 ppm. For the titration experiments, the chemical shift of each peak was recorded, and the 1:1 CD:PFAS association constants were calculated in GraphPad Prism (version 5.03, La Jolla, CA) and Mathworks Matlab (version R2013b, Natick, MA) by Ramos Cabrer, et al.'s method (Chapter 1) (1999).

4.4 Results and Discussion

The chemical shift of the peaks corresponding to each fluorine changed as a function of CD concentration (refer to Appendix 3). This change in chemical shift was monitored and used to calculate the individual association constants of each fluorine with the CD. The average of these individual association constants is reported in Table 4.1 for each short chain PFAS with each β-CD derivative, along with the association constants for native β-CD calculated in previous studies (Chapters 2 and 3).

Table 4.1: Average association constants of short chain PFASs with β-CD derivatives

PFAS	β-CD (M^{-1})	Mono-am-β-CD (M^{-1})	Hepta-am-β-CD (M^{-1})	QACD (M^{-1})	SBECD (M^{-1})
PFBA	$2.90 \pm 0.24 \times 10^{2}$ [a]	$2.16 \pm 1.04 \times 10^{2}$	$1.02 \pm 0.40 \times 10^{3}$	$1.46 \pm 0.31 \times 10^{2}$	No significant association
PFPA	$7.60 \pm 0.44 \times 10^{2}$ [a]	$1.01 \pm 0.61 \times 10^{3}$	$2.62 \pm 0.79 \times 10^{3}$	$6.68 \pm 3.41 \times 10^{2}$	$1.07 \pm 0.18 \times 10^{2}$
PFMOPrA	$1.54 \pm 0.52 \times 10^{2}$ [b]	$6.39 \pm 1.06 \times 10^{2}$	$3.06 \pm 1.33 \times 10^{3}$	$6.92 \pm 1.56 \times 10^{2}$	No significant association
PFMOBA	$1.48 \pm 0.36 \times 10^{3}$ [b]	$1.76 \pm 1.02 \times 10^{3}$	$4.56 \pm 1.22 \times 10^{3}$	$3.29 \pm 0.63 \times 10^{3}$	$9.68 \pm 2.29 \times 10^{1}$
PFPrOPrA	$7.45 \pm 4.27 \times 10^{2}$ [b]	$1.55 \pm 0.62 \times 10^{4}$	$1.86 \pm 1.13 \times 10^{3}$	$4.43 \pm 1.66 \times 10^{2}$	$3.70 \pm 2.32 \times 10^{2}$
PFDMMOBA	$2.66 \pm 0.61 \times 10^{4}$ [b]	$2.75 \pm 0.39 \times 10^{4}$	$2.12 \pm 0.49 \times 10^{5}$	$2.02 \pm 0.57 \times 10^{5}$	$6.49 \pm 2.79 \times 10^{3}$

a: From Chapter 2; b: from Chapter 3

General trends were observed for each β-CD derivative. For the negatively charged SBECD, the association constant decreased compared to native β-CD, with the shortest chain PFASs studied (PFBA and PFMOPrA) experiencing no significant association. All studied PFASs are expected to be negatively charged under the experimental conditions (long chain PFASs have pK_as of approximately 0) (Goss 2008), and thus they are repulsed by SBECD, leading to weaker complexation than neutral β-

CD. For the three positively charged β-CD derivatives (mono-am-β-CD, hepta-am-β-CD, and QACD), complexation with the short chain PFASs generally increased compared to neutral β-CD, due to the electrostatic attraction between the positively charged β-CD derivative and the negatively charged PFAS. For QACD, the legacy PFASs (PFBA and PFPA) and PFPrOPrA (GenX) experience slightly decreased association, whereas the ether PFASs besides PFPrOPrA (PFMOPrA, PFMOBA, and PFDMMOBA) experience increased association. For mono-am-β-CD, the complexation remained similar to β-CD for PFBA, PFMOBA, and PFDMMOBA, and increased for PFPA, PFMOPrA, and PFPrOPrA. Finally, for hepta-am-β-CD, the association constant increased for all studied short chain PFASs compared with the association constant with β-CD.

Our previous studies (Chapters 2 and 3) have elucidated the major factors causing the favorable encapsulation of PFASs by β-CD. PFASs have strong interactions with β-CD due to the cross-sectional sizes of the PFASs and β-CD (28.3 and 30.2 $Å^2$, respectively), leading to favorable van der Waals forces between the PFAS fluorinated chain and the β-CD cavity (Lo Nostro et al. 2003). These hydrophobic interactions dominate the host-guest complex: legacy PFASs have stronger interactions with β-CD than PFECAs, which have ether oxygen moieties interspersed throughout the fluorinated chain, disrupting the van der Waals forces. Secondary to the hydrophobic interactions is the hydrogen-bonding interactions between the PFAS head group (carboxylate, sulfonate, etc.) and the primary hydroxyl groups lining the perimeter of the small side of the β-CD cavity. When this hydrogen-bonding is prevented (as in the case of the β-CD:PFPrOPrA complex, due to branching of the PFAS next to the carboxylate), encapsulation is

weakened; when it is forced (as in the case of the β-CD:PFDMMOBA complex, due to branching of the PFAS at the tail), encapsulation is strengthened.

The calculated association constants for the complexes between the β-CD derivatives and the short chain PFASs provide additional insight into the nature of CD:PFAS host-guest interactions. PFMOPrA, PFPrOPrA, and PFDMMOBA have the largest changes in association constants with the positively charged β-CD derivatives, as seen in Table 4.2. PFPrOPrA has increased complexation with mono-am-β-CD (20 ×), and PFDMMOBA has increased complexation with both QACD (8 ×) and hepta-am-β-CD (8 ×). PFMOPrA has increased complexation with all three studied positively charged β-CD derivatives, especially hepta-am-β-CD (20 ×).

Table 4.2: Increase in β-CD derivative:PFAS association constants compared with β-CD:PFAS association constants

PFAS	Mono-am-β-CD	Hepta-am-β-CD	QACD	SBECD
PFBA	0.7	3.5	0.5	0
PFPA	1.3	3.4	0.9	0.1
PFMOPrA	4.2	20	4.5	0
PFMOBA	1.2	3.1	2.2	0.08
PFPrOPrA	20	2.5	0.6	0.5
PFDMMOBA	1.0	8.0	8.0	0.2

Branching in the PFAS structure is an important factor in the strength of complexation. PFDMMOBA, branched at the tail, must enter β-CD head first (threading the carboxylate through the CD cavity). In native β-CD, once PFDMMOBA has threaded

through the cavity, the primary hydroxyl groups will hydrogen-bond with the PFDMMOBA carboxylate, locking PFDMMOBA in place. For the mono-am-β-CD complex, there is no increase in association constant, suggesting that the complex with β-CD is already so stable that the presence of a single positive charge does not affect the strength of complexation. For the hepta-am-β-CD complex, the presence of seven positive charges, however, does have an effect on the complexation, and increases the association constant relative to the β-CD complex by 8 × (about an order of magnitude). Thus, multiple positives charges can strengthen the complex, whereas the presence of one positive charge has roughly the same effect as the hydrogen-bonding interactions. Furthermore, the QACD:PFDMMOBA association constant is also 8 × stronger than the β-CD complex. The QACD has a propyl linker between the CD cavity and the quaternary amine group (compared with mono-am-β-CD or hepta-am-β-CD which have methylene linkers). The increased length of the linker may allow this side chain to curl back around the PFDMMOBA head group so that both the hydroxyl group in the middle of the linker and the positively charged quaternary amine group at the end of the linker can interact with the PFDMMOBA carboxylate through hydrogen-bonding and electrostatic interactions, respectively. These potential dual interactions could also be a great enough difference compared to the native β-CD neutral hydroxyl groups and the single amino group of the mono-am-β-CD to produce a noticeable increase in association.

Branching also produces changes in the PFPrOPrA complexes. PFPrOPrA can only enter the CD cavity tail first (threading the fluorinated tail through the CD cavity) due to this branching next to the carboxylate head group. The amino groups of mono-am-β-CD and hepta-am-β-CD are substituted on the small side of the CD, which is the

opening that the fluorinated chain of PFPrOPrA must pass through to enter the CD cavity. Although the association constant for the hepta-am-β-CD:PFPrOPrA complex increased compared to the β-CD complex, the increase was smaller than all the other studied PFASs. Most likely this is observed because it is unfavorable for the fluorinated chain to pass through the ring of positively charged amino groups, whereas all the other studied PFASs can enter the CD cavity through the other opening (threading the carboxylate through the CD cavity). The mono-am-β-CD:PFPrOPrA complex, however, is 20 × stronger than the complex with β-CD. For this complex, PFPrOPrA does not have to thread through a ring of multiple positive charges. From the previous results (Chapter 3), the amino group is expected to be too far from the PFPrOPrA carboxylate in the complex. Electrostatic attraction may still occur, however, leading to the large increase in association. For the complex with QACD, the association constant is decreased compared to β-CD. The long side chain may block PFPrOPrA from threading through the CD cavity, leading to decreased interactions.

Finally, PFMOPrA had unusual increases in association constants with the three positively charged β-CD derivatives, especially for hepta-am-β-CD, compared with the other linear PFASs (PFBA, PFPA, and PFMOBA). PFMOPrA is the only PFAS studied that does not have the $–CF_2CF_2CF_2–$ subunit. From the molecular sizes of the PFASs and the β-CD cavity, three fluorinated carbons will be encapsulated in the cavity during the host-guest interactions (Chapter 2; Lo Nostro et al. 2003). As this functionality is extremely hydrophobic, its interactions with the hydrophobic β-CD cavity lead to the favorable van der Waals forces that drive the strong complexation of PFASs by β-CD. PFMOPrA does not have this functionality; it has two fluorinated carbons between the

carboxylate and ether functionalities, with a $–CF_3$ group on the other side of the ether oxygen. Thus, the encapsulation of PFMOPrA by native β-CD is relatively unfavorable due to the hydrophilic ether oxygen within the hydrophobic CD cavity during complexation. Since this complex is unfavorable, complexes with slightly more favorable conditions lead to large increases in association constant. For the mono-am-β-CD:PFMOPrA and QACD:PFMOPrA complexes, the association constants are about 4 × the value of the association constant for the β-CD:PFMOPrA complex. Although the van der Waals interactions are the driving force behind the host-guest complexation and the interactions between the PFAS carboxylate and the hydroxyl groups of the β-CD cavity perimeter are secondary, the change of one of the hydroxyl groups to a positively charged amino group, or the addition of the side chain with a quaternary amine, cause a larger change in the association constant than other PFASs due to the unfavorable hydrophobic interactions in the CD cavity. This association constant is increased further (20 ×) by the replacement of all the primary hydroxyl groups by positively charged amino groups in hepta-am-β-CD. This result indicates that the presence of positively charged groups that can experience ionic bonding interactions with the negatively charged PFAS carboxylate become increasingly important to the favorability of the host-guest complex if there is no $–CF_2CF_2CF_2–$ group present in the PFAS structure. As the van der Waals forces are decreased, electrostatic interactions can help drive the host-guest interactions.

These conclusions further explain why PFBA, PFPA, and PFMOBA experience very similar changes in association constant depending on the β-CD derivative: they all have three fluorinated carbon subunits within their structure, despite PFMOBA having an ether functionality. Almost no increase in complexation is observed when only one or

two positively charged groups are present (mono-am-β-CD and QACD), as the van der Waals forces are still the major driver of the host-guest complex, and the ionic bonding interactions play a minor role. A slight increase (3 ×) in association constant occurs when the seven positively charged groups are present (hepta-am-β-CD), as the electrostatic interactions between the carboxylate and amino groups are more likely and thus become a greater factor in the overall strength of complexation. In contrast, for PFMOPrA, any presence of cationic groups that can facilitate electrostatic attraction will lead to increases in the encapsulation, as the weak van der Waals forces within the cavity are a more minor component in the association.

4.5 Conclusions

Positively charged β-CD derivatives increased encapsulation of short chain PFASs relative to native β-CD. Linear PFASs with a $–CF_2CF_2CF_2–$ group had little or no increase with mono-am-β-CD and QACD, and moderate increase with hepta-am-β-CD, compared to β-CD. Favorable interactions between the hydrophobic fluorinated chain and the CD cavity dominate these complexes, while ionic bonding interactions between the PFAS carboxylate and the CD amino groups are secondary. A linear PFAS without the $–CF_2CF_2CF_2–$ group (PFMOPrA) had moderate increases in complexation with mono-am-β-CD and QACD and a large increase with hepta-am-β-CD compared to β-CD. PFMOPrA does not have strong van der Waals interactions between the PFAS chain and the CD cavity, and thus the electrostatic attraction due to addition of amino groups in the CD structure dominates the host-guest complex. PFDMMOBA, the PFAS branched at the tail, had moderate increases in association with QACD and hepta-am-β-CD compared

with β-CD. The presence of a positively charged side chain (QACD) or multiple positively charged amino groups (hepta-am-β-CD) can further lock PFDMMOBA into the CD cavity and hinder dissociation, increasing the strength of complexation beyond the base hydrophobic interactions. PFPrOPrA, the PFAS branched next to the carboxylate head group, had a large increase in association constant with mono-am-β-CD compared with β-CD, but not with the other positively charged β-CD derivatives. Since PFPrOPrA must enter the CD cavity through the primary hydroxyl, and thus amino-substituted, side, the presence of the positively charged side chain (QACD) or multiple positively charged amino groups (hepta-am-β-CD) make the complex unfavorable, whereas the presence of one positively charged group (mono-am-β-CD) allows PFPrOPrA to enter the CD cavity leading to potential favorable electrostatic interactions.

The addition of positive groups on β-CD allows for greater complexation with short chain PFASs than neutral β-CD. A negatively charged β-CD derivative causes weaker complexation than neutral β-CD. Thus, the interaction between the PFAS carboxylate and the β-CD primary hydroxyl groups, or their substitutions, is important to the strength of the host-guest complex. This interaction, however, is secondary to the hydrophobic interactions between the PFAS fluorinated chain and the β-CD cavity, which are the primary drivers of the host-guest complex. The ionic interactions with the positively charged amino groups are only important to the host-guest interactions (leading to large increases) when the hydrophobic interactions are unfavorable, such as in the case of PFMOPrA, or when branching has either hindered the host-guest complex originally (PFPrOPrA) or stabilized it (PFDMMOBA). These results give further insight

into the host-guest chemistry between PFASs and CDs, and can be utilized in the design of CD-based remediation technologies for short chain and emerging PFASs.

CHAPTER 5

β-Cyclodextrin Reverses Binding of Perfluorooctanoic Acid to Human Serum Albumin

5.1 Abstract

Perfluorooctanoic acid (PFOA), a persistent organic pollutant known to cause adverse health effects, strongly binds to human serum albumin (HSA). β-Cyclodextrin (β-CD), a non-toxic cyclic sugar, strongly complexes PFOA in a host-guest complex, and has been proposed for environmental remediation of PFOA. The interactions between HSA, PFOA, and β-CD were investigated in order to determine if β-CD can reverse the binding of PFOA to HSA, with potential therapeutic applications towards exposure to PFOA. ^{19}F Nuclear magnetic resonance (NMR), circular dichroism, and fluorescence spectroscopies were used to study these interactions. Multiple PFOA binding sites to HSA, one with strong affinity and others with low affinity, are evident from changes in the fluorescence emission spectra of HSA and the fluorescence lifetimes of the single Trp residue in HSA with increasing PFOA concentration. Structural changes in the protein are also evident from changes in the circular dichroism spectra of HSA upon titration of PFOA. Addition of β-CD to PFOA and HSA reversed these changes, indicating that formation of the β-CD:PFOA host-guest complex is favored even in the presence of HSA. Equimolar β-CD to PFOA (1:1 β-CD:PFOA ratio) causes dissociation of the weakly bound PFOA from HSA, whereas excess β-CD relative to PFOA (5:1 β-CD:PFOA ratio) leads to the complete disassociation of the strongly bound PFOA molecule from HSA. The ^{19}F NMR studies further suggest that the 2:1 β-CD:PFOA complex inhibits PFOA binding to HSA. These data demonstrate that β-CD has potential to be used in therapeutic applications for PFOA in human blood.

5.2 Introduction

In this study, we have investigated the interactions between PFOA, HSA, and β-CD by employing ^{19}F NMR, circular dichroism, and fluorescence (both steady state and frequency-resolved) spectroscopies to elucidate the potential for β-CD to reverse the binding of PFOA to HSA. The association between PFOA and β-CD in the presence of HSA was characterized by ^{19}F NMR. Circular dichroism experiments elucidated the conformational changes of HSA upon addition of PFOA. Steady state fluorescence and fluorescence lifetime experiments were employed to examine the binding between PFOA and HSA in the absence/presence of β-CD. Finally, a fluorescence competition study was used to further probe these interactions and determine potential binding sites.

5.3 Experimental Methods

PFOA, hexafluorobenzene, and 8-anilinonaphthalene-1-sulfonic acid (1,8-ANS) were purchased from Sigma-Aldrich. β-CD was purchased from Acros Organics. HSA (66,248 Da, ≥ 99 % by agarose gel electrophoresis, fatty acid and globulin free) and deuterium oxide (99.9 % D) were purchased from Sigma-Aldrich and stored at 4 °C. All chemicals were used without further purification.

5.3.1 Sample Preparation

For the ^{19}F NMR experiments, a solution of 2.42 mM PFOA was prepared in 50 % D_2O and 50 % 100 mM sodium phosphate buffer (pH 7.4) solution in H_2O. Hexafluorobenzene (1.44 mM) was added as an internal standard. Various stoichiometric ratios of β-CD were added to the PFOA solution, and the samples were sonicated to

ensure dissolution (Chapter 2). After analysis, HSA (35 μM) was added to each sample, and the samples were analyzed again.

For the circular dichroism and fluorescence spectroscopy experiments, stock solutions of PFOA (10 mM and 100 μM), β-CD (5 mM), and HSA (20 μM) were prepared with a 50 mM sodium phosphate buffer (pH 7.4) solution in polypropylene tubes (MacManus-Spencer et al. 2010). The concentration for a stock solution of 1,8-ANS (2.77 mM) was calculated by measuring the UV-visible absorbance at 350 nm of the solution and using ε_{350} = 5000 $M^{-1}cm^{-1}$ (Gonzalez and Miksovska 2014). All the stock solutions were shaken to ensure dissolution of each compound.

5.3.2 ^{19}F NMR Spectroscopy

NMR experiments were performed with a 400 MHz Bruker instrument with a quad probe (operating at 376.498 MHz for ^{19}F). Hexafluorobenzene was used as the internal standard with a chemical shift of -164.9 ppm (Chapter 2). The chemical shift of each peak was recorded, and the 1:1 and 2:1 β-CD:PFOA association constants were calculated in GraphPad Prism (version 5.03, La Jolla, CA) and Mathworks Matlab (version R2013b, Natick, MA) by Ramos Cabrer, et al.'s method (Chapter 1) (1999).

5.3.3 Circular Dichroism Spectroscopy

Circular dichroism experiments were performed with a JASCO J-815 CD Spectrometer. The ellipticity was measured between 200 and 300 nm. The concentration of HSA was 10 μM. PFOA was titrated into the sample at various concentrations. The

spectra were corrected to account for dilution. The experiment was performed in triplicate.

5.3.4 Fluorescence Spectroscopy

Steady state emission experiments were performed with a PC1 Fluorometer (ISS Inc, Champaign, IL). The excitation wavelength was 295 nm, and the emission spectra were recorded between 305 and 440 nm using 1 nm slit width for both excitation and emission. The emission spectra were corrected for the inner filter effect; however, the inner filter effect was insignificant at the HSA concentrations used in this study (refer to Appendix 4). Fluorescence lifetime experiments (frequency-resolved) were performed with a ChronoFD Fluorometer (ISS Inc, Champaign, IL). The excitation wavelength was 280 nm and 2,5-diphenyloxazole (PPO) was used as a lifetime reference. The fluorescence decay was modeled using a sum of three exponential decays according to Equation 5.1,

$$I(t) = \sum \alpha_i \, e^{\left(\frac{-t}{\tau_i}\right)} \tag{5.1}$$

where I(t) is the intensity decay at time t, τ is the fluorescence lifetime, and α is the pre-exponential factor (Lakowicz 2006, Ross and Jameson 2008). Data were analyzed using Globals for Spectroscopy Software (Laboratory of Fluorescence Dynamics, Irvine, CA). For both steady state and fluorescence lifetime experiments, the concentration of HSA was 10 μM. PFOA and then β-CD were titrated into the sample at various concentrations and the spectra were corrected to account for dilution. Each experiment was performed in triplicate. The Stern-Volmer quenching constant (K_{SV}) and bimolecular quenching rate constant (k_q) were determined from Stern-Volmer plots by measuring the emission

intensity (I) and average fluorescence lifetime (< τ >) as a function of quencher concentration ([Q]) and using Equations 5.2 and 5.3,

$$\frac{I_o}{I} = 1 + K_{SV}[Q] \tag{5.2}$$

$$\frac{<\tau_o>}{<\tau>} = 1 + k_q < \tau_0 > [Q] \tag{5.3}$$

where I_o and $< \tau_o >$ are the emission intensity and average fluorescence lifetime in the absence of quencher, respectively.

Steady state emission competition experiments with 1,8-ANS were performed with a Cary Eclipse Fluorescence Spectrophotometer. The excitation wavelength was 350 nm, and the emission spectra were measured between 370 and 650 nm. The slit width was 2.5 nm for both excitation and emission. The concentration of HSA was 10 μM. 1,8-ANS, PFOA, and β-CD were titrated into the sample at various concentrations and the spectra were corrected to account for dilution. The experiment was performed in triplicate.

5.4 Results and Discussion

5.4.1 ^{19}F NMR Studies

^{19}F NMR spectroscopy has previously been used to study the 1:1 and 2:1 β-CD:PFOA host-guest complexes formed in aqueous solution (Chapter 2). Changes in the ^{19}F chemical shift of PFOA titrated with β-CD were monitored to compare the host-guest association in the presence and absence of 35 μM HSA (see Appendix 4). The observed change in chemical shift of each fluorine peak varied differently as a function of β-CD concentration. The samples containing HSA showed broadened peaks, suggesting PFOA

is binding to HSA. The 1:1 and 2:1 β-CD:PFOA association constants were calculated by non-linear least-squares regression analysis for each fluorine (see Appendix 4). The association constants for the fluorines closer to the PFOA carboxylate head group with β-CD are weaker in the presence of HSA, whereas the fluorines towards the end of the alkyl chain (tail) experience a stronger interaction with β-CD in the presence of HSA. The 1:1 and 2:1 β-CD:PFOA association constants averaged for all fluorines are listed in Table 5.1. The 1:1 β-CD:PFOA association constant decreases in the presence of HSA likely due to the interaction of the carboxylate group of PFOA with HSA (supported by the changes in the individual fluorines) that weakens the PFOA association to β-CD. The association constants for the formation of 2:1 β-CD:PFOA complexes in the presence and absence of HSA are within the calculated error, suggesting that the formation of the 2:1 complex between β-CD and PFOA inhibits PFOA binding to HSA.

Table 5.1: Association constants for β-CD:PFOA complexes in 50 mM phosphate buffer (pH 7.4)

Condition	$K_{1:1}$, M^{-1}	$K_{2:1}$, M^{-1}
No HSA	$4.16 \pm 0.88 \times 10^5$	$6.42 \pm 1.78 \times 10^2$
35 μM HSA	$1.67 \pm 0.33 \times 10^5$	$9.09 \pm 1.27 \times 10^2$

5.4.2 Steady State Fluorescence and Circular Dichroism

HSA has a single Trp residue (Trp-214) located between IIA and IIB subdomains that is often employed as an internal fluorescence probe to monitor the mechanism of the interactions of organic molecules with HSA (Dugaiczyk et al. 1982, Fanali et al. 2012). As PFOA is titrated into a solution of HSA, both the emission intensity (Figure 5.1a; also

see Appendix 4) as well as the emission maximum (λ_{max}; Figure 5.1b) for the Trp-214 residue changed. At concentrations up to 10 μM PFOA, the 1:1 molar ratio between PFOA and HSA, the fluorescence intensity increased by 20 % without a significant shift in λ_{max}. Further increase in PFOA concentration leads to a decrease in the fluorescence intensity of HSA, and the λ_{max} shifted to shorter wavelengths (from 335 nm to 320 nm). At 200 μM PFOA (the 20:1 ratio between PFOA and HSA), the fluorescence intensity and λ_{max} plateaued suggesting no additional PFOA binding to HSA.

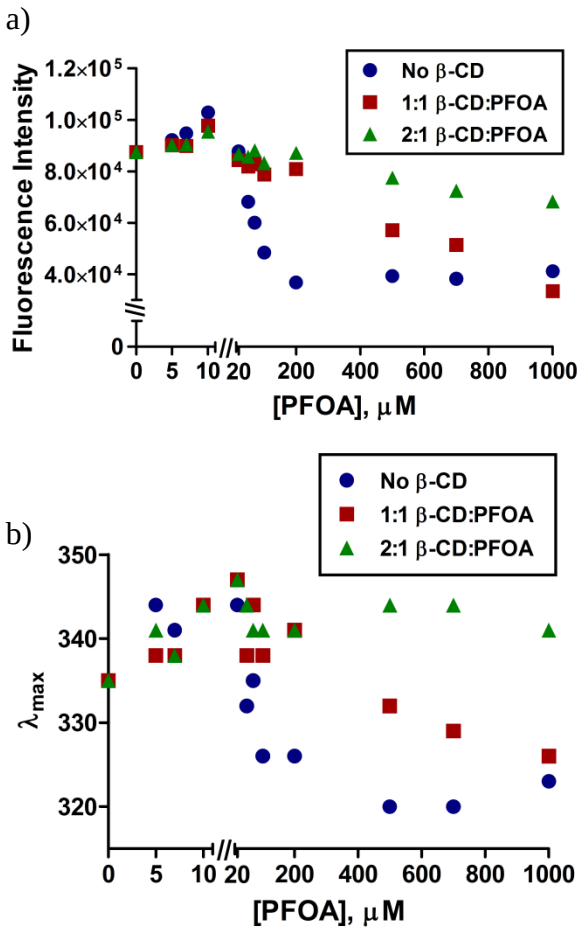

Figure 5.1: a) Fluorescence emission intensity measured at 335 nm and b) the maximum emission wavelength (λ_{max}) of 10 μM HSA titrated with increasing concentrations of PFOA. For each PFOA concentration, β-CD was added to achieve 1:1 and 2:1 β-CD:PFOA ratios. The error bars are within the symbols.

Circular dichroism can be used to determine the secondary structures of proteins by measuring the absorption of circularly polarized light by the peptide bonds at wavelengths less than 240 nm (Kelly et al. 2005). α-Helical secondary structure is evident from circular dichroism ellipticity minimums at 208 and 220 nm. The circular dichroism spectra of HSA as a function of PFOA concentration showed similar changes as the fluorescence spectra (Figure 5.2; also see Appendix 4). At ratios up to 1:1 PFOA:HSA, the ellipticity at 208 and 220 nm decreased by ~ 8 % whereas at PFOA concentrations above the 1:1 ratio, the ellipticity slightly increased (~ 1 %). At a twenty-fold excess of PFOA, the ellipticity plateaued.

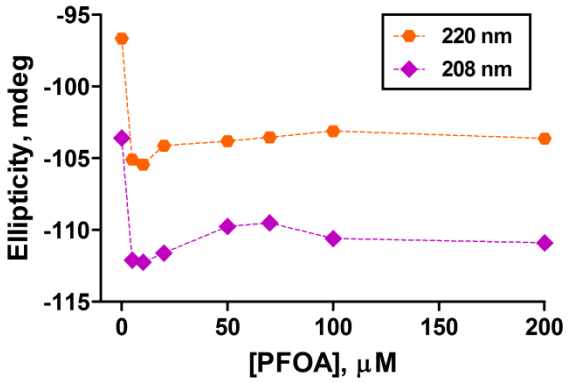

Figure 5.2: Circular dichroism ellipticity measured at 220 and 208 nm for 10 μM HSA titrated with increasing concentrations of PFOA. The error bars are within the symbols.

These results are consistent with previously published data and indicate a presence of multiple binding sites for PFOA in HSA (Wu et al. 2009, Chen and Guo 2009, MacManus-Spencer et al. 2010). The first site, which is significantly populated at the 1:1 molar ratio, has a strong binding constant ($K_{a,1} > 10^5$ M^{-1}), and PFOA association leads to the increase in the α-helical structure of HSA from 47 % in the absence of the

ligand to 52 % upon PFOA binding (refer to Appendix 4). Association of PFOA to additional binding sites slightly destabilizes the protein structure as is evident from the hypsochromic shift of the λ_{max}. Analysis of the fluorescence emission data at PFOA:HSA ratios greater than 1:1 using the double logarithm plot to model fluorescence quenching (Appendix 4) provided an equilibrium binding constant $K_{a,2} = 1.39 \times 10^4$ M^{-1} with one binding site, suggesting the presence of single lower affinity binding site (Wei et al. 2010). An alternative model (the modified Scatchard plot) suggests up to eight low affinity binding sites (see Appendix 4), which agrees more closely with previous studies that observed multiple low affinity sites (Han et al. 2003, Wu et al. 2009, Salvalaglio et al. 2010, Wei et al. 2010). The equilibrium binding constant for the lower affinity site reported herein is consistent with the equilibrium constant reported from ITC measurements ($K_a = 2.47 \times 10^4$ M^{-1}) (Wu et al. 2009), whereas the equilibrium constant for the high affinity site ($K_{a,1}$) is comparable to that determined in previous fluorescence measurements (2.7×10^5 M^{-1}) (Chen and Guo 2009). Finally, at the 20:1 PFOA:HSA ratio, the binding sites are occupied as no further changes in fluorescence intensity, λ_{max}, or ellipticity are observed. Nonetheless, additional PFOA molecules may bind or have weak association with HSA but lead to insignificant changes in the fluorescence or circular dichroism spectra.

For HSA titrations carried out at 1:1 or 2:1 β-CD:PFOA ratios, the fluorescence intensities followed analogous trends as observed in the absence of β-CD, with an increase in emission intensity to the 1:1 PFOA:HSA ratio and subsequent quenching at elevated PFOA concentrations. Reduced fluorescence quenching at elevated PFOA concentrations was observed with an increased ratio of β-CD to PFOA. These results

suggest that β-CD can inhibit the binding of PFOA to HSA. The blue shift in the HSA emission spectra is less pronounced for the 1:1 β-CD:PFOA ratio, and absent for the 2:1 β-CD:PFOA ratio, indicating that β-CD is competing with HSA for PFOA and effectively inhibits associating of PFOA molecules to lower affinity sites on the protein surface. The fluorescence intensity is increased when β-CD is added; however, the values do not return to the intensity values observed for HSA alone, suggesting that β-CD at the 1:1 and 2:1 ratio with PFOA cannot completely reverse the first PFOA binding to HSA.

In order to further investigate this, 500 μM PFOA was added to 10 μM HSA (50:1 PFOA:HSA ratio), and β-CD was titrated into the sample (Figure 5.3). As the β-CD concentration approached the 1:1 β-CD:PFOA ratio (500 μM), the fluorescence intensity and λ_{max} dramatically increased and then experienced much smaller increases around the 2:1 ratio (1000 μM β-CD). At the 5:1 ratio (2500 μM β-CD), the fluorescence intensity and λ_{max} returned to the values observed for HSA in the absence of PFOA. These observations demonstrate that an equimolar concentration of β-CD to PFOA can disrupt the weaker PFOA binding to HSA, and that a 5:1 molar ratio between β-CD and PFOA effectively disrupts PFOA molecules bound to the high affinity site. These data support the hypothesis that an excess of β-CD compared to PFOA can totally reverse PFOA binding to HSA.

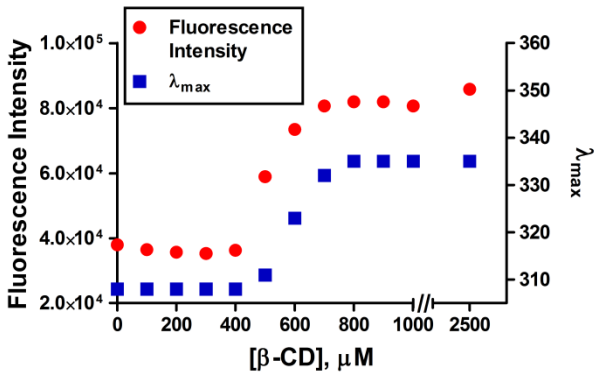

Figure 5.3: Fluorescence emission intensity measured at 335 nm and the maximum emission wavelength (λ_{max}) of 10 μM HSA and 500 μM PFOA titrated with increasing concentrations of β-CD. The error bars are within the symbols.

5.4.3 Lifetimes

The fluorescence lifetimes (τ) for the single Trp residue in HSA (Trp-214) were measured as PFOA was titrated into the sample (Figure 5.4a; for the average lifetime, see Appendix 4). Three lifetimes (τ_1 = 0.48 ns, τ_2 = 3.75 ns, τ_3 = 7.85 ns) were resolved for the single Trp-214 residue, which is consistent with previous studies (Albani 2007, Amiri et al. 2010a, Amiri et al. 2010b). The molecular origin of the three distinct lifetimes observed for the single Trp residue in HSA was investigated previously and associated with the presence of three distinct substructures of Trp in the excited state (Albani 2007, Amiri et al. 2010a). The two shorter lifetimes (τ_1 and τ_2) are similar to those found for Trp residues in aqueous solutions and thus originate from the molecular structure of Trp, whereas the longest lifetime is only observed for Trp in proteins and was attributed to the Trp interactions with hydrophobic residues in the core of the protein (Albani 2007, Amiri et al. 2010a). The addition of PFOA does not alter the shortest fluorescence lifetime, whereas τ_2 and τ_3 increase at low concentrations of PFOA. After the 1:1 PFOA:HSA

ratio, τ_2 and τ_3 decrease. In addition, the pre-exponential factors (α), which represent the fraction of Trp with the corresponding lifetime, are also sensitive to the PFOA association to the protein, with increasing α values after the 1:1 PFOA:HSA ratio (Figure 5.4b). Increase in τ_3, and to a smaller extent τ_2, upon PFOA association to the high affinity site suggest that this site may be located in the vicinity of the Trp residue, and that binding of PFOA increases the hydrophobicity of the Trp-214 environment, which is supported by previous molecular modeling studies (Salvalaglio et al. 2010).

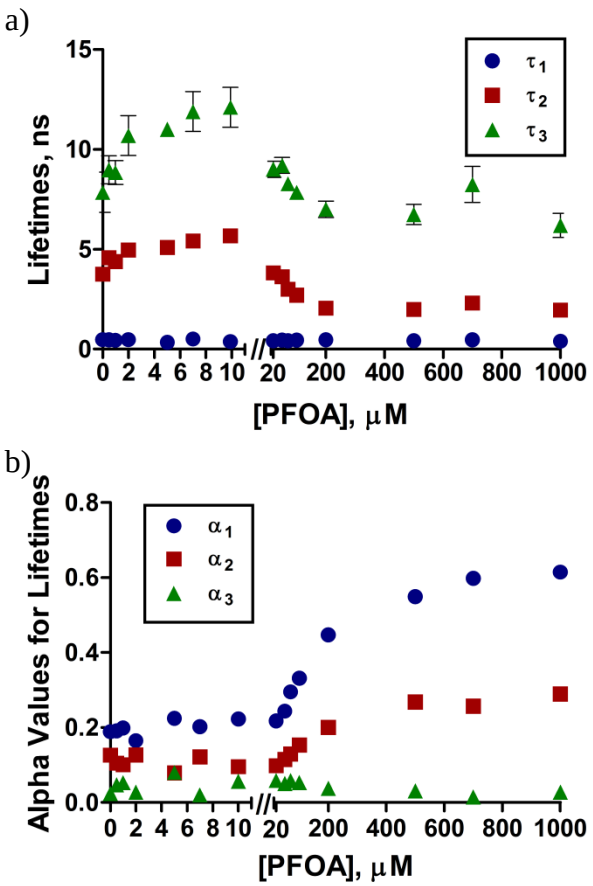

Figure 5.4: a) Fluorescence lifetimes and b) α values for the fluorescence lifetimes of 10 μM HSA titrated with increasing concentrations of PFOA. The error bars, when not apparent, are within the symbols.

The decrease of τ_2 and τ_3 suggests an efficient quenching of Trp emission upon PFOA association to the lower affinity sites. This decrease in the Trp emission and lifetime can be analyzed either in terms of dynamic quenching, dynamic and static quenching, and/or can be associated with the PFOA-triggered changes in protein structure that lead to the alteration of the Trp environment. The absence of spectral overlay between the absorption spectrum of PFOA and the emission spectrum of HSA exclude fluorescence resonance energy transfer (FRET) from being the major mechanism for Trp emission quenching. To determine whether the quenching is dynamic or dynamic and static, Stern-Volmer plots were analyzed for linearity. Stern-Volmer plots using emission intensities and average lifetime data (Figure 5.5) are both linear and provide matching Stern-Volmer constants of 9370 ± 750 M^{-1} and 9400 ± 440 M^{-1}, respectively, suggesting a purely dynamic quenching of Trp emission due to the PFOA association to the low affinity site. The value of the bimolecular quenching rate constant calculated using Equation 5.3, $k_q = 1.54 \times 10^{12}$ $M^{-1}s^{-1}$, is two orders of magnitude larger than a value expected for the diffusion limited process (10^{10} $M^{-1}s^{-1}$), which is consistent with PFOA binding to HSA triggering structural changes in the protein that affect the environment of Trp-214 (Lakowicz 2006).

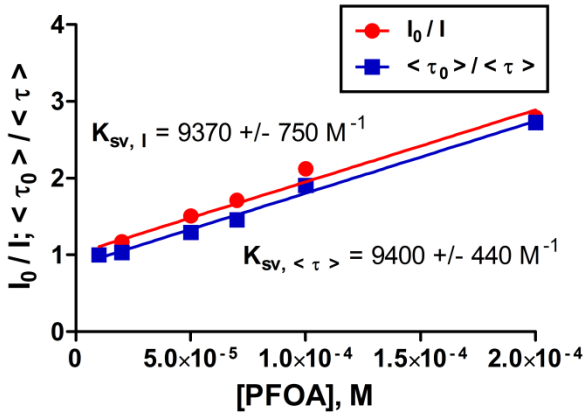

Figure 5.5: Stern-Volmer plots of fluorescence emission intensities and average lifetimes of 10 μM HSA titrated with PFOA.

When β-CD is titrated into a sample of PFOA and HSA (at a 50:1 PFOA:HSA ratio), τ_1 does not change, and τ_2 and τ_3 increase (Figure 5.6a; for the average lifetime, see Appendix 4). The pre-exponential factors (α_1 and α_2 values) for the first and second lifetimes decrease, and the α_3 value slightly increases (Figure 5.6b), suggesting that β-CD inhibits binding of PFOA to the low affinity sites. At the 5:1 β-CD:PFOA ratio, the observed τ and α values decrease and are identical to those determined for HSA in the absence of PFOA. These results again support that β-CD at low concentrations can disrupt the second binding of PFOA to HSA, and that excess β-CD can totally reverse all PFOA binding to HSA.

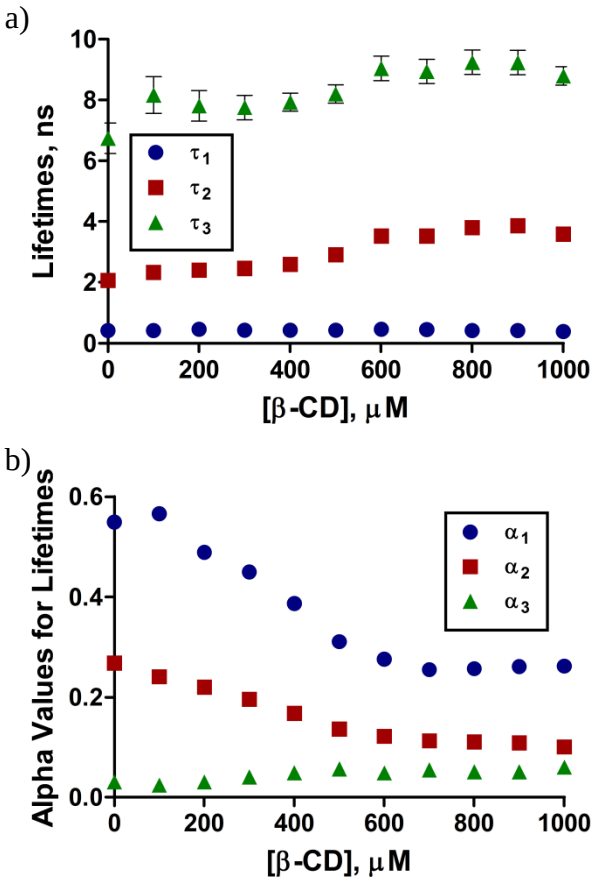

Figure 5.6: a) Fluorescence lifetimes and b) α values for the fluorescence lifetimes of 10 μM HSA and 500 μM PFOA titrated with increasing concentrations of β-CD. The error bars, when not apparent, are within the symbols.

We also determined the impact of β-CD on the protein conformation. Addition of β-CD to HSA in the absence of PFOA resulted in a negligible decrease in HSA emission intensity (less than 2 %) and a slight decrease in fluorescence average lifetime (from 6.14 ns to 6.08 ns) at the highest β-CD concentration (2500 μM). A previous study found that the binding between HSA and β-CD is weak, with an equilibrium constant of 185 M^{-1}, which is much weaker than PFOA affinity for HSA or β-CD (Ghosh et al. 2014). These results indicate that under experimental conditions used in this study, β-CD does not bind

to HSA, and thus the impact of β-CD on the spectroscopic properties of HSA in the presence of PFOA can be associated with the formation of β-CD:PFOA complexes, and thus PFOA dissociation from HSA.

5.4.4 Competition Study with 1,8-ANS

A competition study was performed using steady state fluorescence to further confirm the results. 8-anilinonaphthalene-1-sulfonic acid (1,8-ANS) is a model compound known to bind to hydrophobic pockets in HSA that bind fatty acids, hormones, and drugs (Gasymov and Glasgow 2007, Takehara et al. 2009, Kuznetsova et al. 2012). A previous study found that 1,8-ANS binds to three sites on HSA, including the site in proximity to Trp-214, with very strong binding constants (on the order of 10^5-10^6 M^{-1}), while another study suggests that 1,8-ANS can bind to 14 sites on HSA with slightly weaker binding constants (on the order of 10^3-10^5 M^{-1}) (Takehara et al. 2009, Kuznetsova et al. 2012). Due to similar binding constants, it is expected that PFOA will successfully compete with 1,8-ANS for HSA binding. Furthermore, it is important to note that 1,8-ANS has extremely weak complexation to β-CD, with an association constant of 65 M^{-1}, and thus 1,8-ANS is expected to be bound to HSA or quenched in aqueous solution during the course of the competition study, and that only PFOA will interact meaningfully with β-CD (Schneider et al. 1991).

The fluorescence emission of 1,8-ANS was measured in the presence of HSA, PFOA, and β-CD. First, 10 μM HSA was titrated with 1,8-ANS. The fluorescence intensity at 470 nm increased as the concentration of 1,8-ANS increased until saturation of HSA occurred (at about 60 μM 1,8-ANS). Next, PFOA was titrated into the sample

and the fluorescence intensity decreased, indicating that PFOA replaces 1,8-ANS bound to the protein. The 1,8-ANS fluorescence intensity was not fully quenched even at the highest PFOA concentration (1 mM), however, suggesting that 1,8-ANS binds to sites on HSA that PFOA does not. Significant overlap of binding sites on HSA for 1,8-ANS and PFOA are expected, due to both 1,8-ANS and PFOA being hydrophobic molecules with negatively charged groups (sulfonate in the case of 1,8-ANS and carboxylate in the case of PFOA). Their structures, however, are widely different. 1,8-ANS is aromatic and planar whereas PFOA is aliphatic and linear, and thus they are not expected to completely share all binding sites. When β-CD was titrated into the sample, the 1,8-ANS fluorescence emission intensity at 470 nm increased, and at the 5:1 β-CD:PFOA ratio, the intensity returned to the value observed for 1,8-ANS and HSA in the absence of PFOA (Figure 5.7). These results indicate that β-CD can reverse the binding of PFOA to HSA, further confirming that β-CD strongly encapsulates PFOA, even in the presence of HSA.

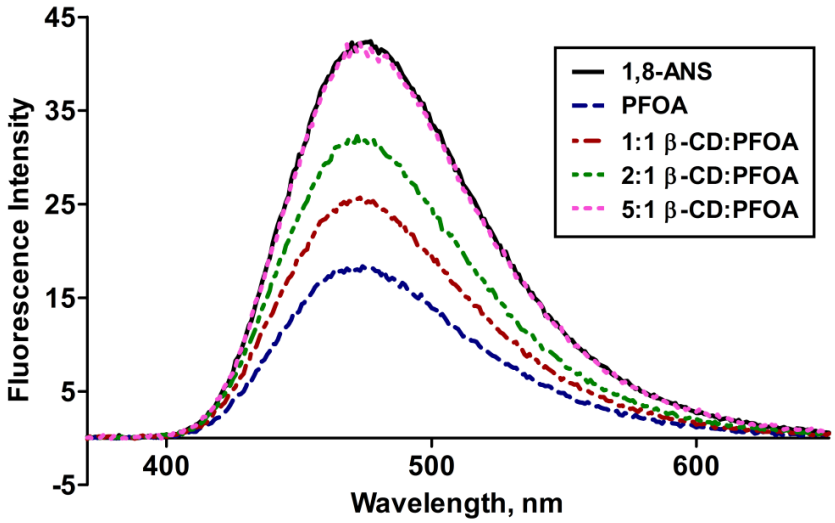

Figure 5.7: Fluorescence emission spectra of 100 μM 1,8-ANS with 10 μM HSA. When PFOA (500 μM pictured) is added, the fluorescence intensity decreases. As β-CD is added to this solution, the fluorescence intensity returns to the original intensity.

5.5 Conclusions

Prior to testing the ability of β-CD to reverse PFOA binding to HSA, the interactions between PFOA and HSA (in the absence of β-CD) were characterized and compared to previous studies. PFOA binds to multiple sites in HSA, with a strong affinity for the first binding site and weaker affinities for the remaining binding sites, as evidenced by the steady state and frequency-resolved fluorescence spectra and the circular dichroism spectra. The strongest binding site is likely located near the Trp-214 residue, as evidenced by the increase in emission intensity and fluorescence lifetimes τ_2 and τ_3, indicating an increase in the hydrophobic environment of the Trp residue. Binding of PFOA to the lower affinity sites, however, causes destabilization of the protein and dynamic quenching of the Trp emission, as indicated by the Stern-Volmer plots. Upon addition of β-CD, PFOA dissociates from the lower affinity sites on HSA and complexes with β-CD via encapsulation of the PFOA tail, while still interacting with hydrophilic moieties on the surface of HSA, as evidenced from the NMR studies. Excess β-CD results in complete dissociation of PFOA from HSA, supported by the return of the fluorescence emission spectra and fluorescence lifetimes of HSA to that of the protein alone. The NMR studies suggest that the 2:1 β-CD:PFOA complex can be formed in these conditions, with the strong β-CD encapsulation of PFOA preventing binding to HSA.

Our results indicate that β-CD can reverse binding of PFOA to HSA, and thus, may attenuate the toxicity of PFOA. The half-life and toxicological properties of PFOA in humans may arise from binding to HSA: PFOA cannot be eliminated from the body while it is bound to HSA, and HSA is known to transport hormones, fatty acids, and other

biological molecules to the liver, kidneys, and thyroid, the organs where PFOA accumulates and exerts its toxic effects. Although our studies were not conducted at physiologically relevant concentrations, the results clearly demonstrate the principle of using β-CD to inhibit and reverse PFOA binding to HSA. These results have possible applications for a therapeutic strategy to address PFOA exposure and contamination, and could possibly be extended to other problematic perfluorinated compounds. Further research is needed at physiologically relevant concentrations and in biological organisms exposed to PFOA to fully investigate the therapeutic potential of β-CD.

CHAPTER 6

β-Cyclodextrin Attenuates Perfluorooctanoic Acid Toxicity in the Zebrafish Embryo Model

6.1 Abstract

Perfluorooctanoic acid (PFOA) has been linked to negative health outcomes including cancer, thyroid disease, infertility, and developmental delays. β-Cyclodextrin (β-CD), a cyclic sugar, has been previously shown to form strong host–guest complexes with PFOA, and is proposed as a means of environmental remediation with respect to this widespread contaminant. In the present study, β-CD was directly examined with regards to possible attenuation of the toxicity of PFOA, specifically employing the zebrafish (*Danio rerio*) embryo model. Zebrafish embryos were exposed to various concentrations of PFOA without β-CD, and with equimolar (1:1) and excess (2:1) molar ratios of β-CD to PFOA, and assessed for lethality and developmental toxicity through seven days post-fertilization (dpf). Rapid onset of lethality with limited morphological abnormalities was observed at relatively low concentrations of PFOA ($LC_{50} \approx 50$ ppm), along with effects on morphometric and neurobehavioral parameters in surviving embryos. A highly significant difference ($p < 0.0001$) was observed between the 2:1 treatment, and both 1:1 and PFOA only treatments, with respect to lethal concentration and apparent neurobehavioral effects, suggesting an effectively reduced toxicity of the fully complexed PFOA. In contrast, however, neither β-CD treatment reduced developmental toxicity with respect to the morphometric endpoint. Whereas LC_{50} of PFOA alone did not change over 7 dpf, the 1:1 and 2:1 values decreased slightly over time, suggesting either delayed or alternative toxic effects on later developmental stages at presumptively lowered levels. This study indicates β-CD may be an effective agent to reduce toxicity of and mitigate environmental health concerns associated with PFOA, but that further study is required to elucidate the mechanism of complexation as it relates to the attenuation of toxicity.

6.2 Introduction

To test the hypothesis that β-CD:PFOA complex will effectively reduce the toxicity of PFOA in the zebrafish embryo, relevant metrics of toxicity (e.g., lethal concentrations, developmental impairment, and neurobehavioral effects) were assessed for PFOA alone, and in the presence of equimolar (1:1) and excess (2:1) β-CD. The goal of the study was to evaluate potential reduction of toxicity in relation to complex formation. Although various human health effects have been linked to much lower environmental concentrations, relatively high concentrations of PFOA (i.e., parts-per-million (ppm) levels) were used in the current study rather than environmentally relevant concentrations such that acute toxicological endpoints, as a proxy of PFOA toxicity, could be assessed. This study provides direct insight into the potential utility of cyclodextrins for attenuating the toxic effects of PFOA.

6.3 Experimental Methods

Perfluorooctanoic acid (PFOA) was purchased from Sigma-Aldrich. β-Cyclodextrin (β-CD) was purchased from Acros Organics. Both chemicals were used without further purification. Stock solutions of PFOA (7.25 mM, i.e., 3000 ppm), 1:1 β-CD:PFOA (β-CD: 7.25 mM, PFOA: 7.25 mM), and 2:1 β-CD:PFOA (β-CD: 14.50 mM, PFOA: 7.25 mM) were prepared with deionized water in polypropylene tubes. The solutions were sonicated until dissolution of the solids was achieved. A control solution of deionized water was also stored in a polypropylene tube. Stock solutions were subsequently diluted over a relevant range of concentrations (see below) for assessment of zebrafish embryo toxicity.

6.3.1 Zebrafish Rearing and Breeding

To obtain embryos, zebrafish (PS strain) were reared and bred as previously described (Berry et al. 2007, Jaja-Chimedza et al. 2017). Briefly, adult zebrafish were maintained in 30-L tanks at 28 °C with 14 h: 10 h light/dark cycle, and bred (from approximately 10–30 individuals) above 10-L tanks in mesh enclosures. Eggs were collected (from the bottom of tanks) within 1 h of the end of the dark cycle, and, following collection and washing, transferred to plates containing E3 medium (Brand et al. 2002). Eggs containing dead or obviously poor quality embryos were removed. The remaining embryos were used, within ~ 2 h post-fertilization (hpf), for toxicity assays. All rearing and breeding was conducted under protocols approved by the University of Miami's Institutional Animal Care and Use Committee (IACUC), and performed by trained investigators.

6.3.2 Zebrafish Embryo Toxicity Assay

Zebrafish embryo toxicity assays were adapted from previously described methods (Berry et al. 2007, Jaja-Chimedza et al. 2017). Assays were conducted in polypropylene 24-well plates (Evergreen Scientific, Los Angeles, CA) with five embryos (4- to 32-cell stage) per replicate, i.e., well (n = 4), in E3 medium for a total of 20 zebrafish embryos per treatment/concentration (Brand et al. 2002). Embryos were exposed via static exposure (i.e., without replenishment) to a range of PFOA concentrations (30, 50, 100, 150, 200, 250 and 300 ppm) alone, and in 1:1 and 2:1 ratios with β-CD, and subsequently observed at 1, 2, 3, 4 and 7 days post-fertilization (dpf) with a dissecting light microscope to assess mortality and relevant developmental toxicity.

Exposures and assessments were repeated several times, in preliminary studies, to determine relevant concentration levels for PFOA, and generally confirm results. Lethality was calculated as the concentration corresponding to 50 % mortality (LC_{50}); the LC_{50} values, and their 95 % confidence intervals, were calculated via Probit Analysis in SPSS (version 22.0, IBM Corporation, Armonk, NY). In addition to lethality, inhibition of embryo development was morphometrically assessed based on the interocular distance between eyes (as a proxy for body size) of 7 dpf embryos (eleuthero-embryo stage) as measured using Olympus DP2-BSW imaging software (2009, Center Valley, PA). Apparent neurobehavioral effects were additionally measured as the percent of 7-dpf eleuthero-embryos displaying listing (i.e., falling to one side) behavior within a 30 s period (with shaking between each measurement to allow embryos to right themselves). All toxicity assays involving zebrafish were conducted under protocols approved by the Florida International University's Institutional Animal Care and Use Committee (IACUC), and performed by trained investigators.

6.3.3 Statistical Analyses

One-way analysis of variance (ANOVA) of the LC_{50} values, as well as the interocular distance and percent listing at 7 dpf, was performed in GraphPad Prism (version 5.03, La Jolla, CA). The significance level was set at $p = 0.05$.

6.4 Results and Discussion

6.4.1 PFOA Toxicity in the Zebrafish Embryo Model

A rapid onset of embryotoxicity was observed for PFOA with mortality, characterized by coagulation of embryos, occurring within a few hours of exposure. By 24 hpf, a significant dose-dependent response with respect to lethality was observed (Figure 6.1) with all embryos dead at PFOA concentrations above 100 ppm. The observed dose response, with respect to mortality, remained largely unchanged, and the calculated LC_{50} values did not significantly change over the course of the exposure (i.e., 7 dpf; Figure 6.2). Notably, aside from a higher number of mortalities, no clear pattern of developmental deformities was observed: by 7 dpf, for example, only ~ 5 % of both control and PFOA-treated embryos showed any discernible deformities, which included bent spines and edemas. Similarly, the hatching rates were unaffected with the majority of surviving embryos, in both control and PFOA treatments, hatched by 3 dpf.

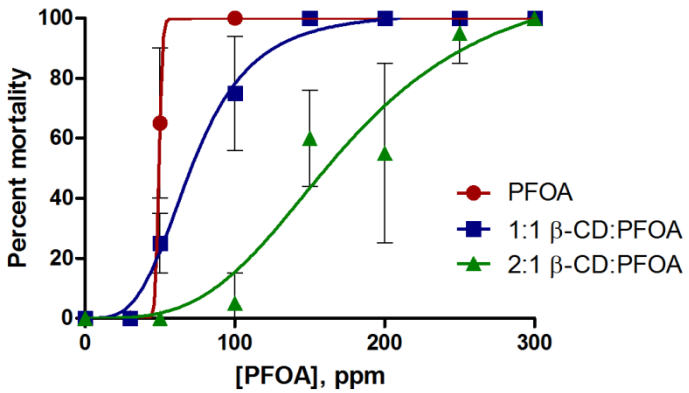

Figure 6.1: Concentration dependent toxicity of PFOA, and 1:1 and 2:1 β-CD:PFOA treatments, in terms of rapid onset lethality. Shown is percent mortality at 24 hpf (error bars represent ± one standard deviation, n = 4) fit by the dose-response curve.

Apparent inhibition of embryo growth (i.e., reduced body size), however, was observed, with the surviving PFOA-treated embryos being smaller at the end of the exposure (i.e., 7 dpf) compared to controls. Inhibition of development was specifically evaluated morphometrically based on interocular distance at 7 dpf: significantly ($p < 0.0001$) reduced interocular distances were measured for surviving PFOA-treated embryos at sub-lethal concentrations (i.e., ≤50 ppm, pooled; 0.25 ± 0.06 mm) versus untreated control (0.41 ± 0.14 mm) embryos (Figure 6.3). In terms of other relevant endpoints, apparent neurobehavioral effects were observed for surviving embryos, and specifically a high frequency of listing was observed for PFOA-treated embryos. At low PFOA concentrations below the LC_{50} (i.e., ≤50 ppm, pooled), the percent of surviving embryos observed to list within a 30 s period (96 ± 9%) was significantly higher ($p < 0.0001$) than controls without PFOA (20 ± 13%; Figure 6.4).

6.4.2 Attenuation of PFOA Toxicity by β-CD

To evaluate the ability of β-CD to reduce the toxicity of PFOA, the LC_{50} values for each treatment (PFOA alone, 1:1 and 2:1 β-CD:PFOA ratios) were calculated and compared. At 1 dpf, a significantly ($p < 0.0001$) higher LC_{50} was observed for 2:1 β-CD:PFOA (159.3 ± 22.9 ppm) compared to both PFOA alone (47.3 ± 3.6 ppm), and the 1:1 β-CD:PFOA treatment (69.9 ± 5.7 ppm). The lethal concentration for 1:1 β-CD:PFOA was higher than PFOA alone, but the difference was not statistically significant. However, whereas LC_{50} did not change over time for PFOA alone, calculated values for both 1:1 and 2:1 β-CD:PFOA treatments notably decreased over 7 days of exposure (Figure 6.2) due to additional, post-hatch mortalities. By 4 dpf, the 1:1 β-

CD:PFOA LC_{50} (48.1 ± 14.2 ppm) was essentially equal to that of PFOA alone. Although the LC_{50} for the 2:1 β-CD:PFOA treatment decreased (e.g., 80.5 ± 9.3 pm by 7 dpf), it was still significantly ($p < 0.0001$) higher than either PFOA alone, or PFOA in a 1:1 ratio with β-CD. No discernible toxicity was observed for β-CD alone, within the range of tested concentrations, including the maximum concentration (i.e., 1645 ppm, or 1.45 mM, β-CD) evaluated in the 2:1 ratio treatments.

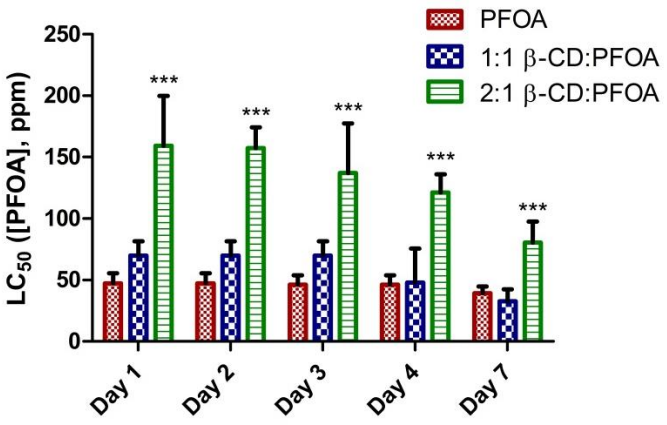

Figure 6.2: Calculated lethal concentrations for 50% of the population (LC_{50} values) for PFOA only, 1:1 β-CD:PFOA, and 2:1 β-CD:PFOA over 7 dpf. The 2:1 β-CD:PFOA LC_{50} values are significantly different (*** = $p < 0.0001$) than PFOA only, and 1:1 β-CD:PFOA. The LC_{50} values for PFOA only and 1:1 β-CD:PFOA are not significantly different from each other. Error bars represent 95% confidence intervals.

In contrast to lethality, β-CD did not reduce apparent developmental toxicity in terms of the morphometric variable (interocular distance) (Figure 6.3). Comparing surviving embryos at, or below, the LC_{50} (i.e., ≤50 ppm), the measure of interocular distance for 7-dpf embryos was significantly ($p < 0.0001$) lower in both 1:1 β-CD:PFOA (0.25 ± 0.07 mm) and 2:1 β-CD:PFOA (0.29 ± 0.07 mm) treatments when compared to controls, and nearly identical to PFOA alone. Similar to lethality, on the other hand, the

apparent neurobehavioral effect (i.e., listing) among 7-dpf embryos was reduced among surviving embryos at sub-lethal concentrations (i.e., ≤50 ppm) in the 2:1 β-CD:PFOA treatment: percent listing in this treatment was not significantly different from untreated controls (Figure 6.4). Frequency of listing in the 1:1 treatment was decreased, compared to that of PFOA alone, but it was still significantly higher ($p < 0.01$) than untreated controls.

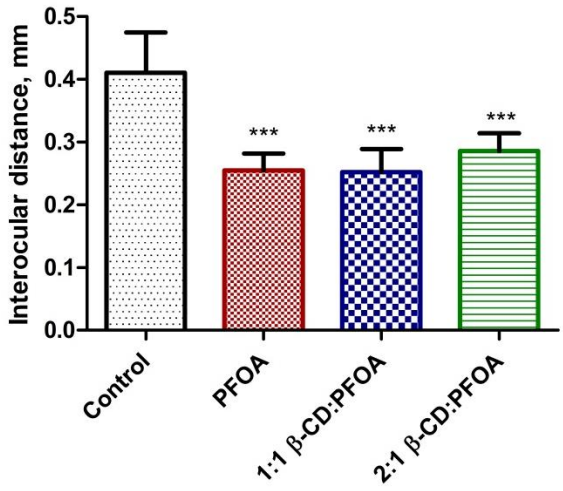

Figure 6.3: Interocular distance, as a morphometric measure of embryo body size, for untreated embryos ("Control") compared to surviving embryos in sub-lethal concentrations (≤50 ppm) of PFOA only, and 1:1 and 2:1 β-CD:PFOA treatments, at 7 dpf. All three treatments are significantly different (*** = $p < 0.0001$) than controls. The three treatments are not significantly different from each other. Error bars represent 95% confidence intervals.

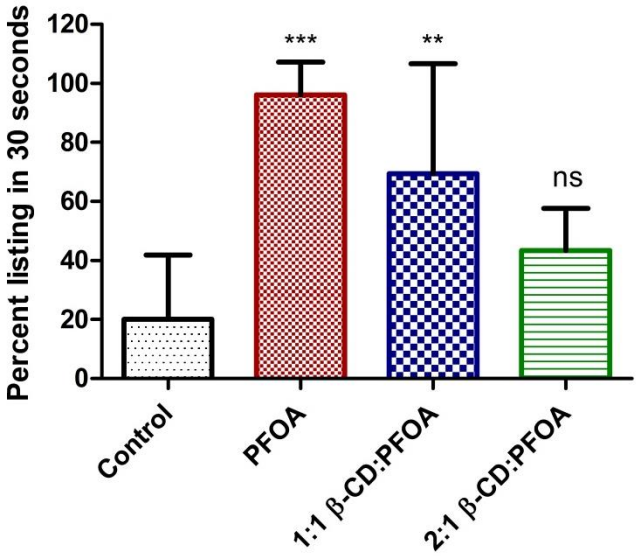

Figure 6.4. Percent listing after 30 s for the untreated embryos ("Control") compared to surviving embryos in sub-lethal concentrations (≤50 ppm) of PFOA only, and 1:1 and 2:1 β-CD:PFOA treatments, at 7 dpf. The control values are significantly different from PFOA only (*** = $p < 0.0001$) and 1:1 β-CD:PFOA (** = $p < 0.01$). The 2:1 β-CD:PFOA values were not significantly different from controls ("ns"). Error bars represent 95% confidence intervals.

6.4.3 Discussion

Toxicity of PFOA in the zebrafish embryo model, including embryotoxicity, reduced body size, and neurobehavioral effects observed in the present study, is generally consistent with prior studies (Hagenaars et al. 2011, Zheng et al. 2011, Hagenaars et al. 2013). Aligned with these previous studies (Zheng et al. 2011), a rapid onset of lethality (≤24 hpf) and relatively limited occurrence of developmental deformities, including bent spines and edemas, were similarly observed in the current study. Lethal concentrations for PFOA in the current study, however, were considerably lower than measured in prior studies, which have typically reported LC_{50} values above 500 ppm and/or test ranges (Hagenaars et al. 2011, Rainieri et al. 2017), although others (Zheng et al. 2011, Ding et al. 2013) have reported somewhat lower values (e.g., 262 and 371 ppm, respectively). It

has been suggested (Jantzen et al. 2016a) that the LC_{50} of PFOA may be, in fact, ten times lower than originally reported, which would put it within the range presently observed. Variability in lethal concentrations is presumably due to genetic differences of zebrafish lines used and/or other experimental conditions, and were not addressed further in the present study. Both reduced body size and locomotory effects have been, likewise, reported for PFOA-treated zebrafish embryos at sub-lethal concentrations (Hagenaars et al. 2011, Jantzen et al. 2016a, Jantzen et al. 2016b, Jantzen et al. 2017). Notably, these sub-lethal effects were observed in previous studies (Jantzen et al. 2016b, Jantzen et al. 2017) at considerably lower (i.e., micro- to nanomolar) exposure concentrations, and effects extended into (following embryonic exposure) adult stages.

Consistent with formation of host–guest complexes, β-CD generally reduced toxicity of PFOA. Although a 1:1 ratio decreased both rapid lethality at early embryonic stages (i.e., ≤3 dpf), and neurobehavioral effects, only the measured decreases (approximately two-fold) associated with the 2:1 ratio were statistically significant through 7 dpf. That being said, neither β-CD treatment significantly attenuated a morphometric variable (interocular distance) indicative of reduced embryo growth and body size associated with PFOA toxicity. Furthermore, while the LC_{50} of PFOA alone did not change during the exposure, values decreased over 7 dpf for both 1:1 and 2:1 ratios. These latter observations suggest a toxicity toward post-hatch larvae at either presumably lowered concentrations of non-complexed PFOA or alternatively less toxic and/or bioavailable complexes, which are uncoupled from the potent embryotoxicity associated with rapid onset lethality at early embryonic stages.

The mechanism whereby β-CD reduces toxicity via complex formation remains to be clarified in future studies. However, the current state of knowledge with respect to the formation of the β-CD:PFOA host–guest complex points to a few possibilities. It appears that the ratio of β-CD, rather than the concentration of β-CD, determines the inhibition of PFOA toxicity. Differences in bioavailability, and thus uptake, of the two complexes, may explain the differential toxicity observed between 1:1 and 2:1 β-CD treatments. Indeed, it has been shown that relative lipophilicity significantly effects and is correlated with uptake in the zebrafish embryo model (De Koning et al. 2015). It would be expected that increased complexation of PFOA would decrease log P values and, thus, uptake.

This model, however, largely assumes stoichiometric, stepwise and stable host–guest complexes. Alternatively, it is possible that non-stoichiometric and/or non-sequential complex formation could lead to non-stoichiometrically reduced levels of free PFOA which would, in turn, be quantitatively dependent on the relative β-CD concentration. Such an alternative model could explain quantitative differences in toxicity between 1:1 and 2:1 ratios whereby formation of 2:1 complexes under equimolar (1:1) conditions would lead to persistence of uncomplexed (and thus toxic) PFOA. Presence of free PFOA in solution, and corresponding sub-lethal toxicity might, in this regard, be further exacerbated by bioaccumulation of PFOA, and subsequent release at later stages. Previous studies have shown high levels of bioconcentration of PFOA in zebrafish embryos including intestine and bile (and potential enterohepatic recirculation), as well as yolk, as a means of bioaccumulation and release at later embryonic stages (Ulhaq et al. 2015). Competition between bioaccumulation and complex formation might explain toxicity at higher concentrations even in 2:1 treatments including both post-hatch

toxicity, and inability of either β-CD treatment to effectively reduce developmental toxicity, in terms of morphometric parameters. Quantitative analysis of PFOA and β-CD complexes with respect to both exposure medium and bioaccumulation/uptake (e.g., critical body residue), including tissue specific bioavailability, in future studies could address these interrelated mechanisms.

6.5 Conclusions

The results of this study directly suggest that β-CD, particularly in excess molar ratios, can largely attenuate the toxicity of PFOA in solution as evidenced by reduced toxicity in the zebrafish embryo model. The ratio of β-CD to PFOA, rather than the concentration of β-CD, drives this attenuation. It is proposed that the host–guest complex may exhibit less biological activity, or alter bioavailability, compared to PFOA alone. Alternatively, β-CD may simply reduce by way of the variable formation of 1:1 and 2:1 complexes levels of free PFOA in solution in a concentration-dependent manner. Further research is needed to understand the mechanism of decreased toxicity, as well as to determine efficacy of β-CD at environmentally relevant concentrations of PFOA, and with respect to non-acute toxicological endpoints (specifically relevant to human health). However, these findings suggest that β-CD is a potentially promising tool for environmental remediation and mitigation of toxic effects of PFOA and, perhaps, related perfluorinated compounds as they relate to environmental health concerns.

CHAPTER 7

General Conclusions

The fundamental host-guest interactions between PFASs and CDs are of paramount importance when developing CD-based environmental remediation and therapeutic strategies for PFAS contamination. The driving force behind the host-guest complexation is the favorable hydrophobic interactions between the PFAS fluorinated chain and the CD cavity. These van der Waals interactions are strongest for the complex between β-CD and legacy PFASs, due to the molecular sizes of these compounds, as well as the fully fluorinated chain of the legacy PFASs. Emerging ether PFASs also interact most favorably with β-CD, though these interactions are weaker than the legacy PFASs due to the insertion of hydrophilic ether oxygens along the perfluorinated backbone, disrupting the van der Waals forces. Second to the hydrophobic interactions arising from the fluorinated chain within the CD cavity are the hydrophilic interactions between the PFAS head group (carboxylate, sulfonate, sulfonamide) and the groups along the perimeter of the CD cavity. In native β-CD, hydrogen-bonding can occur between the PFAS head group and the primary hydroxyl groups. The host-guest complex is always formed in this configuration (PFAS head group oriented towards the smaller side of β-CD with the primary hydroxyl groups) even in cases of branching in the PFAS structure. Branching that favors this hydrogen bonding, such as branching near the PFAS tail, increases the strength of the complex; branching that inhibits or weakens this hydrogen bonding, such as branching near the PFAS head group, decreases the strength of the complex. Positively charged derivatives of β-CD can increase the strength of the complex, while negatively charged derivatives will weaken it. The effect of the positive charge depends upon the preexisting van der Waals forces and branching in the PFAS structure. PFASs that already have favorable hydrophobic interactions with the CD cavity

will only experience a slight to moderate increase in association with positively charged β-CD derivatives due to ionic bonding being stronger than hydrogen-bonding, whereas PFASs with weak preexisting van der Waals forces with the CD cavity will experience a large increase in association. Branching can either have a moderate to large increase in association or, alternatively, no change in association with positively charged β-CD derivatives, depending upon position of the branching and number of positively charged groups on the CD. Finally, 2:1 β-CD:PFAS interactions are most dependent upon PFAS chain length, with these complexes only being observed for PFASs with greater than six carbons or oxygens in a linear chain.

Studies with one of the most problematic legacy PFASs, PFOA, and β-CD suggest that β-CD has the potential to be used in real world therapeutic or remediation strategies. Addition of β-CD to the PFOA-HSA complex reversed the binding of PFOA to HSA, especially when using excess β-CD. Furthermore, a 2:1 β-CD:PFOA ratio corresponded to a highly significant increase in LC_{50} of zebrafish embryos compared to PFOA only or 1:1 β-CD:PFOA ratio conditions, suggesting that excess β-CD can inhibit the toxic effects of PFOA. These results agree with the NMR studies in which the β-CD:PFOA complex was not significantly disturbed in different environmental conditions and while in the presence of competing CD guests.

The conclusions gained from the fundamental studies, paired with the demonstration of principle with HSA and the zebrafish embryos, give insight into the mechanisms, dynamics, strength and structure of the host-guest complexation between CDs and PFASs. The unique structural characteristics of PFASs make them ideal guests for β-CD encapsulation. PFASs were found to have some of the strongest association

constants with β-CD and its derivatives reported in the literature. Thus, it is expected that β-CD and its derivatives will be highly selective towards encapsulation of PFASs in environmental and biological samples. Future research should be directed towards capitalizing upon these favorable host-guest interactions to develop remediation and therapeutic technologies for PFAS removal and sequestration.

REFERENCES

Albani, J. R. New insights in the interpretation of tryptophan fluorescence. *J. Fluoresc.* **2007**, *17*, 406-417.

Amiri, M.; Jankeje, K.; Albani, J.R. Origin of fluorescence lifetimes in human serum albumin. Studies on native and denatured protein. *J. Fluoresc.* **2010a**, *20*, 651-656.

Amiri, M.; Jankeje, K.; Albani, J.R. Characterization of human serum albumin forms with pH. Fluorescence lifetime studies. *J. Pharm. Biomed. Anal.* **2010b**, *51*, 1097-1102.

Arun, R.; Ashok Kumar, C.K.; Sravanthi, V.V.N.S.S. Cyclodextrins as drug carrier molecule: a review. *Sci. Pharm.* **2008**, *76*, 567-598.

Arvaniti, O.S.; Stasinakis, A.S. Review on the occurrence, fate, and removal of perfluorinated compounds during wastewater treatment. *Sci. Total Environ.* **2015**, *524-525*, 81-92.

Barry, V.; Winquist, A.; Steenland, K. Perfluorooctanoic Acid (PFOA) Exposures and incident cancers among adults living near a chemical plant. *Environ. Health Perspect.* **2013**, *121*, 1313-1318.

Barzen-Hanson, K.A.; Roberts, S.C.; Choyke, S.; Oetjen, K.; McAlees, A.; Riddell, N.; McCrindle, R.; Ferguson, P.L.; Higgins, C.P.; Field, J.A. Discovery of 40 classes of per- and polyfluoroalkyl substances in historical aqueous film-forming foams (AFFFs) and AFFF-impacted groundwater. *Environ. Sci. Technol.* **2017**, *51*, 2047-2057.

Battiste, J.; Newmark, R.A. Applications of ^{19}F multidimensional NMR. *Prog. Nucl. Magn. Reson. Spectrosc.* **2006**, *48*, 1-23.

Bergeron, R.J.; Channing, M.A.; Gibeily, G.J.; Pillor, D.M. Disposition requirements for binding in aqueous solution of polar substrates in the cyclohexaamylose cavity. *J. Am. Chem. Soc.* **1977**, *99*, 5146-5151.

Bergeron, R.J.; Channing, M.A.; McGovern, K.A. Dependence of cycloamylose-substrate binding on charge. *J. Am. Chem. Soc.* **1978**, *100*, 2878-2883.

Berry, J.P.; Gantar, M.; Gibbs, P.D.; Schmale, M.C. The zebrafish (*Danio rerio*) embryo as a model system for identification and characterization of developmental toxins from marine and freshwater microalgae. *Comp. Biochem. Physiol. C Toxicol. Pharmacol.* **2007**, *145*, 61–72.

Betts, K.S. Perfluoroalkyl acids: what is the evidence telling us? *Environ. Health Perspect.* **2007**, *115*, A250-A256.

Bischel, H.N.; MacManus-Spencer, L.A.; Luthy, R.G. Noncovalent interactions of long-chain perfluoroalkyl acids with serum albumin. *Environ. Sci. Technol.* **2010**, *44*, 5263-5269.

Bolattin, M.B.; Nandibewoor, S.T.; Joshi, S.D.; Dixit, S.R.; Chimatadar, S.A. Interaction of hydralazine with human serum albumin and effect of β-cyclodextrin on binding: insights from spectroscopic and molecular docking techniques. *Ind. Eng. Chem. Res.* **2016**, *55*, 5454-5464.

Brand, M.; Granato, M.; Nüsslein-Volhard, C. Keeping and raising zebrafish. In *Zebrafish*; Nüsslein-Volhard, C., Dahm, R., Eds.; Oxford University Press: Oxford, UK, 2002; pp. 7–37.

Buck, R.C.; Franklin, J.; Berger, U.; Conder, J.M.; Cousins, I.T.; de Voogt, P.; Jensen, A.A.; Kannan, K.; Mabury, S.A.; van Leeuwen, S.P.J. Perfluoroalkyl and polyfluoroalkyl substances in the environment: terminology, classification, and origins. *Integr. Enviro. Assess. Manage.* **2011**, *7*, 513-541.

Calafat, A.M.; Wong, L.-Y.; Kuklenyik, Z.; Reidy, J.A.; Needham, L.L. Polyfluoroalkyl chemicals in the U.S. population: data from the National Health and Nutrition Examination Survey (NHANES) 2003-2004 and comparisons with NHANES 1999-2000. *Environ. Health Perspect.* **2007**, *115*, 1597-1602.

Chen, Y.-M.; Guo, L.-H. Fluorescence study on site-specific binding of perfluoroalkyl acids to human serum albumin. *Arch. Toxicol.* **2009**, *83*, 255-261.

Choppinet, P.; Jullien, L.; Valeur, B. Multichromophoric cyclodextrins as fluorescent sensors. Interaction of heptachromophoric β-cyclodextrins with surfactants. *J. Chem. Soc., Perkin Trans. 2* **1999**, 249-255.

Cousins, I.T.; Kong, D.; Vestergren, R. Reconciling measurement and modelling studies of the sources and fate of perfluorinated carboxylates. *Environ. Chem.* **2011**, *8*, 339-354.

Crini, G. Recent developments in polysaccharide-based materials used as adsorbents in wastewater treatment. *Prog. Polym. Sci.* **2005**, *30*, 38-70.

Crini, G.; Morcellet, M. Synthesis and applications of adsorbents containing cyclodextrins. *J. Sep. Sci.* **2002**, *25*, 789-813.

D'Hollander, W., de Voogt, P. Coen, W.D.; Bervoets, L. Perfluorinated substances in human food and other sources of human exposure. *Rev. Environ. Contam. Toxicol.* **2010**, *208*, 179-215.

Dawson, W.H.; Hunter, D.H.; Willis, C.J. "*syn-anti*- Isomerization" of the *N*-heptafluoroisopropylimine of hexafluoroacetone; steric effects of negative hyperconjugation? *J. Chem. Soc., Chem. Commun.* **1980**, 874-875.

De Koning, C.; Beekhuijzen, M.; Tobor-Kaplon, M.; de Vries-Buitenweg, S.; Schoutsen, D.; Leeigen, N.; van de Waart, B.; Emmen, H. Visualizing compound distribution during zebrafish embryo development: The effects of lipophilicity and DMSO. *Birth Defects Res. B Dev. Reprod. Toxicol.* **2015**, *104*, 253–272.

Ding, G.; Zhang, J.; Chen, Y.; Wang, L.; Wang, M.; Xiong, D.; Sun, Y. Combined effects of PFOS and PFOA on zebrafish (Danio rerio) embryos. *Arch. Environ. Contam. Toxicol.* **2013**, *64*, 668–675.

Dudley, L.-A.; Arevalo, E.C; Knappe, D.R.U. *Removal of Perfluoroalkyl Substances by PAC Adsorption and Anion Exchange*. Water Research Foundation: Denver, CO, 2015.

Dugaiczyk, A.; Law, S.W.; Dennison, O.E. Nucleotide sequence and the encoded amino acids of human serum albumin mRNA. *Proc. Natl. Acad. Sci. USA* **1982**, *79*, 71-75.

Eftink, M.R.; Andy, M.L.; Bystrom, K.; Perlmutter, H.D.; Kristol, D.S. Cyclodextrin inclusion complexes: studies of the variation in the size of alicyclic guests. *J. Am. Chem. Soc.* **1989**, *111*, 6765-6772.

Fact Sheet: PFOA & PFOS Drinking Water Health Advisories; EPA 800-F-16-003; U.S. Environmental Protection Agency, U.S. Government Printing Office: Washington, DC, 20000.

Fanali, G.; di Masi, A.; Trezza, V.; Marino, M.; Fasano, M.; Ascenzi, P. Human serum albumin: From bench to bedside. *Mol. Aspects Med.* **2012**, *33*, 209-290.

Faraji, H.; Husain, S.W.; Helalizadeh, M. β-Cyclodextrin-bonded silica particles as novel sorbent for stir bar sorptive extraction of phenolic compounds. *J. Chromatogr. Sci.* **2011**, *49*, 482-487.

Frisbee, S.J.; Brooks, A.P.; Maher, A.; Flensborg, P.; Arnold, S.; Fletcher, T.; Steenland, K.; Shankar, A.; Knox, S.S.; Pollard, C.; Halverson, J.A.; Vieira, V.M.; Jin, C.; Leyden, K.M.; Ducatman, A.M. The C8 Health Project: design, methods, and participants. *Environ. Health Perspect.* **2009**, *117*, 1873-1882.

Frömming, K.-H.; Szejtli, J. *Cyclodextrins in Pharmacy*, Springer Science & Business Media: New York, 2013.

Gasymov, O.K.; Glasgow, B.J. ANS fluorescence: Potential to augment the identification of the external binding sites of proteins. *Biochim. Biophys. Acta.* **2007**, *1774*, 403-411.

Gebbink, W.A.; van Asseldonk, L.; van Leeuwan, S.P.J. Presence of Emerging Per- and Polyfluoroalkyl Substances (PFASs) in River and Drinking Water near a Fluorochemical Production Plant in the Netherlands. *Environ. Sci. Technol.* **2017**, *51*, 11057-11065.

Ghosh, S.; Paul, B. K.; Chattopdhyay, N. Interaction of cyclodextrins with human and bovine serum albumins: A combined spectroscopic and computational investigation. *J. Che. Sci.* **2014**, *126*, 931-944.

Glassmeyer, S.T.; Furlong, E.T.; Kolpin, D.W.; Batt, A.L.; Benson, R.; Boone, J.S.; Conerly, O.; Donohue, M.J.; King, D.N.; Kostich, M.S.; Mash, H.E.; Pfaller, S.L.; Schenck, K.M.; Simmons, J.E.; Varughese, E.A.; Vesper, S.J.; Villegas, E.N.; Wilson, V.S. Nationwide reconnaissance of contaminants of emerging concern in source and treated drinking waters of the United States. *Sci. Total Environ.* **2017**, *581-582*, 909-922.

Gomis, M.I.; Vestergren, R.; Borg, D.; Cousins, I.T. Comparing the toxic potency in vivo of long-chain perfluoroalkyl acids and fluorinated alternatives. *Environ. Int.* **2018**, *113*, 1-9.

Gomis, M.I.; Wang, Z.; Scheringer, M.; Cousins, I.T. A modeling assessment of the physicochemical properties and environmental fate of emerging and novel per- and polyfluoroalkyl substances. *Sci. Total Environ.* **2015**, *505*, 981-991.

Gonzalez, W.G.; Miksovska, J. Application of ANS fluorescent probes to identify hydrophobic sites on the surface of DREAM. *Biochim. Biophys. Acta.* **2014**, *1844*, 1472-1480.

Goss, K. The pK_a values of PFOA and other highly fluorinated carboxylic acids. *Environ. Sci. Technol.* **2008**, *42*, 456-458.

Guo, W.; Fung, B.M.; Christain, S.D. NMR study of cyclodextrin inclusion of fluorocarbon surfactants in solution. *Langmuir* **1992**, *8*, 446-451.

Hagenaars, A.; Vergauwen, L.; Benoot, D.; Laukens, K.; Knapen, D. Mechanistic toxicity study of perfluorooctanoic acid in zebrafish suggests mitochondrial dysfunction to play a key role in PFOA toxicity. *Chemosphere* **2013**, *91*, 844–856.

Hagenaars, A.; Vergauwen, L.; De Coen, W.; Knapen, D. Structure-activity relationship assessment of four perfluorinated chemicals using a prolonged zebrafish early life stage test. *Chemosphere* **2011**, *82*, 764–772.

Han, X.; Snow, T.A.; Kemper, R.A.; Jepson, G.W. Binding of perfluorooctanoic acid to rat and human plasma proteins. *Chem. Res. Toxicol.* **2003**, *16*, 775-781.

Hebert, P. C.; MacManus-Spencer, L. A. Development of a fluorescent model for the binding of medium- to long-chain perfluoroalkyl acids to human serum albumin through a mechanistic evaluation of spectroscopic evidence. *Anal. Chem.* **2010**, *82*, 6463-6471.

Herrera, V.L.O. Removal of perfluorooctane sulfonate (PFOS) and related compounds from industrial effluents. Ph.D. Dissertation. University of Arizona, Tucson, Arizona, 2008.

Hinton, D.E.; Kullman, S.W.; Hardman, R.C.; Volz, D.C.; Chen, P.J.; Carney, M.; Bencic, D.C. Resolving mechanisms of toxicity while pursuing ecotoxicological relevance? *Mar. Pollut. Bull.* **2005**, *51*, 635–648.

Houde, M.; Martin, J.W.; Letcher, R.J.; Solomon, K.R.; Muir, D.C.G. Biological monitoring of polyfluoroalkyl substances: a review. *Environ. Sci. Technol.* **2006**, *40*, 3463-3473.

Hu, X.C.; Andrews, D.Q.; Lindstrom, A.B.; Bruton, T.A.; Schaider, L.A.; Grandjean, P.; Lohmann, R.; Carignan, C.C.; Blum, A.; Balan, S.A.; Higgins, C.P.; Sunderland, E.M. Detection of Poly- and Perfluoroalkyl Substances (PFASs) in US Drinking Water Linked to Industrial Sites, Military Fire Training Areas, and Wastewater Treatment Plants. *ES&T Letters* **2016**, *3*, 344-350.

Hughes, R.P.; Smith, J. M.; Liable-Sands, L.M.; Concolino, T.E.; Lam, K.-C.; Incarvito, C.; Rheingold, A.L. Syntheses and crystallographic studies of $[Ir(\eta^5\text{-}C_5Me_5)(L)(R_F)I]$ (L = CO, PMe_3; R_F= CF_2CF_3, $CF_2CF_2CF_3$, $CF_2C_6F_5$, $CF(CF_3)_2$) complexes. Cone and solid angle steric parameters for perfluoroalkyl ligands. *J. Chem. Soc., Dalton Trans.* **2000**, 873-879.

Ito, N.; Yoshida, N.; Ichikawa, K. Fluorescence detection of the electrostatic interactions in the molecular recognition between protonated amino-cyclodextrins and some anilinonapthalenesulfonate anions. *J. Chem. Soc., Perkin Trans. 2* **1996**, 965-972.

Jaja-Chimedza, A.; Sanchez, K.; Gantar, M.; Gibbs, P.; Schmale, M.C.; Berry, J.P. Carotenoid glycosides from cyanobacteria are teratogenic in the zebrafish (*Danio rerio*) embryo model. *Chemosphere* **2017**, *174*, 478–489.

Jantzen, C.E.; Annunziato, K.A.; Bugel, S.M.; Cooper, K.R. PFOS, PFNA, and PFOA sub-lethal exposure to embryonic zebrafish have different toxicity profiles in terms of morphometrics, behavior and gene expression. *Aquat. Toxicol.* **2016a**, *175*, 160–170.

Jantzen, C.E.; Annunziato, K.M.; Cooper, K.R. Behavioral, morphometric, and gene expression effects in adult zebrafish (*Danio rerio*) embryonically exposed to PFOA, PFOS and PFNA. *Aquat. Toxicol.* **2016b**, *180*, 123–130.

Jantzen, C.E.; Toor, F.; Annunziato, K.A.; Cooper, K.R. Effects of chronic perfluorooctanoic acid (PFOA) at low concentrations on morphometrics, gene expression, and fecundity in zebrafish (*Danio rerio*). *Reprod. Toxicol.* **2017**, *69*, 34–42.

Jensen, A.A.; Leffers, H. Emerging endocrine disrupters: perfluoroalkylated substances. *Int. J. Androl.* **2008**, *31*, 161-169.

Job, P. Formation and stability of inorganic complexes in solution. *Ann. Chim.* **1928**, *9*, 113-203.

Kannan, K. Perfluoroalkyl and polyfluoroalkyl substances: current and future perspectives. *Environ. Chem.* **2011**, *8*, 333-338.

Karoyo, A.H.; Borisov, A.S.; Wilson, L.D.; Hazendonk, P. Formation of host-guest complexes of β-cyclodextrin and perfluorooctanoic acid. *J. Phys. Chem. B* **2011**, *115*, 9511-9527.

Karoyo, A.H.; Sidhu, P.; Wilson, L.D.; Hazendonk, P. Characterization and dynamic properties for the solid inclusion complexes of β-cyclodextrin and perfluorooctanoic acid. *J. Phys. Chem. B* **2013**, *117*, 8269-8282.

Karoyo, A.H.; Sidhu, P.S.; Wilson, L.D.; Hazendonk, P.; Borisov, A. Counterion anchoring effect on the structure of the solid-state inclusion complexes of β-cyclodextrin and sodium perfluorooctanoate. *J. Phys. Chem. C* **2015**, *119*, 22225-22243.

Karoyo, A.B.; Wilson, L.D. Tunable macromolecular-based materials for the adsorption of perfluorooctanoic and octanoic acid anions. *J. Colloid Interface Sci.* **2013**, *402*, 196-203.

Karoyo, A.H.; Wilson, L.D. Nano-sized cyclodextrin-based molecularly imprinted polymer adsorbents for perfluorinated compounds – a mini review. *Nanomaterials* **2015**, *5*, 981-1003.

Karoyo, A.H.; Wilson, L.D. Investigation of the adsorption processes of fluorocarbon and hydrocarbon anions at the solid-solution interface of macromolecular imprinted polymer materials. *J. Phys. Chem. C* **2016**, *120*, 6553-6568.

Kelly, S.M.; Jess, T.J.; Price, N.C. How to study proteins by circular dichroism. *Biochim. Biophys. Acta.* **2005**, *1751*, 119-139.

Kitae, T.; Nakayama, T.; Kano, K. Chiral recognition of α-amino acids by charged cyclodextrins through cooperative effects of Coulomb interaction and inclusion. *J. Chem. Soc., Perkin Trans. 2* **1998**, 207-212.

Krafft, M.P.; Riess, J.G. Chemistry, physical chemistry, and uses of molecular fluorocarbon-hydrocarbon diblocks, triblocks, and related compounds – unique "apolar" components for self-assembled colloid and interface engineering. *Chem. Rev.* **2009**, *109*, 1714-1792.

Kuznetsova, I.M.; Sulatskaya, A.I.; Povarova, O.I.; Turoverov, K.K. Reevaluation of ANS binding to human and bovine serum albumins: Key role of equilibrium microdialysis in ligand-receptor binding characterization. *PLoS One* **2012**, *7*, 1-9.

Kwak, E.S.; Gomez, F.A. Determination of the binding of β-cyclodextrin derivatives to adamantane carboxylic acids using capillary electrophoresis. *Chromatographia* **1996**, *43*, 659-662.

Lakowicz, J.R. *Principles of fluorescence spectroscopy*. Springer US: New York, 2006.

Le Saux, T; Hisamoto, H.; Terabe, S. Measurement of monomolecular binding constants of neutral phenols into the β-cyclodextrin by continuous frontal analysis in capillary and microchip electrophoresis via a competitive assay. *J. Chromatogr. A* **2006**, *1104*, 352-358.

Li, C.; Ji, R.; Schaffer, A.; Sequaris, J.-M.; Amelung, W.; Vereecken, H.; Klumpp, E. Sorption of a branched nonylphenol and perfluorooctanoic acid on Yangtze River sediments and their model components. *J. Environ. Monit.* **2012**, *14*, 2653-2658.

Lima, S.; Andrade-Dias, C.; Dias, A.M.A.; Marrucho, I.M.; Coutinho, J.A.P.; Teixeira-Dias, J.J.C. How does β-cyclodextrin affect the aggregation of sodium perfluoroheptanoate in aqueous solution: a ^{19}F NMR study. *J. Incl. Phenom. Macrocycl. Chem.* **2007**, *57*, 157-162.

Lipkowitz, K.B. Applications of computational chemistry to the study of cyclodextrins. *Chem. Rev.* **1998**, *98*, 1829-1873.

Liu, W.; Jiang, X.; Chen, X. A novel method of synthesizing cyclodextrin grafted multiwall carbon nanotubes/iron oxides and its adsorption of organic pollutant. *Appl. Surf. Sci.* **2014**, *320*, 764-771.

Liu, C.; Naismith, N.; Economy, J. Advanced mesoporous organosilica material containing microporous β-cyclodextrins for the removal of humic acid from water. *J. Chromatogr. A* **2004**, *1036*, 113-118.

Liu, L.; Song, K.-S.; Li, Z.-S.; Guo, Q.-X. Charge-transfer interaction: a driving force for cyclodextrin inclusion complexation. *J. Incl. Phenom. Macrocycl. Chem.* **2001**, *40*, 35-39.

Lo Meo, P.; D'Anna, F.; Riela, S.; Gruttadauria, M.; Noto, R. Host-guest interactions involving cyclodextrins: useful complementary insights achieved by polarimetry. *Tetrahedron* **2007**, *63* 9163-9171.

Lo Nostro, P.; Santoni, I.; Bonini, M.; Baglioni, P. Inclusion compound from a semifluorinated alkane and β-cyclodextrin. *Langmuir* **2003**, *19*, 2313-2317.

Lopez-Espinosa, M.J.; Mondal, D.; Armstrong, B.; Bloom, M.S.; Fletcher, T. Thyroid function and perfluoroalkyl acids in children living near a chemical plant. *Environ. Health Perspect.* **2012**, *120*, 1036-1041.

MacManus-Spencer, L.A.; Tse, M.L.; Hebert, P.C.; Bischel, H.N.; Luthy, R.G. Binding of perfluorocarboxylates to serum albumin: A comparison of analytical methods. *Anal. Chem.* **2010**, *82*, 974-981.

Martin Del Valle, E.M. Cyclodextrins and their uses: a review. *Process Biochem.* **2004**, *39*, 1033-1046.

Merino, N.; Qu, Y.; Deeb, R.A.; Hawley, E.L.; Hoffman, M.R.; Mahendra, S. Degradation and removal methods for perfluoroalkyl and polyfluoroalkyl substances in water. *Environ. Eng. Sci.* **2016**, *33*, 615-649.

Morin-Crini, N.; Crini, G. Environmental applications of water-insoluble β-cyclodextrin-epichlorohydrin polymers. *Prog. Polym. Sci.* **2013**, *38*, 344-368.

Moulahcene, L.; Skiba, M.; Senhadji, O.; Milon, N.; Benamor, M.; Lahiani-Skiba, M. Inclusion and removal of pharmaceutical residues from aqueous solution using water-insoluble cyclodextrin polymers. *Chem. Eng. Res. Des.* **2015**, *97*, 145-158.

Nagy, Z.M.; Molnár, M.; Fekete-Kertész, I.; Molnár-Perl, I.; Fenyvesi, E.; Gruiz, K. Removal of emerging micropollutants from water using cyclodextrin. *Sci. Total Environ.* **2014**, *485-486*, 711-719.

Olsen, G.W.; Burris, J.M.; Ehresman, D.J.; Froehlich, J.W.; Seacat, A.M.; Butenhoff, J.L.; Zobel, L.R. Half-life of serum elimination of perfluorooctanesulfonate, perfluorohexanesulfonate, and perfluorooctanoate in retired fluorochemical production workers. *Environ. Health Perspect.* **2007**, *115*, 1298-1305.

Overhauser, A.W. Polarization of nuclei in metals. *Phys. Rev.* **1953**, *92*, 411-415.

Palepu, R.; Reinsborough, V.C. Solution inclusion complexes of cyclodextrins with sodium perfluorooctanoate. *Can. J. Chem.* **1989**, *67*, 1550-1553.

Palepu, R.; Richardson, J.E. Binding constants of β-cyclodextrin/surfactant inclusion by conductivity measurements. *Langmuir* **1989**, *5*, 218-221.

Pérez, F.; Nadal, M.; Navarro-Ortega, A.; Fàbrega, F.; Domingo, J.L.; Barceló, D.; Farré, M. Accumulation of perfluoroalkyl substances in human tissues. *Environ. Int.* **2013**, *59*, 354-362.

Pessine, F.B.T.; Calderini, A.; Alexandrino, G.L. Review: cyclodextrin inclusion complexes probed by NMR techniques. In *Mass Resonance Spectroscopy*; Kim, D., Ed.; InTech, 2012; pp 237-264.

Petrakis, L., Sederholm, C.H. NMR fluorine-fluorine coupling constants in saturated organic compounds. *J. Chem. Phys.* **1961**, *35*, 1243-1248.

Planchart, A.; Mattingly, C.J.; Allen, D.; Ceger, P.; Casey, W.; Hinton, D.; Kanungo, J.; Kullman, S.W.; Tal, T.; Bondesson, M.; et al. Advancing toxicology research using in vivo high throughput toxicology with small fish models. *ALTEX* **2016**, *33*, 435–452.

Prevedouros, K.; Cousins, I.T.; Buck, R.C.; Korzeniowski, S.H. Source, fate, and transport of perfluorocarboxylates. *Environ. Sci. Technol.* **2006**, *40*, 32-44.

Rainieri, S.; Conlledo, N.; Langerholc, T.; Madorran, E.; Sala, M.; Barranco, A. Toxic effects of perfluorinated compounds at human cellular level and on a model vertebrate. *Food Chem. Toxicol.* **2017**, *104*, 14–25.

Ramos Cabrer, P.R.; Alvarez-Parrilla, E.; Meijide, F.; Seijas, J.A.; Rodríguez Núñez, E.R.; Vázquez Tato, J.V. Complexation of sodium cholate and sodium deoxycholate by β-cyclodextrin and derivatives. *Langmuir* **1999**, *15*, 5489-5495.

Rekharsky, M.V.; Inoue, Y. Complexation thermodynamics of cyclodextrins. *Chem. Rev.* **1998**, *98*, 1875-1918.

Ross, J.A.; Jameson, D.M. Time-resolved methods in biophysics. 8. Frequency domain fluorometry: applications to intrinsic protein fluorescence. *Photochem. Photobiol. Sci.* **2008**, *7*, 1301-1312.

Saenger, W.; Steiner, T. Cyclodextrin inclusion complexes: host-guest interactions and hydrogen-bonding networks. *Acta. Cryst.* **1998**, *A54*, 798-805.

Saha, S.; Roy, A.; Roy, K.; Roy, M.N. Study to explore the mechanism to form inclusion complexes of β-cyclodextrin with vitamin molecules. *Sci. Rep.* **2016**, *6*, 35764.

Salvalaglio, M.; Muscionico, I.; Cavallotti, C. Determination of energies and sites of binding of PFOA and PFOS to human serum albumin. *J. Phys. Chem. B* **2010**, *114*, 14860-14874.

Sarmah, S.; Marrs, J.A. Zebrafish as a vertebrate model system to evaluate effects of environmental toxicants on cardiac development and function. *Int. J. Mol. Sci.* **2016**, *17*, 2123 -2139.

Schaider, L.A.; Balan, S.A.; Blum, A.; Andrews, D.Q.; Strynar, M.J.; Dickinson, M.E.; Lunderberg, D.M.; Lang, J.R.; Peaslee, G.F. Fluorinated compounds in U.S. fast food packaging. *Environ. Sci. Technol. Lett.* **2017**, *4*, 105-111.

Schneider, H.-J.; Blatter, T.; Simova, S. NMR and fluorescence studies of cyclodextrin complexes with guest molecules containing both phenyl and naphthyl units. *J. Am. Chem. Soc.* **1991**, *113*, 1996-2000.

Schneider, H.-J.; Hacket, F.; Rüdiger, V. NMR studies of cyclodextrins and cyclodextrin complexes. *Chem. Rev.* **1998**, *98*, 1755-1785.

Scholz, S.; Fischer, S.; Gündel, U.; Küster, E.; Luckenbach, T.; Voelker, D. The zebrafish embryo model in environmental risk assessment—Applications beyond acute toxicity testing. *Environ. Sci. Pollut. Res. Int.* **2008**, *15*, 394–404.

Sheng, N.; Cui, R.; Wang, J.; Guo, Y.; Wang, J.; Dai, J. Cytotoxicity of novel fluorinated alternatives to long-chain perfluoroalkyl substances to human liver cell line and their binding capacity to human liver fatty acid binding protein. *Arch. Toxicol.* **2018**, *92*, 359-369.

Simova, S.; Schneider, H.-J. NMR analyses of cyclodextrin complexes with substituted benzoic acids and benzoate anions. *J. Chem. Soc., Perkin Trans. 2* **2000**, 1717-1722.

Solomon, I. Relaxation processes in a system of two spins. *Phys. Rev.* **1955**, *99*, 559-566.

Strynar, M.; Dagnino, S.; McMahen, R.; Liang, S.; Lindstrom, A.; Andersen, E.; McMillan, L.; Thurman, M.; Ferrer, I.; Ball, C. Identification of novel perfluoroalkyl ether carboxylic acids (PFECAs) and sulfonic acids (PFESAs) in natural waters using accurate mass time-of-flight mass spectrometry (TOFMS). *Environ. Sci. Technol.* **2015**, *49*, 11622-11630.

Sun, M.; Arevalo, E.; Strynar, M.; Lindstrom, A.; Richardson, M.; Kearns, B.; Pickett, A.; Smith, C.; Knappe, D.R.U. Legacy and emerging perfluoroalkyl substances are important drinking water contaminants in the Cape Fear River watershed of North Carolina. *Environ. Sci. Technol. Lett.* **2016**, *3*, 415-419.

Szejtli, J. Introduction and general overview of cyclodextrin chemistry. *Chem. Rev.* **1998**, *98*, 1743-1753.

Szente, L.; Szejtli, J. Highly soluble cyclodextrin derivatives: chemistry, properties, and trends in development. *Adv. Drug Deliv. Rev.* **1999**, *36*, 17-28.

Takahashi, K. Organic reactions mediated by cyclodextrins. *Chem. Rev.* **1998**, *98*, 2013-2033.

Takehara, K.; Yuki, K.; Shirasawa, M.; Yamasaki, S.; Yamada, S. Binding properties of hydrophobic molecules to human serum albumin studied by fluorescence titration. *Anal. Sci.* **2009**, *25*, 115-120.

Ulatowski, F.; Dąbrowa, K.; Bałakier, T.; Jurczak, J. Recognizing the limited applicability of job plots in studying host-guest interactions in supramolecular chemistry. *J. Org. Chem.* **2016**, *81*, 1746-1756.

Ulhaq, M.; Sundström, M.; Larsson, P.; Gabrielsson, J.; Bergman, A.; Norrgren, L.; Örn, S. Tissue uptake, distribution and elimination of (14)C-PFOA in zebrafish (*Danio rerio*). *Aquat. Toxicol.* **2015**, *163*, 148–157.

Valente, A.J.M.; Söderman, O. The formation of host-guest complexes between surfactants and cyclodextrins. *Adv. Colloid Interface Sci.* **2014**, *205*, 156-176.

Vieira, V.M.; Hoffman, K.; Shin, H.M.; Weinberg, J.M.; Webster, T.F.; Fletcher, T. Perfluorooctanoic acid exposure and cancer outcomes in a contaminated community: a geographic analysis. *Environ. Health Perspect.* **2013**, *121*, 318-323.

Wagner, B.D. Hydrogen bonding of excited states in supramolecular host-guest inclusion complexes. *Phys. Chem. Chem. Phys.* **2012**, *14*, 8825-8835.

Wang, E.J.; Chen, G.Y. Crystal structure of β-cyclodextrin-4-chlorobenzoic acid complex: unusual C-Cl$^{\cdots}\pi$ interaction between 4-chlorobenzoic acids in β-cyclodextrin dimer. *Chin. Chem. Lett.* **2011**, *22*, 847-850.

Wang, Z.; Cousins, I.T.; Scheringer, M.; Hungerbühler, K. Fluorinated alternatives to long-chain perfluoroalkyl carboxylic acids (PFCAs), perfluoroalkane sulfonic acids (PFSAs) and their potential precursors. *Environ. Int.* **2013**, *60*, 242-248.

Wang, Z.; Cousins, I.T.; Scheringer, M.; Hungerbuehler, K. Hazard assessment of fluorinated alternatives to long-chain perfluoroalkyl acids (PFAAs) and their precursors: status quo, ongoing challenges and possible solutions. *Environ. Int.* **2015**, *75*, 172-179.

Wang, Z.; DeWitt, J.C.; Higgins, C.P.; Cousins, I.T. A never-ending story of per- and polyfluoroalkyl substances (PFASs)? *Environ. Sci. Technol.* **2017**, *51*, 2508-2518.

Wang, N.; Zhou, L.; Guo, J.; Ye, Q.; Lin, J.; Yuan, J. Adsorption of environmental pollutants using magnetic hybrid nanoparticles modified with β-cyclodextrin. *Appl. Surf. Sci.* **2014**, *305*, 267-273.

Watanbe, M.; Nakamura, H.; Matsuo, T. Formation of through-ring α-cyclodextrin complexes with α,ω-alkanedicarboxylate anion. Effects of the aliphatic chain length and electrostatic factors on the complexation behavior. *Bull. Chem. Soc. Jpn.* **1992**, *65*, 164-169.

Wei, X.L.; Xiao, J.B.; Wang, Y.; Bai, Y. Which model based on fluorescence quenching is suitable to study the interaction between *trans*-resveratrol and BSA? *Spectrochim. Acta A* **2010**, *75*, 299-304.

Wenz, G.; Strassnig, C.; Thiele, C.; Engelke, A.; Morgenstern, B.; Hegetschweiler, K. Recognition of ionic guests by ionic β-cyclodextrin derivatives. *Chem. Eur. J.* **2008**, *14*, 7202-7211.

Wilson, L.D. Binding studies of cyclodextrin-surfactant complexes. Ph.D. Dissertation, University of Saskatchewan, Saskatoon, Canada, 1998.

Wilson, L.D.; Verrall, R.E. ^{19}F and ^{1}H NMR investigation of cyclodextrin/fluorocarbon alkyl carboxylate surfactant inclusion complexes. *Langmuir* **1998a**, *14*, 4710-4717.

Wilson, L.D.; Verrall, R.E. A ^{1}H NMR study of cyclodextrin-hydrocarbon surfactant inclusion complexes in aqueous solutions. *Can. J. Chem.* **1998b**, *76*, 25-34.

Wilson, L.D.; Verrall, R.E. A volumetric study of cyclodextrin-α,ω-alkyl dicarboxylate anion complexes in aqueous solutions. *J. Phys. Chem. B* **2000**, *104*, 1880-1886.

Wu, L.-L.; Gao, H.-W.; Gao, N.-Y.; Chen, F.-F.; Chen, L. Interaction of perfluorooctanoic acid with human serum albumin. *BMC Struct.* **2009**, *Biol. 9*, 31.

Xiao, L.; Ling, Y.; Alsbaiee, A.; Li, C.; Helbling, D.E.; Dichtel, W.R. β-Cyclodextrin polymer network sequesters perfluorooctanoic acid at environmentally relevant concentrations. *J. Am. Chem. Soc.* **2017**, *139*, 7689-7692.

Xing, H.; Lin, S.-S.; Yan, P.; Xiao, J.-X.; Chen, Y.-M. NMR studies of selectivity of β-cyclodextrin to fluorinated/hydrogenated surfactant mixtures. *J. Phys. Chem. B* **2007**, *111*, 8089-8095.

Yang, L.; Ho, N.Y.; Alshut, R.; Legradi, J.; Weiss, C.; Reischl, M.; Mikut, R.; Liebel, U.; Müller, F.; Strähle, U. Zebrafish embryos as models for embryotoxicity and teratological effects of chemicals. *Reprod. Toxicol.* **2009**, *28*, 245–253.

Zheng, X.M.; Liu, H.L.; Shi, W.; Wei, S.; Giesy, J.P.; Yu, H.X. Effects of perfluorinated compounds on development of zebrafish embryos. *Environ. Sci. Pollut. Res. Int.* **2011**, *19*, 2498–2505.

APPENDICES

Appendix 1: Chapter 2

Structures

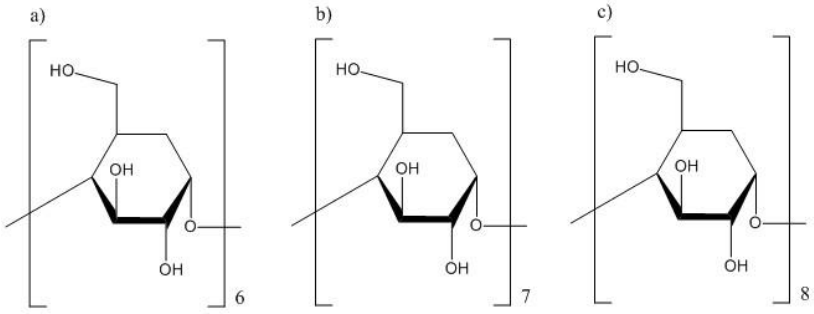

Figure A1: Structures of cyclodextrins: a) α-CD; b) β-CD; c) γ-CD.

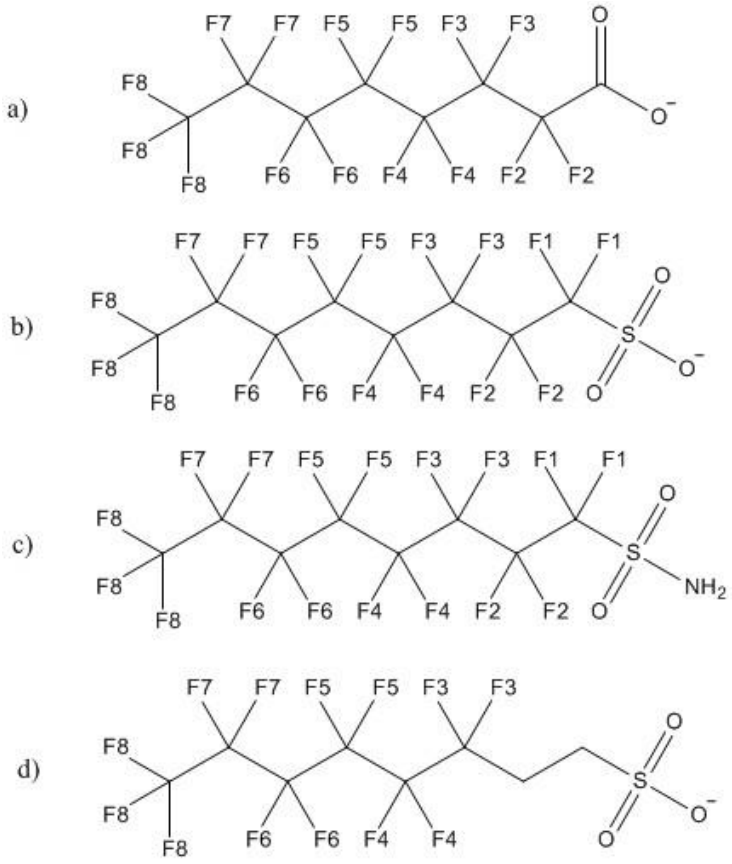

Figure A2: PFASs included in this study: a) perfluorooctanoic acid (PFOA), a representative perfluorocarboxylic acid (four others were studied with carbon number of 4, 5, 7, and 9); b) perfluorooctane sulfonate (PFOS); c) perfluorooctanesulfonamide (PFOSA); and d) 6:2 fluorotelomer sulfonate (6:2 FTS). Fluorines labeled by position.

^{19}F NMR Spectra of CD:PFAS Interactions

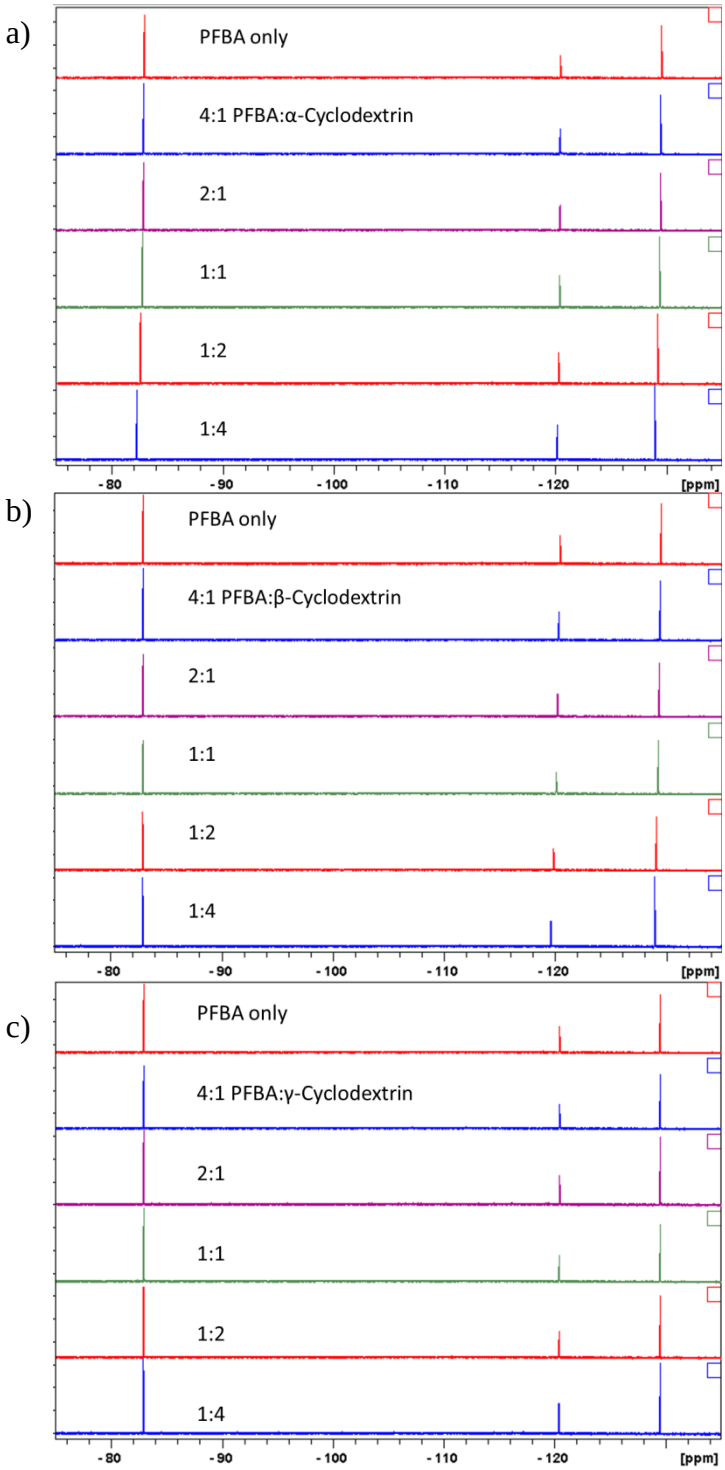

Figure A3: ^{19}F NMR spectra of perfluorobutanoic acid with a) α-CD; b) β-CD; and c) γ-CD. [PFBA] = 0.00242 M, pH 7, 50% D_2O/50% H_2O, 400 MHz NMR. Peaks from left to right: F4, F2, F3.

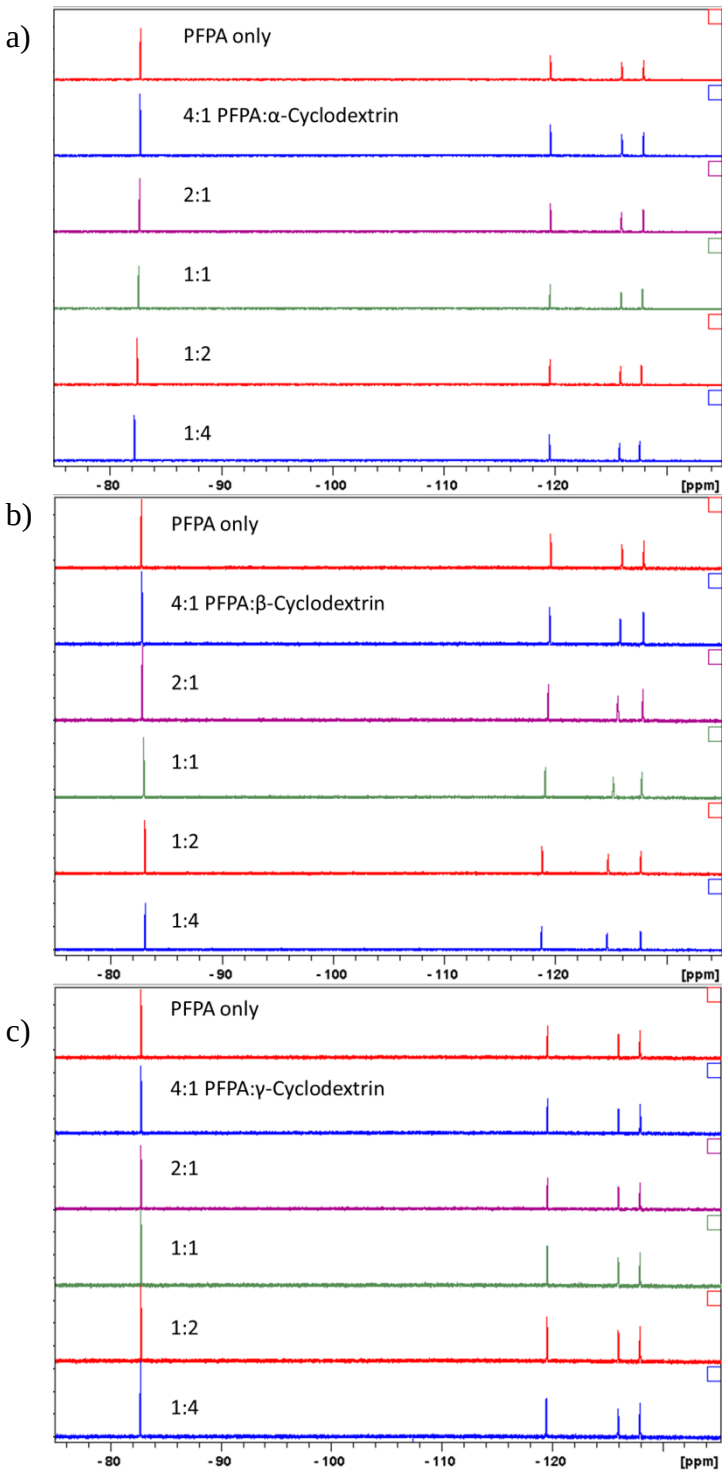

Figure A4: ^{19}F NMR spectra of perfluoropentanoic acid with a) α-CD; b) β-CD; and c) γ-CD. [PFPA] = 0.00242 M, pH 7, 50% D_2O/50% H_2O, 400 MHz NMR. Peaks from left to right: F5, F2, F3, F4.

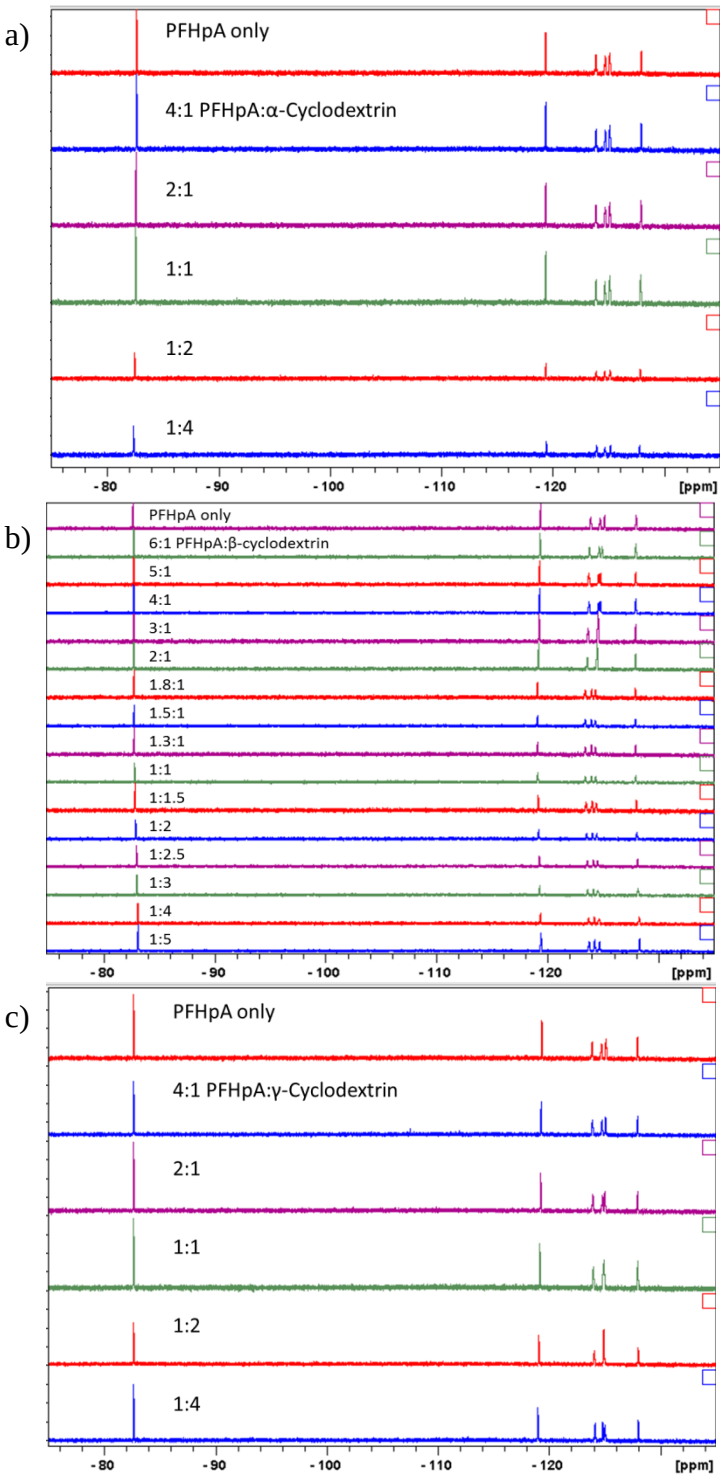

Figure A5: ^{19}F NMR spectra of perfluoroheptanoic acid with a) α-CD; b) β-CD; and c) γ-CD. [PFHpA] = 0.00242 M, pH 7, 50% D_2O/50% H_2O, 400 MHz NMR. Peaks from left to right: F7, F2, F4, F5, F3, F6.

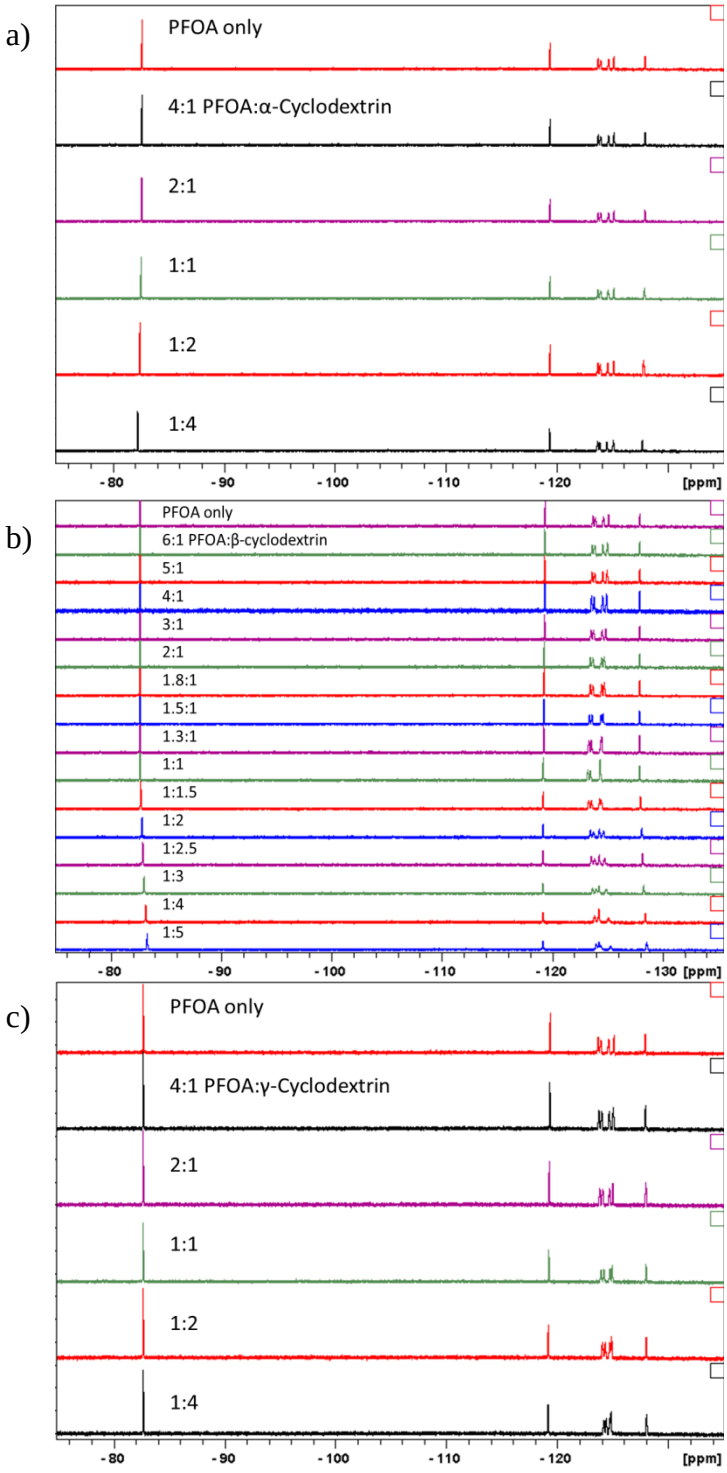

Figure A6: ^{19}F NMR spectra of perfluorooctanoic acid with a) α-CD; b) β-CD; and c) γ-CD. [PFOA] = 0.00242 M, pH 7, 50% D_2O/50% H_2O, 400 MHz NMR. Peaks from left to right: F8, F2, F4, F5, F3, F6, F7.

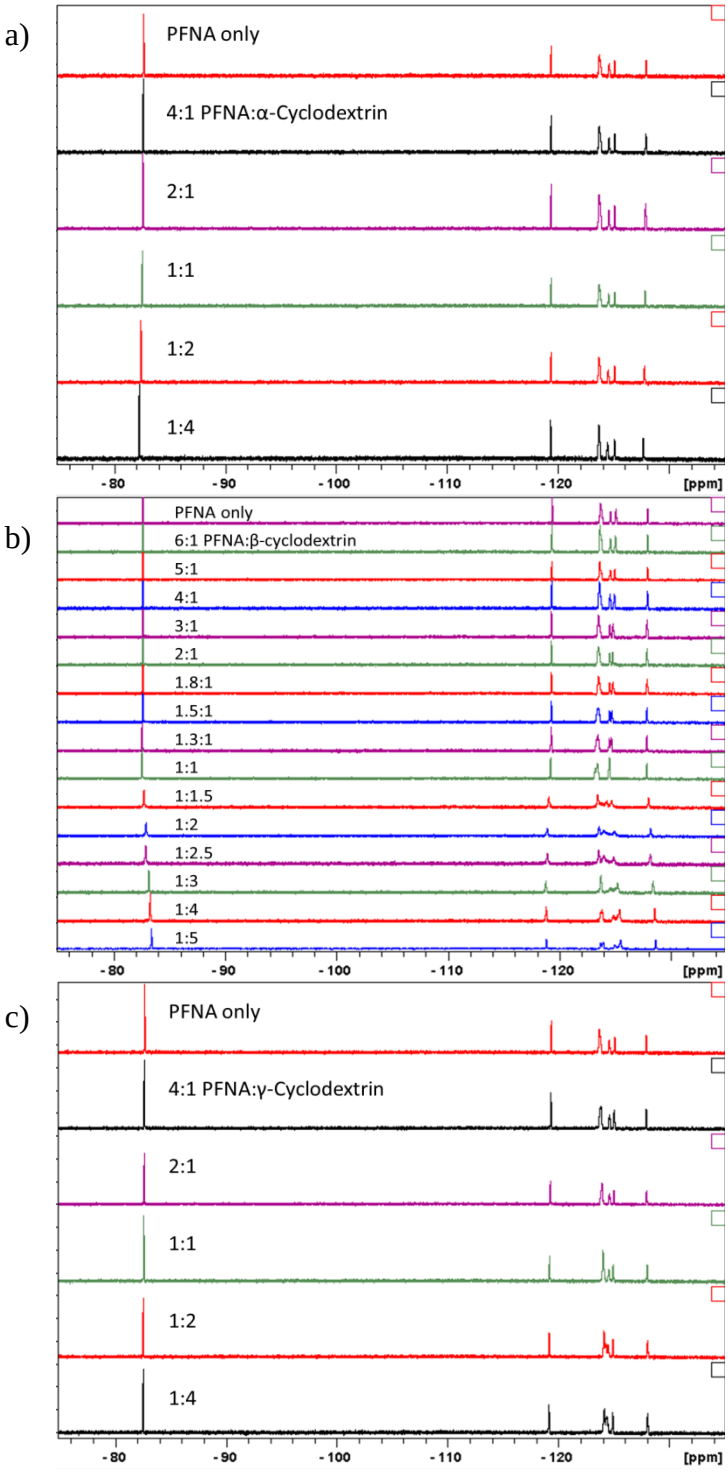

Figure A7: ^{19}F NMR spectra of perfluorononanoic acid with a) α-CD; b) β-CD; and c) γ-CD. [PFNA] = 0.00242 M, pH 7, 50% D_2O/50% H_2O, 400 MHz NMR. Peaks from left to right: F9, F2, F4-6, F3, F7, F8.

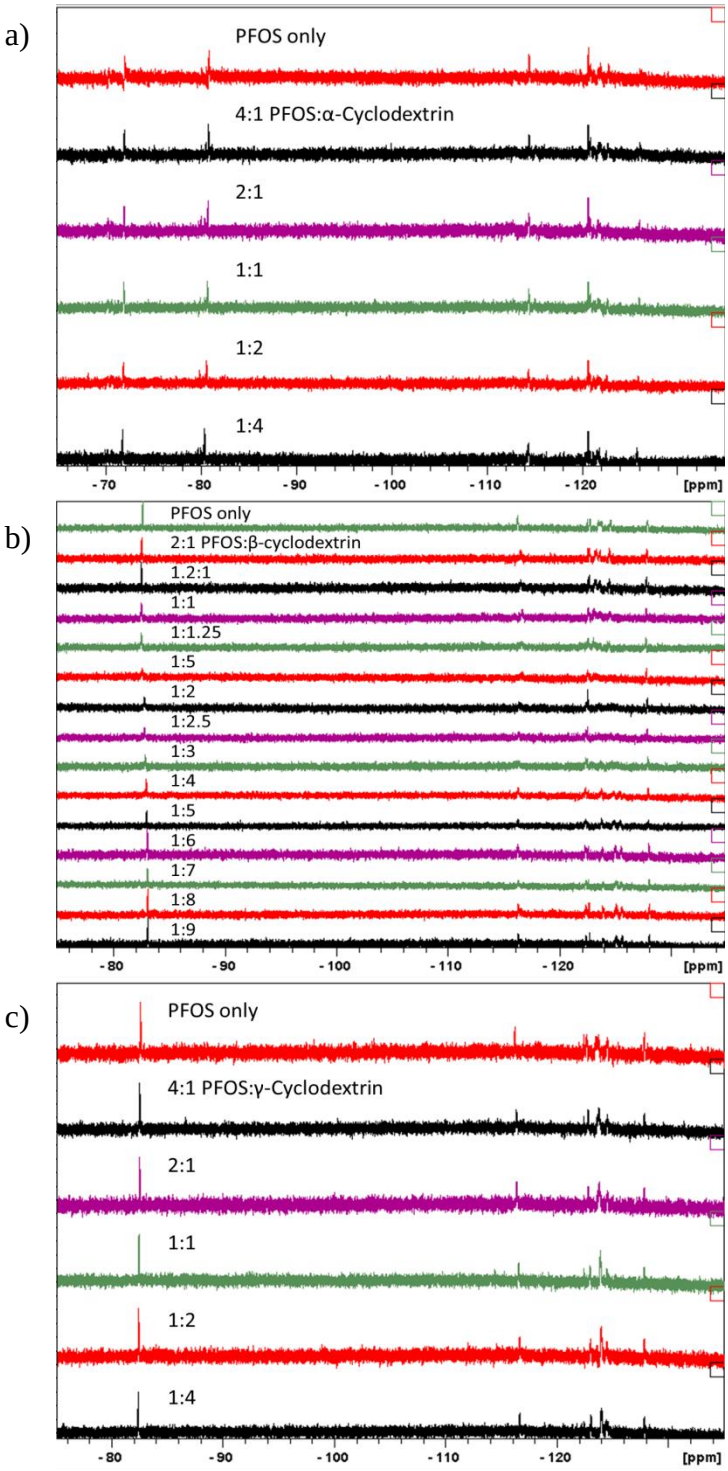

Figure A8: ^{19}F NMR spectra of perfluorooctane sulfonate with a) α-CD; b) β-CD; and c) γ-CD. [PFOS] = 6.05 x 10^{-4} M, pH 7, 50% D_2O/50% H_2O, 400 MHz NMR. Peaks from left to right: F8, F1, F3, F4-5, F2, F6, F7.

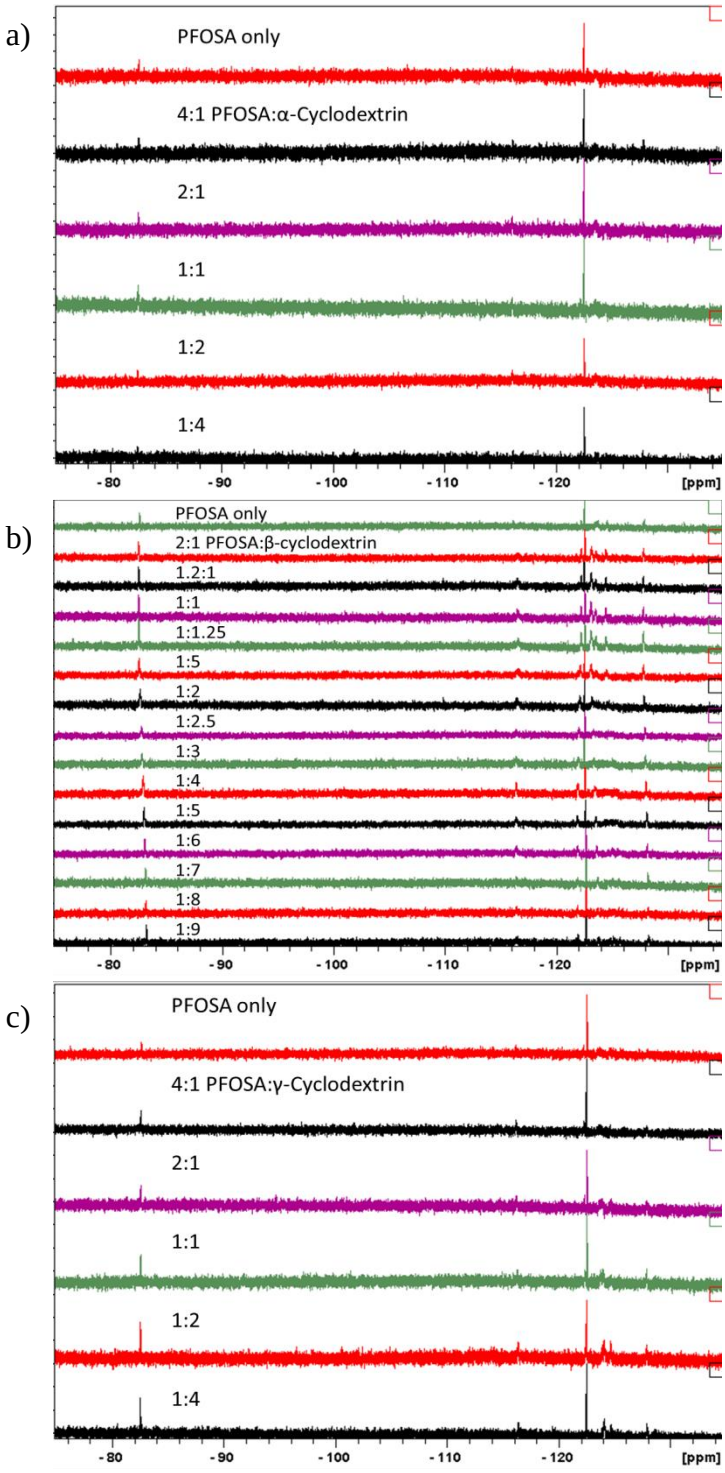

Figure A9: ^{19}F NMR spectra of perfluorooctanesulfonamide with a) α-CD; b) β-CD; and c) γ-CD. [PFOSA] = 6.05 x 10^{-4} M, pH 7, 50% D_2O/50% H_2O, 400 MHz NMR. Peaks from left to right: F8, F1, F3, F2, F4, F5, F6, F7.

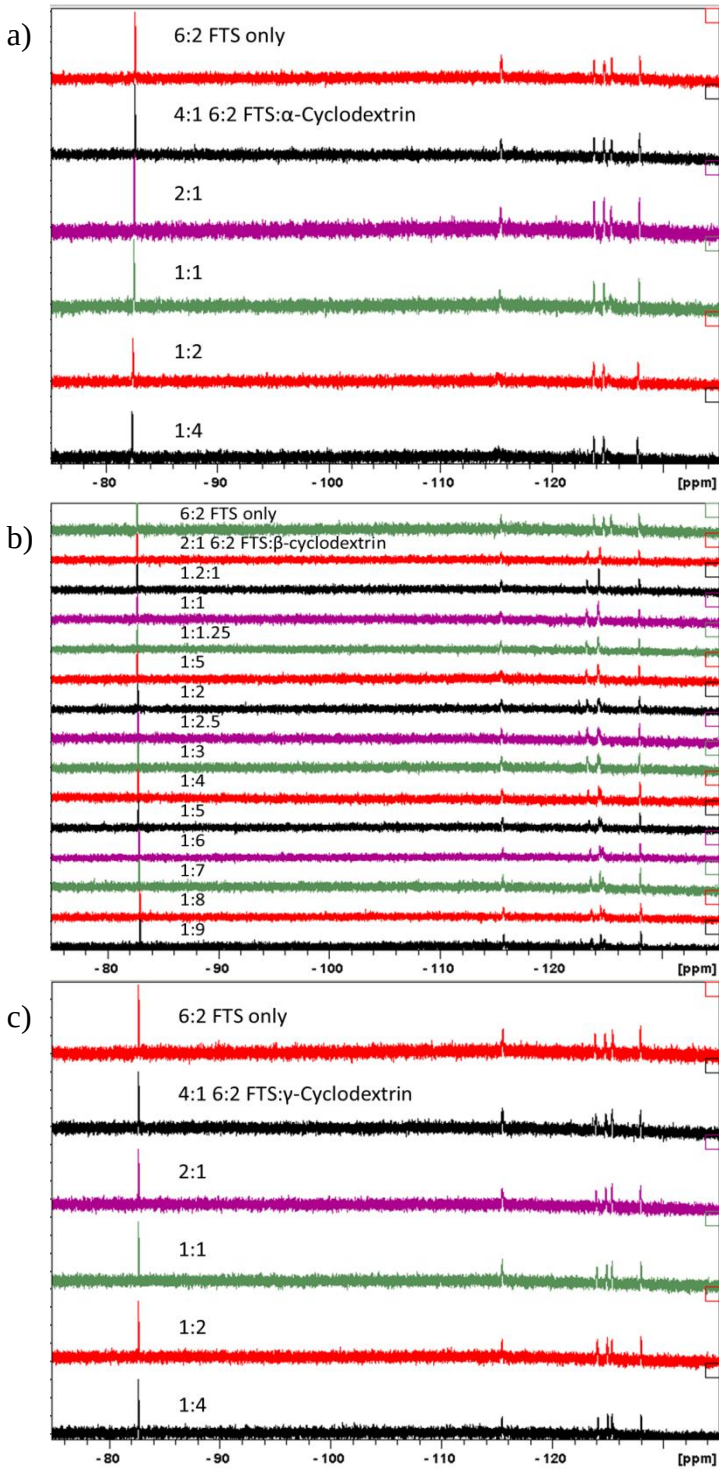

Figure A10: ^{19}F NMR spectra of 6:2 fluorotelomer sulfonate with a) α-CD; b) β-CD; and c) γ-CD. [6:2 FTS] = 6.05 x 10^{-4} M, pH 7, 50% D_2O/50% H_2O, 400 MHz NMR. Peaks from left to right: F8, F3, F5, F6, F4, F7.

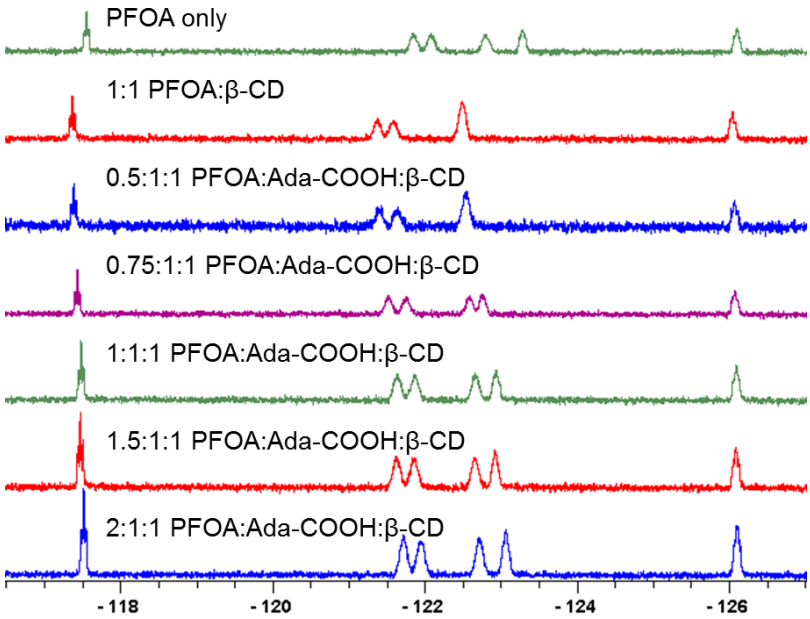

Figure A11: ^{19}F NMR spectra of adamantane-carboxylic acid competition study, detail of F2-F7 of PFOA. D_2O, 400 MHz NMR.

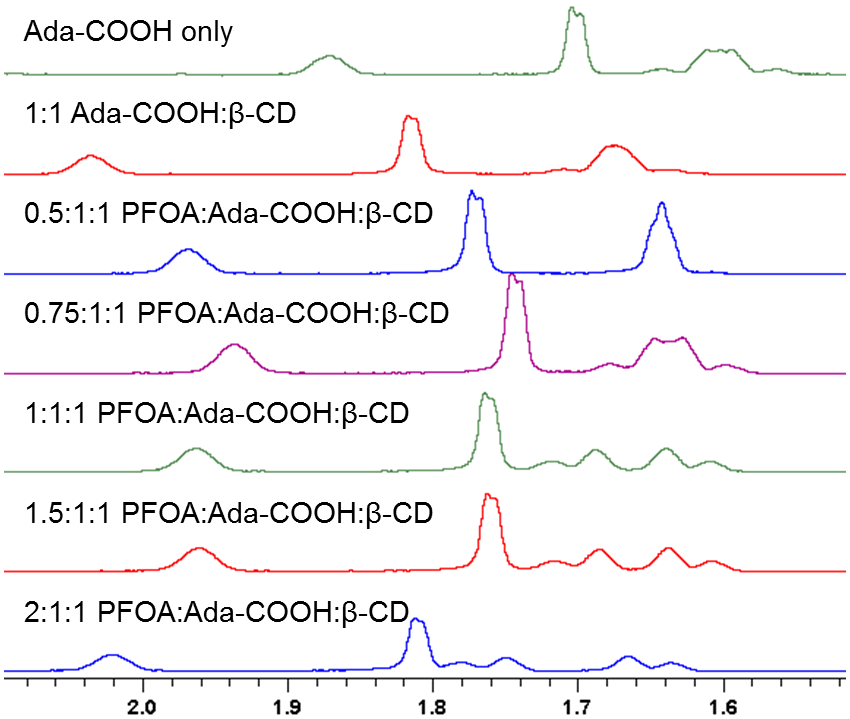

Figure A12: ^{1}H NMR spectra of adamantane-carboxylic acid competition study, detail of adamantane-carboxylic acid protons. D_2O, 400 MHz NMR.

Phenol Competition Study

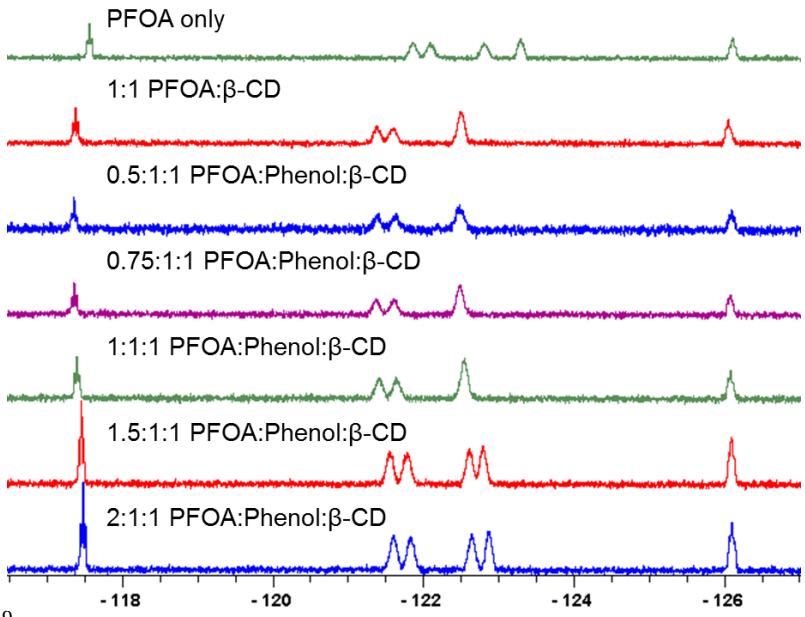

Figure A13: ^{19}F NMR spectra of phenol competition study, detail of F2-F7 of PFOA. D_2O, 400 MHz NMR.

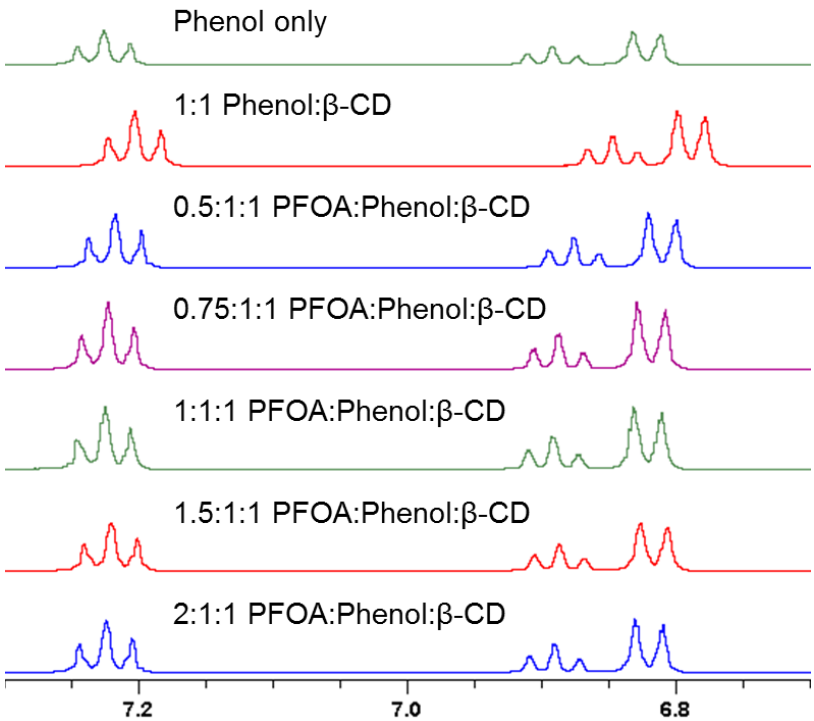

Figure A14: ^{1}H NMR spectra of phenol competition study, detail of phenol protons. D_2O, 400 MHz NMR.

Job Analysis of β-CD:PFOA Interactions

Table A1: Job Analysis of β-Cyclodextrin and Perfluorooctanoic Acid Interactions

PFOA (μL)	β-CD (μL)	PFOA (mM)	β-CD (mM)	χ_{PFOA} ([PFOA]/([PFOA]+[CD])
100	900	0.484	4.356	0.1
200	800	0.968	3.872	0.2
300	700	1.452	3.388	0.3
400	600	1.936	2.904	0.4
500	500	2.420	2.420	0.5
600	400	2.904	1.936	0.6
700	300	3.388	1.452	0.7
800	200	3.872	0.968	0.8
900	100	4.356	0.484	0.9
1000	0	4.840	0.000	1.0

Average Association Constants of CD:PFAS Interactions

Table A2: Average Association Constants for α-, β-, and γ-CD with PFASs

PFAS (#C)	α-CD (M^{-1})	β-CD (M^{-1})	γ-CD (M^{-1})
PFBA (4C)	$8.2 \pm 5.4 \times 10^{0}$	$2.90 \pm 0.24 \times 10^{2}$	No significant association
PFPA(5C)	$3.1 \pm 1.6 \times 10^{1}$	$7.60 \pm 0.44 \times 10^{2}$	No significant association
PFHpA (7C)	No significant association	$4.30 \pm 0.85 \times 10^{5}$ (1:1) $2.30 \pm 0.27 \times 10^{3}$ (2:1)	$3.50 \pm 0.38 \times 10^{2}$
PFOA (8C)	No significant association	$5.00 \pm 0.10 \times 10^{5}$ (1:1) $1.20 \pm 0.50 \times 10^{3}$ (2:1)	$8.80 \pm 1.40 \times 10^{2}$
PFNA (9C)	$4.7 \pm 2.1 \times 10^{1}$	$3.37 \pm 0.35 \times 10^{5}$ (1:1) $7.80 \pm 0.66 \times 10^{3}$ (2:1)	$1.80 \pm 0.96 \times 10^{3}$
PFOS (8C)	No significant association	$6.96 \pm 0.79 \times 10^{5}$ (1:1) $5.95 \pm 1.70 \times 10^{4}$ (2:1)	$1.07 \pm 0.42 \times 10^{3}$
PFOSA (8C)	No significant association	$1.02 \pm 0.16 \times 10^{5}$ (1:1) $2.70 \pm 0.57 \times 10^{4}$ (2:1)	$9.80 \pm 3.00 \times 10^{2}$
6:2 FTS (8C)	$2.60 \pm 1.80 \times 10^{2}$	$8.99 \pm 0.36 \times 10^{4}$ (1:1) $1.35 \pm 0.38 \times 10^{3}$ (2:1)	$6.70 \pm 1.60 \times 10^{2}$

Individual Association Constants of CD:PFAS Interactions

Table A3: Regression Analysis Results for Perfluorobutanoic Acid and α-, β-, and γ-Cyclodextrin

CD	Fluorine	$K_{1:1}$, M^{-1}	$\Delta\delta_{cd\text{-}F}$, ppm	R^2
α	2	$9.3 \pm 5.6 \times 10^0$	3.4 ± 1.9	0.999
	3	$8.7 \pm 5.4 \times 10^0$	7.6 ± 4.4	0.999
	4	$6.7 \pm 5.2 \times 10^0$	11.1 ± 8.1	0.999
β	2	$2.30 \pm 0.23 \times 10^2$	1.3 ± 0.1	0.999
	3	$2.30 \pm 0.23 \times 10^2$	0.91 ± 0.04	0.999
	4	$4.10 \pm 0.27 \times 10^2$	0.025 ± 0.005	0.945
γ	2	No significant association		
	3			
	4			

Table A4: Regression Analysis Results for Perfluoropentanoic Acid and α-, β-, and γ-Cyclodextrin

CD	Fluorine	$K_{1:1}$, M^{-1}	$\Delta\delta_{cd\text{-}F}$, ppm	R^2
α	2	$1.37 \pm 17.2 \times 10^0$	8.50 ± 10.50	0.989
	3	$2.48 \pm 1.61 \times 10^1$	1.13 ± 0.59	0.995
	4	$3.22 \pm 1.59 \times 10^1$	1.65 ± 0.63	0.996
	5	$3.58 \pm 1.36 \times 10^1$	2.21 ± 0.63	0.997
β	2	$7.80 \pm 0.44 \times 10^2$	1.02 ± 0.13	0.975
	3	$7.62 \pm 0.43 \times 10^2$	1.63 ± 0.22	0.974
	4	$7.25 \pm 0.41 \times 10^2$	0.37 ± 0.05	0.974
	5	$7.72 \pm 0.46 \times 10^2$	-0.42 ± 0.06	0.972
γ	2	No significant association		
	3			
	4			
	5			

Table A5: Regression Analysis Results for Perfluoroheptanoic Acid and α-, β-, and γ-Cyclodextrin

CD	Fluorine	$K_{1:1}$, M^{-1}	$K_{2:1}$, M^{-1}	$\Delta\delta_{cd\text{-}F}$, ppm	$\Delta\delta_{2cd\text{-}F}$, ppm	R^2
α	2	No significant association				
	3					
	4					
	5					
	6					
	7					
β	2	$6.20 \pm 0.24 \times 10^5$	$7.56 \pm 1.20 \times 10^2$	0.35 ± 0.01	-15.2 ± 3.5	0.953
	3	$2.62 \pm 0.21 \times 10^4$	$7.74 \pm 0.41 \times 10^3$	1.3 ± 0.1	-6.5 ± 5.4	0.949
	4	$1.06 \pm 0.43 \times 10^6$	$2.49 \pm 0.12 \times 10^3$	0.77 ± 0.04	-3.9 ± 1.0	0.794
	5	$6.92 \pm 0.44 \times 10^5$	$7.61 \pm 1.66 \times 10^2$	0.57 ± 0.10	-17.3 ± 11.8	0.943
	6	$7.81 \pm 0.40 \times 10^4$	$8.90 \pm 5.30 \times 10^2$	0.14 ± 0.01	-16.3 ± 2.4	0.993
	7	$9.22 \pm 0.41 \times 10^4$	$1.15 \pm 0.28 \times 10^3$	0.0023 ± 0.0011	-13.1 ± 8.2	0.995
γ	2	$4.18 \pm 0.50 \times 10^2$	Not observed	0.47 ± 0.02	Not observed	0.999
	3	$6.71 \pm 0.38 \times 10^2$	Not observed	0.35 ± 0.05	Not observed	0.966
	4	$2.15 \pm 0.39 \times 10^2$	Not observed	-0.41 ± 0.03	Not observed	0.997
	5	$3.09 \pm 0.15 \times 10^2$	Not observed	-0.43 ± 0.07	Not observed	0.976
	6	$1.25 \pm 0.46 \times 10^2$	Not observed	-0.13 ± 0.03	Not observed	0.992
	7	No significant association				

Table A6: Regression Analysis Results for Perfluorooctanoic Acid and α-, β-, and γ-Cyclodextrin

CD	Fluorine	$K_{1:1}$, M^{-1}	$K_{2:1}$, M^{-1}	$\Delta\delta_{cd\text{-}F}$, ppm	$\Delta\delta_{2cd\text{-}F}$, ppm	R^2
α	2	No significant association				
	3					
	4					
	5					
	6					
	7					
	8					
β	2	$3.27 \pm 0.94 \times 10^3$	Not observed	0.212 ± 0.006	Not observed	0.987
	3	$1.73 \pm 0.28 \times 10^3$	Not observed	0.448 ± 0.011	Not observed	0.993
	4	$6.77 \pm 0.39 \times 10^5$	$1.01 \pm 0.35 \times 10^3$	0.729 ± 0.027	-21.8 ± 5.8	0.997
	5	$4.04 \pm 0.87 \times 10^5$	$1.30 \pm 0.42 \times 10^3$	0.815 ± 0.028	-22.1 ± 7.2	0.997
	6	$1.36 \pm 0.14 \times 10^6$	$1.18 \pm 0.53 \times 10^3$	1.08 ± 0.05	-23.6 ± 7.9	0.993
	7	$2.27 \pm 0.83 \times 10^4$	$1.32 \pm 0.98 \times 10^3$	0.302 ± 0.110	-16.1 ± 8.0	0.988
	8	$6.07 \pm 0.73 \times 10^4$	$1.17 \pm 0.21 \times 10^3$	0.281 ± 0.020	-17.5 ± 2.3	0.999
γ	2	$1.55 \pm 0.31 \times 10^3$	Not observed	0.21 ± 0.01	Not observed	0.997
	3	No significant association				
	4	$3.91 \pm 0.51 \times 10^2$	Not observed	-0.66 ± 0.03	Not observed	0.998
	5	$7.46 \pm 1.04 \times 10^2$	Not observed	-0.59 ± 0.02	Not observed	0.998
	6	$1.10 \pm 0.14 \times 10^3$	Not observed	0.30 ± 0.01	Not observed	0.999
	7	$6.35 \pm 0.87 \times 10^2$	Not observed	-0.15 ± 0.01	Not observed	0.998
	8	No significant association				

Table A7: Regression Analysis Results for Perfluorononanoic Acid and α-, β-, and γ-Cyclodextrin

CD	Fluorine	$K_{1:1}$, M^{-1}	$K_{2:1}$, M^{-1}	$\Delta\delta_{cd\text{-}F}$, ppm	$\Delta\delta_{2cd\text{-}F}$, ppm	R^2
α	2	No significant association				
	3	$4.43 \pm 1.48 \times 10^1$	Not observed	0.532 ± 0.128	Not observed	0.997
	4,5,6	$9.19 \pm 6.42 \times 10^1$	Not observed	0.104 ± 0.042	Not observed	0.970
	7	$1.45 \pm 0.50 \times 10^1$	Not observed	0.286 ± 0.860	Not observed	0.927
	8	$4.31 \pm 1.49 \times 10^1$	Not observed	0.884 ± 0.220	Not observed	0.997
	9	$4.25 \pm 0.74 \times 10^1$	Not observed	1.41 ± 0.18	Not observed	0.999
β	2	$2.82 \pm 0.12 \times 10^5$	$1.43 \pm 0.28 \times 10^4$	-0.396 ± 0.030	4.18 ± 1.59	0.969
	3	No significant association				
	4,5,6	$6.12 \pm 0.75 \times 10^5$	$4.37 \pm 0.34 \times 10^3$	0.664 ± 0.126	-6.35 ± 0.68	0.948
	7	$7.36 \pm 0.83 \times 10^5$	$6.43 \pm 1.30 \times 10^3$	1.30 ± 0.10	-10.6 ± 0.8	0.992
	8	$3.09 \pm 0.12 \times 10^4$	$6.89 \pm 0.21 \times 10^3$	0.756 ± 0.424	-8.80 ± 0.38	0.999
	9	$2.66 \pm 0.51 \times 10^4$	$7.10 \pm 0.80 \times 10^3$	0.813 ± 0.048	-9.03 ± 0.52	0.999
γ	2	$2.52 \pm 0.63 \times 10^3$	Not observed	0.222 ± 0.007	Not observed	0.997
	3	No significant association				
	4,5,6	$9.87 \pm 6.50 \times 10^2$	Not observed	-0.572 ± 0.079	Not observed	0.969
	7	$3.98 \pm 2.50 \times 10^3$	Not observed	0.208 ± 0.013	Not observed	0.980
	8	$7.42 \pm 5.50 \times 10^2$	Not observed	-0.169 ± 0.031	Not observed	0.957
	9	$9.04 \pm 4.80 \times 10^2$	Not observed	0.135 ± 0.016	Not observed	0.979

Table A8: Regression Analysis Results for Perfluorooctane Sulfonate and α-, β-, and γ-Cyclodextrin

CD	Fluorine	$K_{1:1}$, M^{-1}	$K_{2:1}$, M^{-1}	$\Delta\delta_{cd\text{-}F}$, ppm	$\Delta\delta_{2cd\text{-}F}$, ppm	R^2
α	1	No significant association				
	2					
	3					
	4,5					
	6					
	7					
	8					
β	1	$6.14 \pm 0.46 \times 10^5$	$6.24 \pm 1.92 \times 10^4$	-0.530 ± 0.125	4.00 ± 0.26	0.821
	2	$8.97 \pm 1.26 \times 10^5$	$9.49 \pm 3.78 \times 10^4$	1.16 ± 0.31	-15.8 ± 7.9	0.975
	3	No significant association				
	4,5	$1.41 \pm 0.21 \times 10^6$	$7.76 \pm 1.10 \times 10^4$	0.837 ± 0.066	-8.55 ± 1.91	0.982
	6	$2.30 \pm 0.49 \times 10^5$	$8.21 \pm 2.03 \times 10^4$	0.794 ± 0.044	-12.2 ± 1.2	0.982
	7	$3.10 \pm 0.22 \times 10^5$	$2.42 \pm 0.49 \times 10^4$	0.201 ± 0.011	-4.50 ± 0.51	0.993
	8	$7.15 \pm 0.21 \times 10^5$	$1.62 \pm 0.88 \times 10^4$	0.193 ± 0.500	-11.1 ± 1.6	0.931
γ	1	$1.53 \pm 0.65 \times 10^3$	Not observed	-0.557 ± 0.065	Not observed	0.965
	2	$8.92 \pm 2.70 \times 10^2$	Not observed	-0.400 ± 0.043	Not observed	0.984
	3	No significant association				
	4,5					
	6	$1.68 \pm 0.25 \times 10^2$	Not observed	0.221 ± 0.022	Not observed	0.914
	7	No significant association				
	8	$1.69 \pm 0.75 \times 10^3$	Not observed	0.206 ± 0.024	Not observed	0.959

Table A9: Regression Analysis Results for Perfluorooctanesulfonamide and α-, β-, and γ-Cyclodextrin

CD	Fluorine	$K_{1:1}$, M^{-1}	$K_{2:1}$, M^{-1}	$\Delta\delta_{cd\text{-}F}$, ppm	$\Delta\delta_{2cd\text{-}F}$, ppm	R^2
α	1	No significant association				
	2					
	3					
	4					
	5					
	6					
	7					
	8					
β	1	No significant association				
	2	$8.00 \pm 1.08 \times 10^3$	$1.34 \pm 0.48 \times 10^3$	0.0592 ± 0.0081	-27.8 ± 7.0	0.995
	3	No significant association				
	4	$6.34 \pm 1.23 \times 10^4$	$3.59 \pm 1.37 \times 10^4$	0.849 ± 0.200	-9.88 ± 1.17	0.972
	5	$3.20 \pm 0.66 \times 10^4$	$2.58 \pm 0.58 \times 10^4$	0.922 ± 0.081	-27.9 ± 4.7	0.991
	6	$1.99 \pm 0.37 \times 10^5$	$4.46 \pm 0.66 \times 10^4$	0.885 ± 0.057	-17.4 ± 1.3	0.996
	7	$1.76 \pm 0.25 \times 10^5$	$2.15 \pm 0.36 \times 10^4$	0.240 ± 0.015	-7.77 ± 0.88	0.996
	8	$1.33 \pm 0.14 \times 10^5$	$3.30 \pm 0.42 \times 10^4$	0.370 ± 0.024	-9.59 ± 0.81	0.996
γ	1	$8.25 \pm 0.28 \times 10^2$	Not observed	-0.373 ± 0.005	Not observed	1.000
	2	No significant association				
	3	$1.00 \pm 0.20 \times 10^3$	Not observed	-0.300 ± 0.020	Not observed	0.993
	4	$6.21 \pm 1.40 \times 10^2$	Not observed	-0.567 ± 0.053	Not observed	0.993
	5					
	6	$9.97 \pm 0.46 \times 10^3$	Not observed	-0.132 ± 0.007	Not observed	0.966
	7	No significant association				
	8	$1.47 \pm 0.65 \times 10^3$	Not observed	0.123 ± 0.015	Not observed	0.955

Table A10: Regression Analysis Results for 6:2 Fluorotelomer Sulfonate and α-, β-, and γ-Cyclodextrin

CD	Fluorine	$K_{1:1}$, M^{-1}	$K_{2:1}$, M^{-1}	$\Delta\delta_{cd\text{-}F}$, ppm	$\Delta\delta_{2cd\text{-}F}$, ppm	R^2
α	3	$6.86 \pm 5.69 \times 10^1$	Not observed	1.64 ± 1.11	Not observed	0.991
	4	$1.79 \pm 1.97 \times 10^2$	Not observed	0.877 ± 0.630	Not observed	0.949
	5	$1.89 \pm 1.05 \times 10^3$	Not observed	0.0678 ± 0.0094	Not observed	0.937
	6	$8.92 \pm 5.70 \times 10^2$	Not observed	0.127 ± 0.029	Not observed	0.937
	7	$7.82 \pm 6.03 \times 10^1$	Not observed	0.954 ± 0.585	Not observed	0.990
	8	$8.65 \pm 3.72 \times 10^1$	Not observed	1.09 ± 0.37	Not observed	0.997
β	3	$1.98 \pm 0.36 \times 10^4$	$1.10 \pm 0.47 \times 10^3$	0.0507 ± 0.0116	-38.4 ± 2.5	0.993
	4	No significant association				
	5	$1.47 \pm 0.37 \times 10^5$	$7.13 \pm 0.11 \times 10^3$	0.831 ± 0.117	-18.8 ± 2.1	0.918
	6	$2.14 \pm 1.35 \times 10^5$	$6.74 \pm 0.31 \times 10^2$	0.553 ± 0.041	-59.4 ± 3.2	0.875
	7	$1.13 \pm 0.18 \times 10^4$	$1.76 \pm 0.55 \times 10^3$	0.00653 ± 0.00323	-15.8 ± 2.5	0.987
	8	$5.76 \pm 0.29 \times 10^4$	$1.86 \pm 0.73 \times 10^3$	0.00906 ± 0.00595	-24.79 ± 1.31	0.995
γ	3	$2.71 \pm 1.02 \times 10^3$	Not observed	0.0642 ± 0.0051	Not observed	0.967
	4	$8.59 \pm 0.88 \times 10^2$	Not observed	0.0578 ± 0.0214	Not observed	0.818
	5	$7.55 \pm 1.38 \times 10^2$	Not observed	-0.358 ± 0.024	Not observed	0.995
	6	$8.83 \pm 1.40 \times 10^2$	Not observed	-0.336 ± 0.019	Not observed	0.996
	7	$4.57 \pm 1.34 \times 10^2$	Not observed	-0.127 ± 0.018	Not observed	0.990
	8	$3.73 \pm 2.90 \times 10^2$	Not observed	0.0267 ± 0.0105	Not observed	0.934

Cross-Sectional Sizes

Table A11: Cyclodextrin Cavity Size Compared with Size of Fluorinated Chain Fragment [5]

Molecule	Diameter (Å) CD: Cavity, PFAS: Molecule	Cross Section ($Å^2$) CD: Cavity, PFAS: Molecule	Volume ($Å^3$) CD: Cavity, PFAS: Molecule
α-CD	4.9	18.9	174
β-CD	6.2	30.2	262
γ-CD	7.9	49.0	427
$CF_2CF_2CF_2$	6.0	28.3	249

^{19}F NMR Spectra of β-CD:PFOA Interactions in Different Environmental Conditions

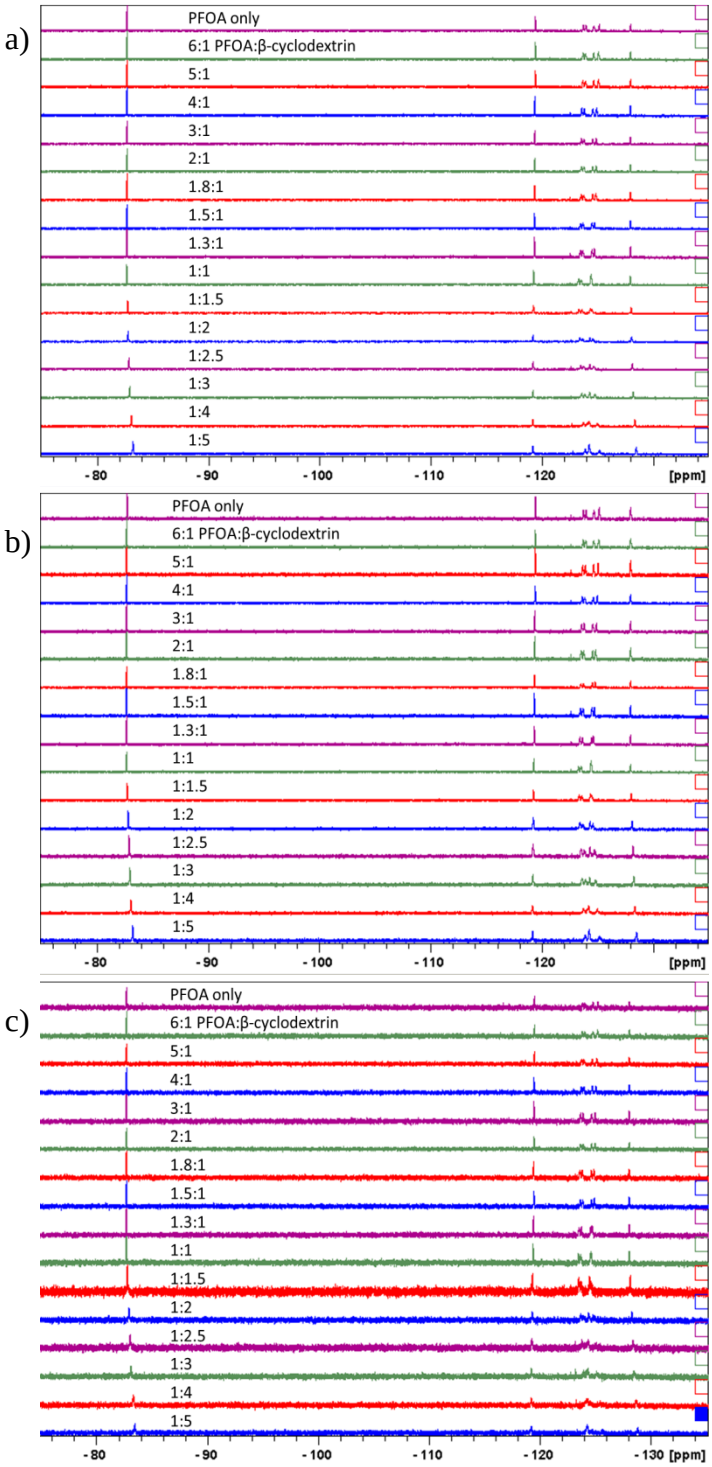

Figure A15: ^{19}F NMR spectra of PFOA and β-CD with a) 0.01 M NaCl; b) 0.1 M NaCl; and c) 1.0 M NaCl. [PFOA] = 0.00242 M, pH 7, 50% D_2O/50% H_2O, 400 MHz NMR.

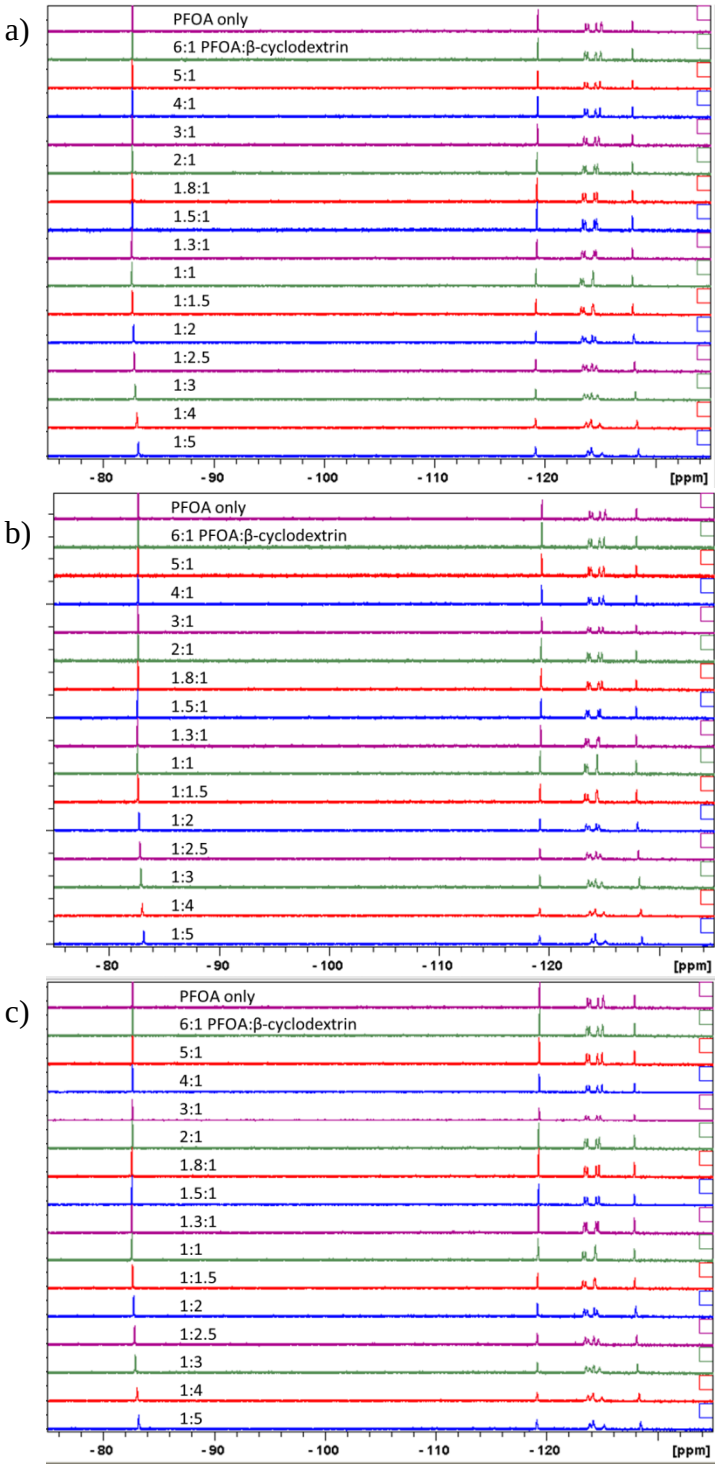

Figure A16: ^{19}F NMR spectra of PFOA and β-CD in a) pH 2; b) pH 4; and c) pH 10. [PFOA] = 0.00242 M, 50% D_2O/50% H_2O, 400 MHz NMR.

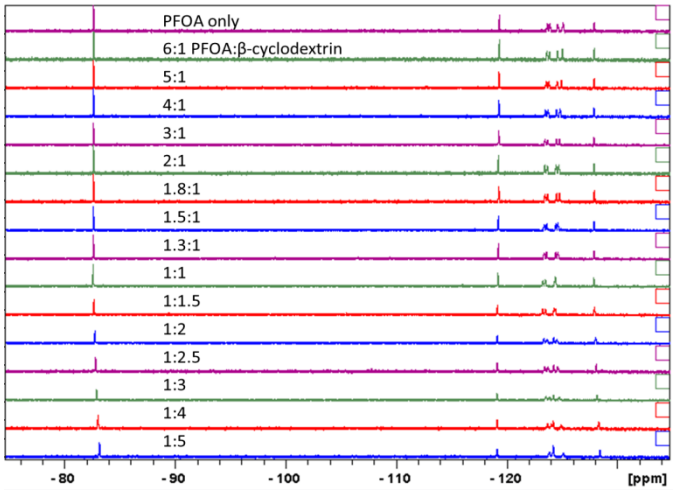

Figure A17: ^{19}F NMR spectra of PFOA and β-CD with 0.5 g/L Humic acid. [PFOA] = 0.00242 M, pH 7, 50% D_2O/50% H_2O, 400 MHz NMR.

Association Constants of β-CD:PFOA Interactions in Different Environmental Conditions

Table A12: Regression Analysis Results for Effects of Ionic Strength on β-CD:PFOA Complex

[NaCl], M	Fluorine	$K_{1:1}$, M^{-1}	$K_{2:1}$, M^{-1}	$\Delta\delta_{cd\text{-}F}$, ppm	$\Delta\delta_{2cd\text{-}F}$, ppm	R^2
0.01	2	$7.60 \pm 1.98 \times 10^2$	Not observed	0.270 ± 0.017	Not observed	0.977
	3	$6.19 \pm 1.25 \times 10^2$	Not observed	0.508 ± 0.027	Not observed	0.985
	4	$1.75 \pm 0.55 \times 10^6$	$5.98 \pm 1.20 \times 10^2$	0.582 ± 0.027	-23.1 ± 2.4	0.944
	5	$1.19 \pm 0.14 \times 10^6$	$6.41 \pm 0.81 \times 10^2$	0.646 ± 0.029	-27.8 ± 8.8	0.963
	6	$7.55 \pm 0.23 \times 10^5$	$6.33 \pm 1.73 \times 10^2$	0.899 ± 0.048	-26.6 ± 3.3	0.930
	7	$1.64 \pm 0.46 \times 10^5$	$1.74 \pm 0.51 \times 10^2$	0.153 ± 0.007	-67.0 ± 5.9	0.998
	8	$2.78 \pm 0.15 \times 10^5$	$3.30 \pm 0.2 \times 10^2$	0.189 ± 0.003	-39.3 ± 5.8	0.999
0.1	2	$6.35 \pm 1.43 \times 10^2$	Not observed	0.302 ± 0.017	Not observed	0.981
	3	$6.06 \pm 1.31 \times 10^2$	Not observed	0.535 ± 0.030	Not observed	0.983
	4	$5.55 \pm 0.27 \times 10^5$	$3.82 \pm 0.4 \times 10^2$	0.600 ± 0.012	-36.6 ± 8.3	0.984
	5	$6.05 \pm 0.93 \times 10^5$	$7.14 \pm 0.45 \times 10^2$	0.668 ± 0.025	-26.6 ± 9.0	0.991
	6	$8.30 \pm 0.81 \times 10^5$	$5.25 \pm 0.34 \times 10^2$	0.942 ± 0.032	-34.7 ± 4.4	0.976
	7	$3.11 \pm 0.51 \times 10^5$	$5.40 \pm 0.58 \times 10^2$	0.181 ± 0.0076	-24.8 ± 3.3	0.997
	8	$2.80 \pm 0.16 \times 10^5$	$6.55 \pm 0.27 \times 10^2$	0.202 ± 0.017	-21.5 ± 2.7	0.997
1.0	2	$2.39 \pm 0.37 \times 10^2$	Not observed	0.460 ± 0.029	Not observed	0.991
	3	$3.30 \pm 0.41 \times 10^2$	Not observed	0.693 ± 0.030	Not observed	0.994
	4	$2.31 \pm 0.73 \times 10^4$	$1.59 \pm 0.18 \times 10^3$	0.791 ± 0.270	-18.7 ± 3.4	0.948
	5	$6.10 \pm 0.99 \times 10^4$	$1.23 \pm 0.43 \times 10^3$	0.821 ± 0.051	-27.0 ± 3.1	0.980
	6	$2.04 \pm 0.75 \times 10^5$	$5.35 \pm 0.77 \times 10^2$	0.944 ± 0.100	-48.7 ± 6.0	0.974
	7	$3.50 \pm 0.57 \times 10^4$	$1.78 \pm 0.41 \times 10^3$	0.317 ± 0.044	-14.5 ± 2.0	0.998
	8	$2.10 \pm 0.50 \times 10^5$	$1.13 \pm 0.23 \times 10^3$	0.275 ± 0.020	-20.2 ± 3.0	0.999

Table A13: Regression Analysis Results for Effects of pH on β-CD:PFOA Complex

pH	Fluorine	$K_{1:1}$, M^{-1}	$K_{2:1}$, M^{-1}	$\Delta\delta_{cd\text{-}F}$, ppm	$\Delta\delta_{2cd\text{-}F}$, ppm	R^2
2	2	$1.56 \pm 0.47 \times 10^3$	Not observed	0.234 ± 0.012	Not observed	0.977
	3	$8.32 \pm 1.68 \times 10^2$	Not observed	0.492 ± 0.022	Not observed	0.986
	4	$5.93 \pm 1.18 \times 10^5$	$1.54 \pm 0.22 \times 10^2$	0.633 ± 0.022	-95.4 ± 3.8	0.980
	5	$7.41 \pm 0.61 \times 10^5$	$2.02 \pm 0.52 \times 10^2$	0.658 ± 0.034	-85.2 ± 12.4	0.986
	6	$7.61 \pm 1.36 \times 10^5$	$1.64 \pm 0.66 \times 10^2$	0.956 ± 0.040	-107 ± 8	0.972
	7	$6.46 \pm 0.30 \times 10^4$	$1.60 \pm 0.32 \times 10^2$	0.169 ± 0.008	-78.5 ± 2.3	0.998
	8	$1.56 \pm 0.11 \times 10^4$	$1.40 \pm 0.50 \times 10^2$	0.206 ± 0.011	-94.5 ± 9.3	0.998
4	2	$1.56 \pm 0.37 \times 10^3$	Not observed	0.244 ± 0.016	Not observed	0.969
	3	$1.06 \pm 0.23 \times 10^3$	Not observed	0.478 ± 0.021	Not observed	0.984
	4	$9.39 \pm 0.99 \times 10^5$	$6.38 \pm 0.77 \times 10^2$	0.650 ± 0.015	-25.4 ± 8.1	0.984
	5	$8.25 \pm 0.30 \times 10^5$	$1.25 \pm 0.31 \times 10^3$	0.724 ± 0.022	-18.0 ± 3.1	0.988
	6	$7.93 \pm 0.16 \times 10^5$	$8.56 \pm 0.33 \times 10^2$	0.993 ± 0.029	-23.9 ± 6.4	0.974
	7	$3.32 \pm 0.17 \times 10^5$	$6.73 \pm 1.94 \times 10^2$	0.193 ± 0.008	-20.9 ± 2.1	0.995
	8	$4.87 \pm 0.28 \times 10^4$	$4.63 \pm 1.18 \times 10^2$	0.215 ± 0.005	-30.7 ± 4.4	0.996
10	2	$8.57 \pm 1.60 \times 10^2$	Not observed	0.263 ± 0.011	Not observed	0.988
	3	$6.01 \pm 0.77 \times 10^2$	Not observed	0.518 ± 0.018	Not observed	0.994
	4	$6.23 \pm 0.35 \times 10^5$	$3.44 \pm 0.88 \times 10^2$	0.592 ± 0.058	-39.7 ± 11.4	0.961
	5	$3.72 \pm 0.20 \times 10^5$	$6.12 \pm 0.87 \times 10^2$	0.669 ± 0.078	-31.4 ± 7.8	0.968
	6	$7.47 +/- 0.21 \times 10^5$	$2.61 \pm 0.11 \times 10^2$	0.904 ± 0.075	-61.8 ± 3.3	0.944
	7	$1.98 \pm 0.46 \times 10^4$	$2.00 \pm 0.91 \times 10^3$	0.279 ± 0.079	-9.59 ± 2.39	0.993
	8	$2.55 \pm 0.15 \times 10^4$	$1.83 \pm 0.15 \times 10^3$	0.293 ± 0.019	-10.5 ± 3.0	0.992

Table A14: Regression Analysis Results for Effects of Presence of Humic Acid on β-CD:PFOA Complex

Fluorine	$K_{1:1}$, M^{-1}	$K_{2:1}$, M^{-1}	$\Delta\delta_{cd\text{-}F}$, ppm	$\Delta\delta_{2cd\text{-}F}$, ppm	R^2
2	$1.63 \pm 0.46 \times 10^3$	Not observed	0.226 ± 0.010	Not observed	0.980
3	$8.53 \pm 1.72 \times 10^2$	Not observed	0.476 ± 0.021	Not observed	0.986
4	$9.55 \pm 1.50 \times 10^5$	$4.26 \pm 0.30 \times 10^2$	0.615 ± 0.071	-34.0 ± 9.4	0.962
5	$8.23 \pm 0.44 \times 10^5$	$4.96 \pm 0.20 \times 10^2$	0.658 ± 0.046	-36.5 ± 2.2	0.975
6	$1.05 \pm 0.41 \times 10^6$	$4.23 \pm 0.97 \times 10^2$	0.922 ± 0.160	-40.8 ± 2.6	0.953
7	$1.36 \pm 0.80 \times 10^5$	$5.46 \pm 0.40 \times 10^2$	0.196 ± 0.010	-25.6 ± 2.2	0.999
8	$9.97 \pm 0.22 \times 10^4$	$5.79 \pm 2.49 \times 10^2$	0.216 ± 0.020	-25.4 ± 9.2	0.998

Appendix 2: Chapter 3

Numbering System of PFECAs

Table A15: Structures of Studied Perfluoroethercarboxylic Acids

Name (Abbreviation)	Oxygen content (#O / chain length)	Structure
Perfluoro(3-oxabutanoic) acid (PFMOPrA)	HOC (0.6)	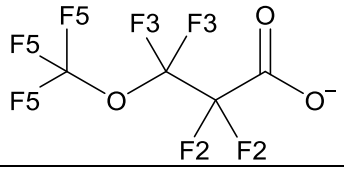
Perfluoro(4-oxapentanoic) acid (PFMOBA)	HOC (0.5)	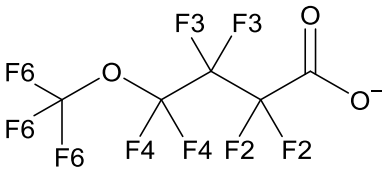
Perfluoro(2-methyl-3-oxahexanoic) acid (PFPrOPrA, "GenX")	HOC (0.5)	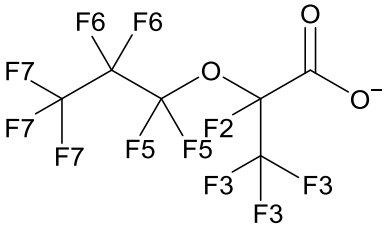
Perfluoro(5-oxa-6-dimethylhexanoic) acid (PFDMMOBA)	LOC (0.4)	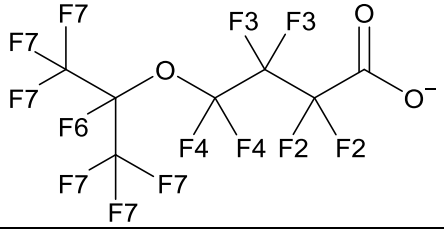
Perfluoro(3,6-dioxaheptanoic) acid (PFO2HpA)	HOC (0.6)	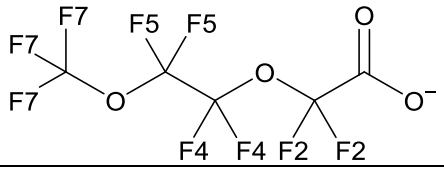
Perfluoro(3,6-dioxadecanoic) acid (PFO2DA)	LOC (0.4)	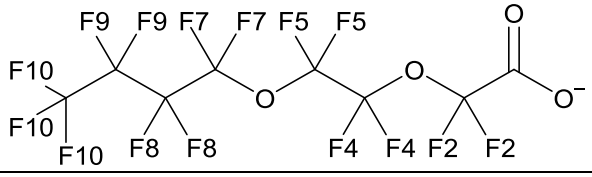

Perfluoro(3,6,9-trioxadecanoic) acid (PFO3DA)	HOC (0.5)	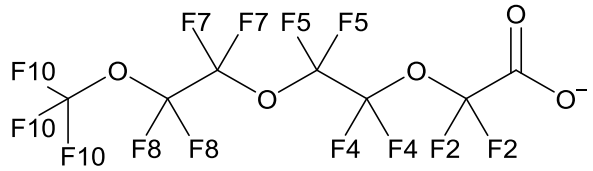
Perfluoro(3,6,9-trioxatridecanoic) acid (PFO3TDA)	LOC (0.4)	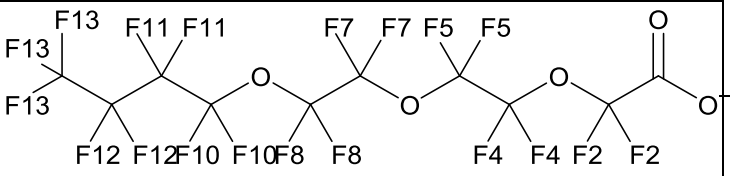

Characterization of PFECAs by ^{19}F and ^{13}C NMR

Note: ^{19}F coupling constants depend on conformation of the compound

Perfluoro(3-oxabutanoic) acid (PFMOPrA): ^{19}F NMR (D_2O; referenced to hexafluorobenzene) δ = -57.0 (t, *J* = 9.1 Hz, 3F), -90.0 (m, 2F), -122.7 (t, *J* = 3.2 Hz, 2F). ^{13}C NMR ($CDCl_3$; referenced to $CDCl_3$) δ = 160.0, 119.1, 114.9, 106.2.

Perfluoro(4-oxapentanoic) acid (PFMOBA): ^{19}F NMR (D_2O; referenced to hexafluorobenzene) δ = -57.8 (t, *J* = 9.3 Hz, 3F), -87.7 (q, *J* = 9.3 Hz, 2F), -119.9 (t, *J* = 9.3 Hz, 2F), -129.4 (s, 2F). ^{13}C NMR ($CDCl_3$; referenced to $CDCl_3$) δ = 160.9, 119.0, 114.7, 108.1, 107.6.

Perfluoro(2-methyl-3-oxahexanoic) acid (PFPrOPrA, "GenX"): ^{19}F NMR (D_2O; referenced to hexafluorobenzene) δ = -82.8 (m, 1F), -83.1 (t, *J* = 7.4 Hz, 3F), -84.3 (d, *J* = 3.3 Hz, 3F), -87.6 (m, 1F), -128.7 (d, *J* = 21.0, 1F), -131.7 (s, 2F). ^{13}C NMR ($CDCl_3$; referenced to $CDCl_3$) δ = 161.5, 117.8, 117.0, 115.8, 106.4, 100.3.

Perfluoro(5-oxa-6-dimethylhexanoic) acid (PFDMMOBA): ^{19}F NMR (D_2O; referenced to hexafluorobenzene) δ = -82.3 (td, *J* = 5.8 Hz, 2.2 Hz, 6F), -83.2 (br, 2F), -119.6 (t, *J* = 8.0 Hz, 2F), -128.8 (t, *J* = 3.2 Hz, 2F), -147.1 (t, *J* = 21.3 Hz, 1F). ^{13}C NMR ($CDCl_3$; referenced to $CDCl_3$) δ = 160.2, 117.4, 115.9, 108.3, 107.6, 101.8.

Perfluoro(3,6-dioxaheptanoic) acid (PFO2HpA): ^{19}F NMR (D_2O; referenced to hexafluorobenzene) δ = -57.0 (t, *J* = 8.9 Hz, 3F), -79.6 (t, *J* = 10.4 Hz, 2F), -90.3 (t, *J* = 10.4 Hz, 2F), -92.5 (q, *J* = 8.9 Hz, 2F). ^{13}C NMR ($CDCl_3$; referenced to $CDCl_3$) δ = 159.4, 119.1, 114.0, 113.3, 112.9.

Perfluoro(3,6-dioxadecanoic) acid (PFO2DA): ^{19}F NMR (D_2O; referenced to hexafluorobenzene) δ = -79.7 (t, *J* = 10.5 Hz, 2F), -82.9 (t, *J* = 9.2 Hz, 3F), -85.4 (br, 2F), -90.5 (m, 4F), -128.3 (t, *J* = 9.2 Hz, 2F), -128.4 (br, 2F). ^{13}C NMR ($CDCl_3$; referenced to $CDCl_3$) δ = 159.2, 117.1, 115.5, 114.4, 114.0, 112.2, 108.1, 107.9.

Perfluoro(3,6,9-trioxadecanoic) acid (PFO3DA): ^{19}F NMR (D_2O; referenced to hexafluorobenzene) δ = -57.0 (t, *J* = 9.0 Hz, 3F), -79.7 (t, *J* = 10.4 Hz, 2F), -90.3 (m, 4F), -90.5 (m, 2F), -92.3 (q, *J* = 9.0 Hz, 2F). ^{13}C NMR ($CDCl_3$; referenced to $CDCl_3$) δ = 159.3, 119.1, 114.3, 114.1, 114.0, 113.1, 112.9.

Perfluoro(3,6,9-trioxatridecanoic) acid (PFO3TDA): ^{19}F NMR (D_2O; referenced to hexafluorobenzene) δ = -79.6 (t, *J* = 10.9 Hz, 2F), -82.9 (t, *J* = 8.5 Hz, 3F), -85.4 (br, 2F), -90.6 (m, 4F), -90.8 (s, 4F), -128.4 (br, 2F), -128.5 (br, 2F). ^{13}C NMR ($CDCl_3$; referenced to $CDCl_3$) δ = 158.8, 117.0, 115.5, 114.3, 114.2, 114.1, 113.9, 112.9, 108.0, 107.9.

^{19}F NMR Spectra of CD:PFECA Interactions

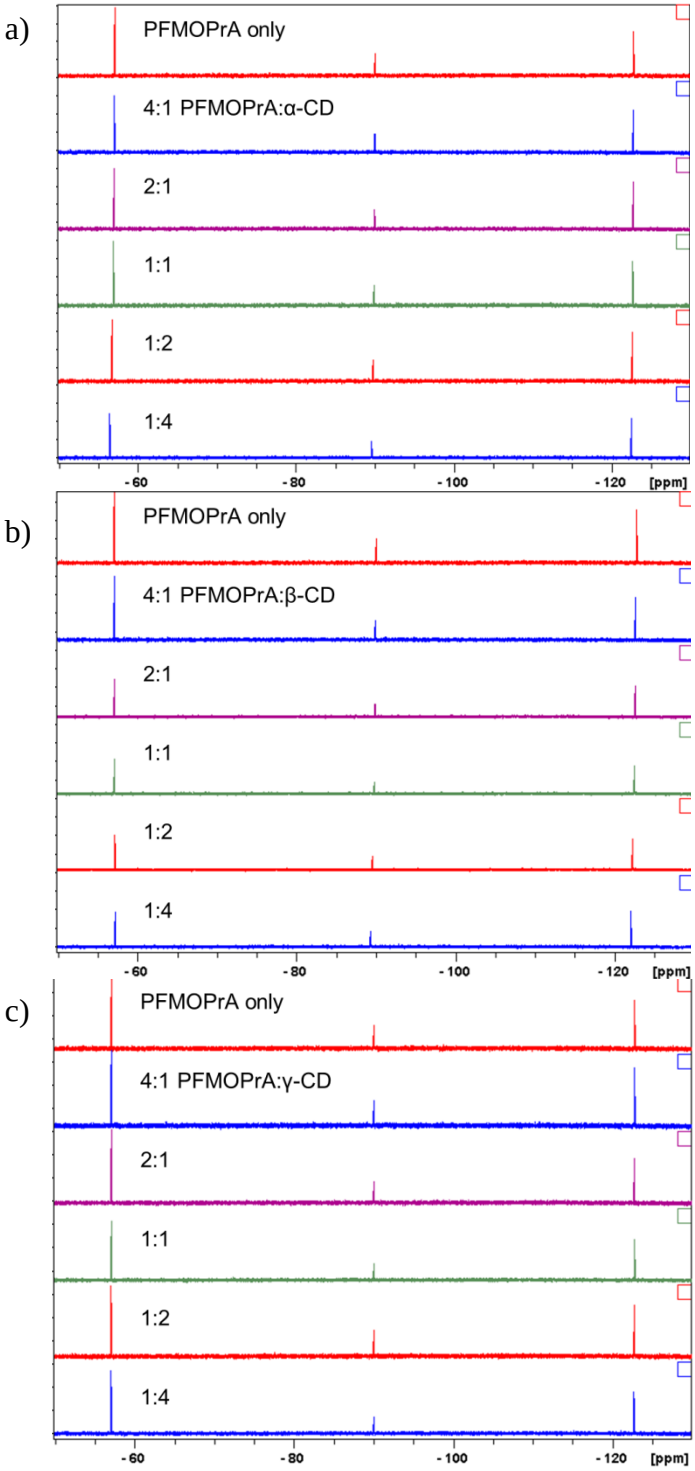

Figure A18: ^{19}F NMR spectra of perfluoro(3-oxabutanoic) acid with a) α-CD; b) β-CD; and c) γ-CD. [PFMOPrA] = 0.00242 M, pH 7, 50% D_2O/50% H_2O, 400 MHz NMR. Peaks from left to right: F5, F3, F2.

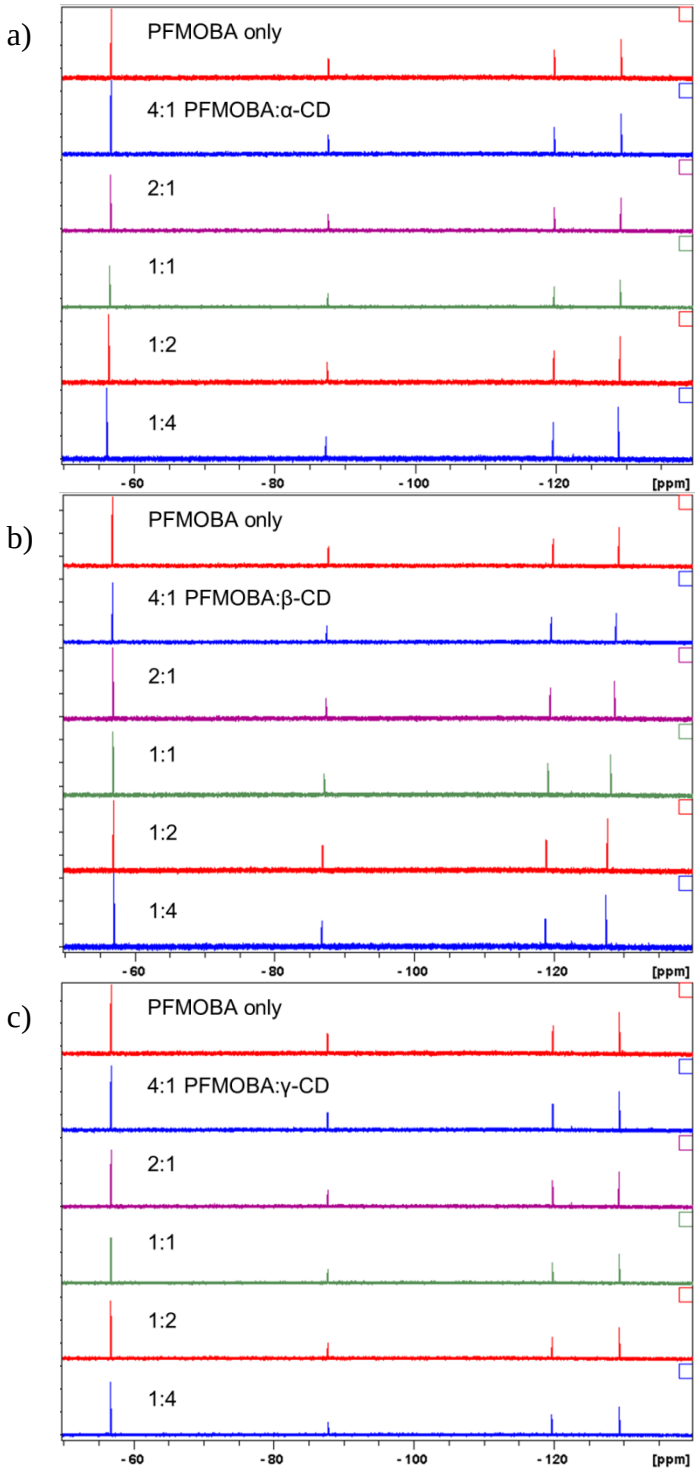

Figure A19: ^{19}F NMR spectra of perfluoro(4-oxapentanoic) acid with a) α-CD; b) β-CD; and c) γ-CD. [PFMOBA] = 0.00242 M, pH 7, 50% D_2O/50% H_2O, 400 MHz NMR. Peaks from left to right: F6, F4, F2, F3.

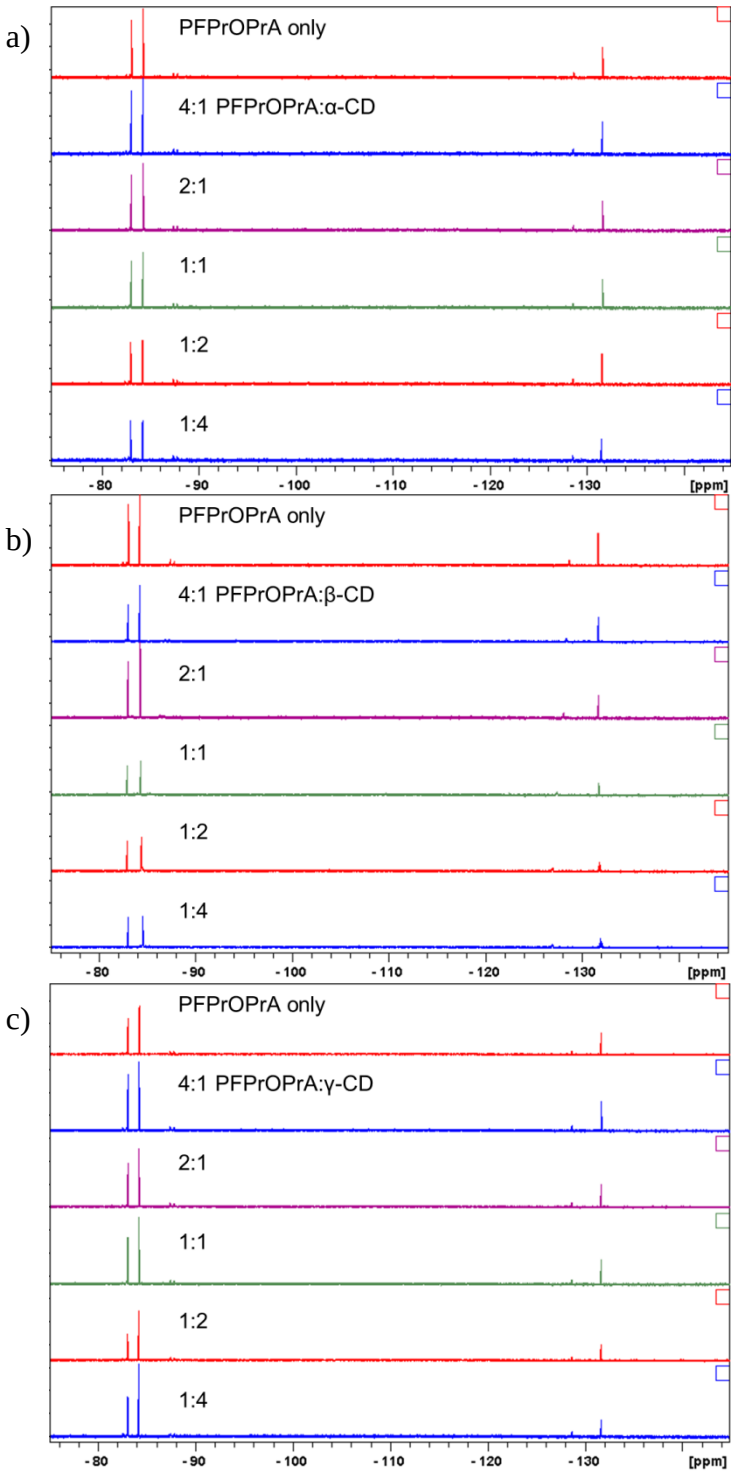

Figure A20: ^{19}F NMR spectra of perfluoro(2-methyl-3-oxahexanoic) acid with a) α-CD; b) β-CD; and c) γ-CD. [PFPrOPrA] = 0.00242 M, pH 7, 50% D_2O/50% H_2O, 400 MHz NMR. Peaks from left to right: F5a, F7, F3, F5b, F2, F6.

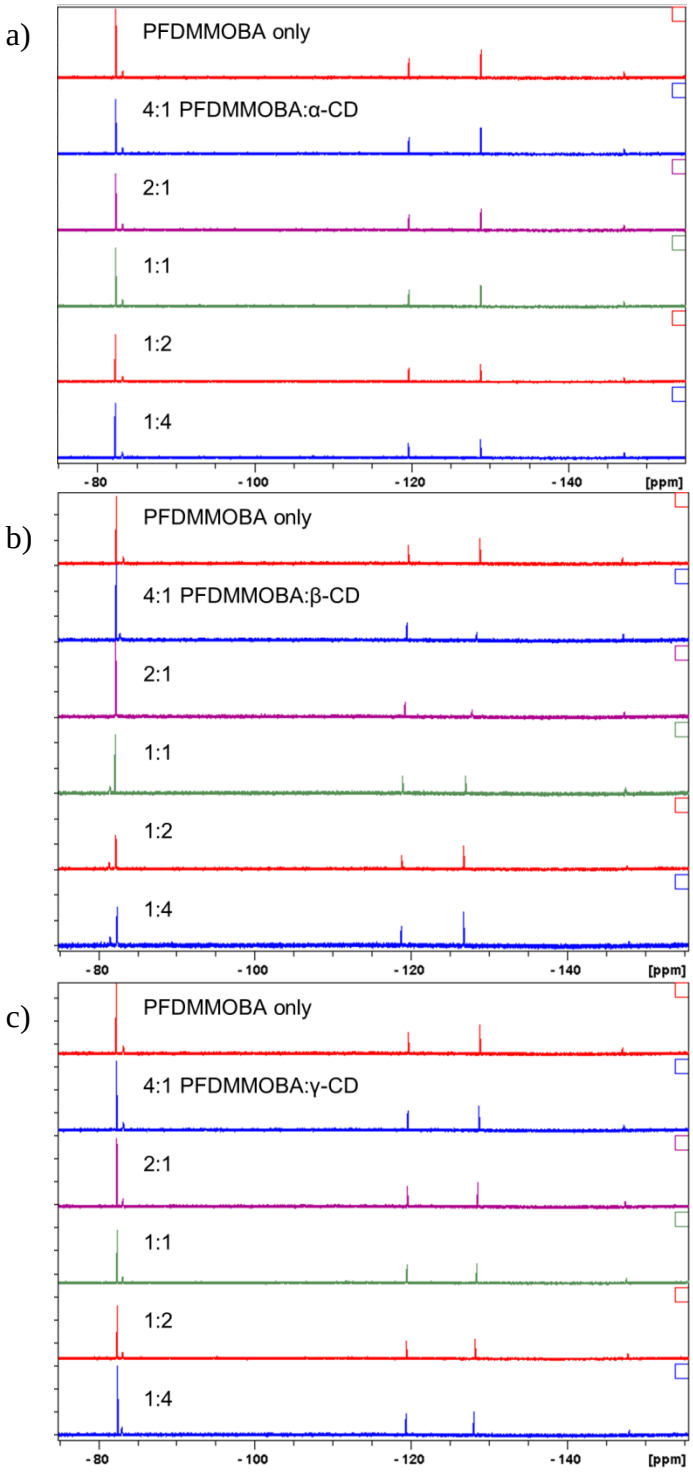

Figure A21: ^{19}F NMR spectra of perfluoro(5-oxa-6-dimethylhexanoic) acid with a) α-CD; b) β-CD; and c) γ-CD. [PFDMMOBA] = 0.00242 M, pH 7, 50% D_2O/50% H_2O, 400 MHz NMR. Peaks from left to right: F7, F4, F2, F3, F6.

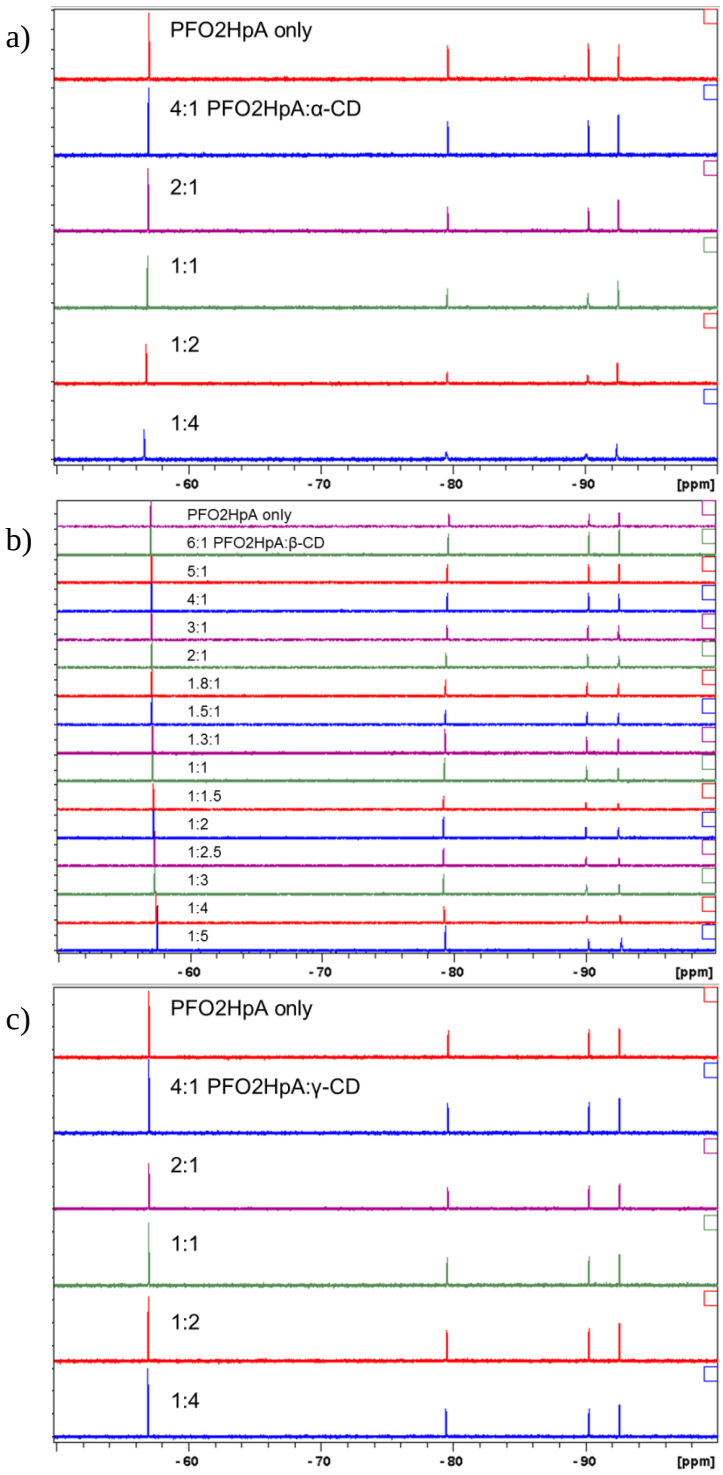

Figure A22: ^{19}F NMR spectra of perfluoro(3,6-dioxaheptanoic) acid with a) α-CD; b) β-CD; and c) γ-CD. [PFO2HpA] = 0.00242 M, pH 7, 50% D_2O/50% H_2O, 400 MHz NMR. Peaks from left to right: F7, F2, F4, F5.

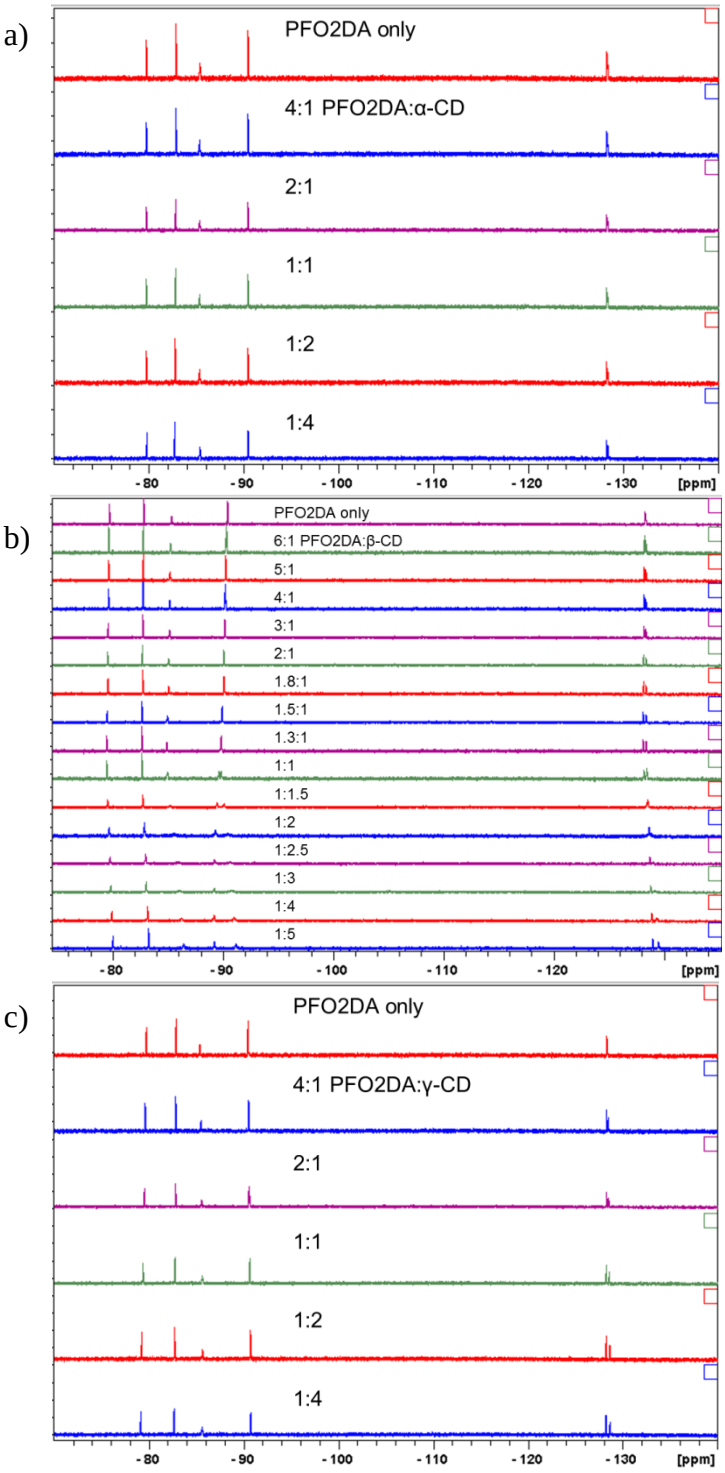

Figure A23: ^{19}F NMR spectra of perfluoro(3,6-dioxadecanoic) acid with a) α-CD; b) β-CD; and c) γ-CD. [PFO2DA] = 0.00242 M, pH 7, 50% D_2O/50% H_2O, 400 MHz NMR. Peaks from left to right: F2, F10, F7, F4-F5, F8, F9.

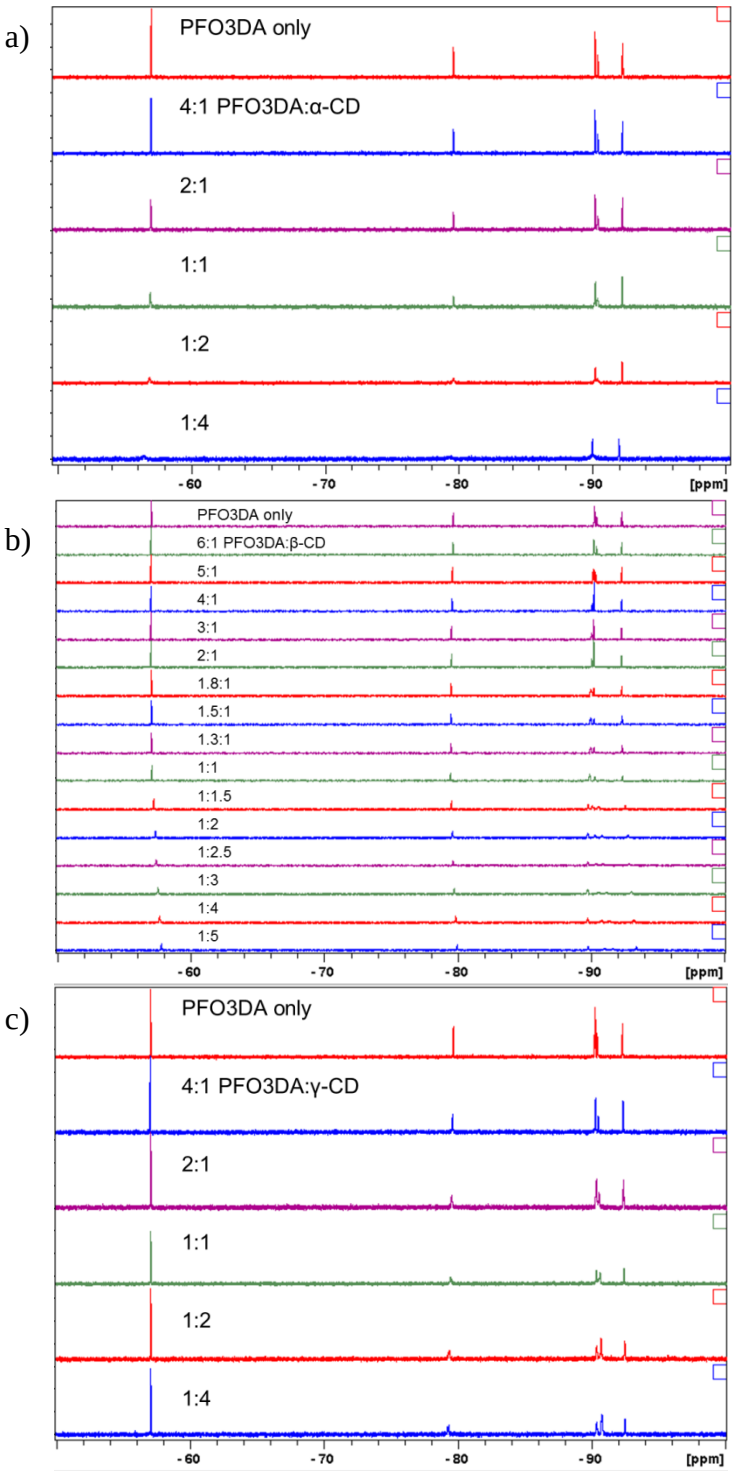

Figure A24: ^{19}F NMR spectra of perfluoro(3,6,9-trioxadecanoic) acid with a) α-CD; b) β-CD; and c) γ-CD. [PFO3DA] = 0.00242 M, pH 7, 50% D_2O/50% H_2O, 400 MHz NMR. Peaks from left to right: F10, F2, F4-5, F7, F8.

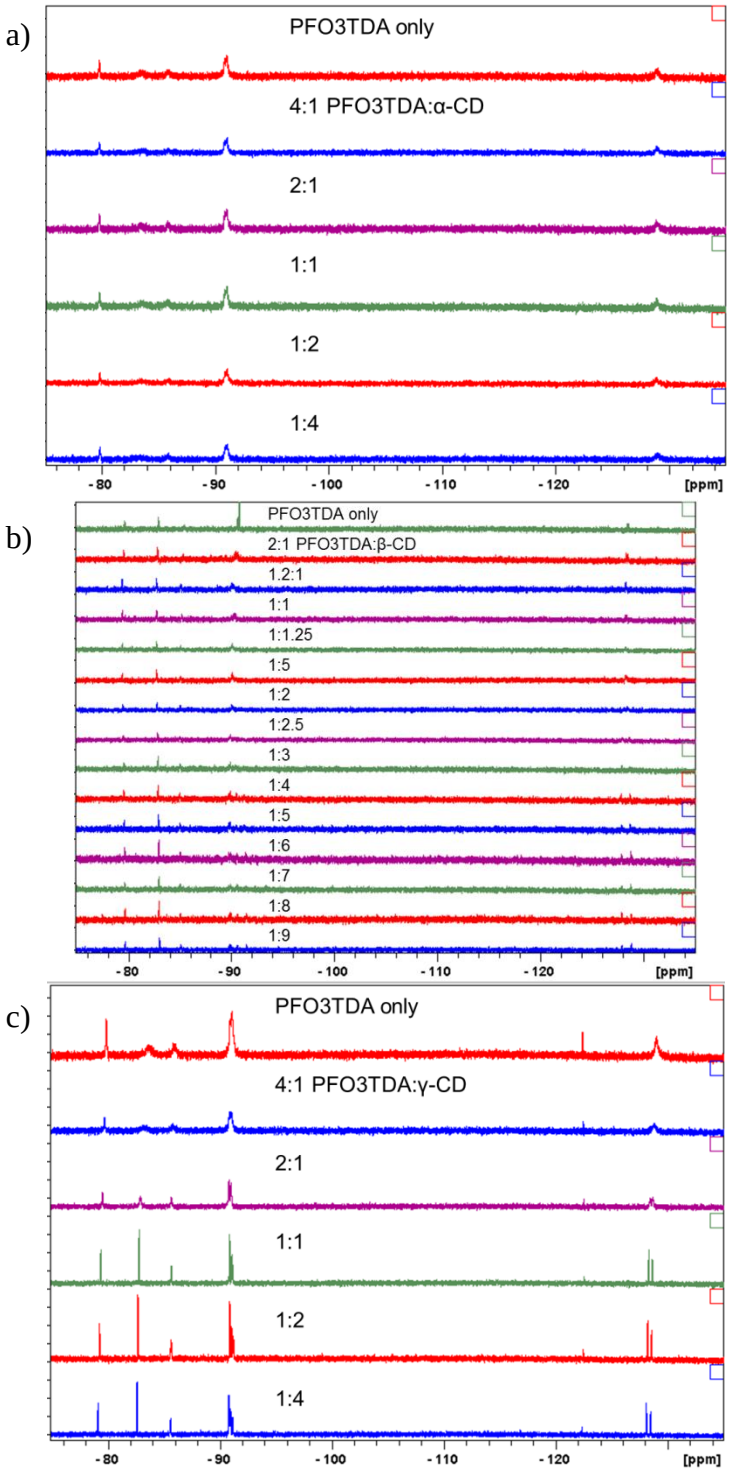

Figure A25: ^{19}F NMR spectra of perfluoro(3,6,9-trioxatridecanoic) acid with a) α-CD; b) β-CD; and c) γ-CD. [PFO3TDA] = 6.05 x 10^{-4} M, pH 7, 50% D_2O/50% H_2O, 400 MHz NMR. Peaks from left to right: F2, F13, F10, F4-5, F7-8, F11, F12.

Individual Association Constants of CD:PFECA Interactions

Table A16: Regression Analysis Results for PFMOPrA and α-, β-, and γ-Cyclodextrin

CD	Fluorine	$K_{1:1}$, M^{-1}	$\Delta\delta_{cd\text{-}F}$, ppm	R^2
α	2	$2.50 \pm 1.54 \times 10^1$	1.24 ± 0.62	0.995
	3	$2.62 \pm 1.03 \times 10^1$	2.37 ± 0.75	0.998
	5	$2.67 \pm 0.84 \times 10^1$	3.15 ± 0.79	0.999
β	2	$1.17 \pm 0.47 \times 10^2$	1.37 ± 0.29	0.989
	3	$1.23 \pm 0.47 \times 10^2$	1.44 ± 0.29	0.990
	5	$2.22 \pm 0.63 \times 10^2$	-0.206 ± 0.024	0.992
γ	2	No significant association		
	3			
	5			

Table A17: Regression Analysis Results for PFMOBA and α-, β-, and γ-Cyclodextrin

CD	Fluorine	$K_{1:1}$, M^{-1}	$\Delta\delta_{cd\text{-}F}$, ppm	R^2
α	2	$3.10 \pm 1.57 \times 10^1$	0.85 ± 0.33	0.996
	3	$3.69 \pm 1.44 \times 10^1$	1.53 ± 0.45	0.997
	4	$3.62 \pm 1.28 \times 10^1$	1.48 ± 0.39	0.997
	6	$3.05 \pm 1.30 \times 10^1$	2.98 ± 0.99	0.997
β	2	$1.47 \pm 0.36 \times 10^3$	1.20 ± 0.05	0.995
	3	$1.46 \pm 0.37 \times 10^3$	2.10 ± 0.09	0.995
	4	$1.45 \pm 0.36 \times 10^3$	1.01 ± 0.04	0.995
	6	$1.55 \pm 0.35 \times 10^3$	-0.193 ± 0.007	0.996
γ	2	No significant association		
	3			
	4			
	6			

Table A18: Regression Analysis Results for PFPrOPrA and α-, β-, and γ-Cyclodextrin

CD	Fluorine	$K_{1:1}$, M^{-1}	$\Delta\delta_{cd\text{-}F}$, ppm	R^2
α	2	$1.74 \pm 0.95 \times 10^2$	0.177 ± 0.045	0.974
	3	$1.56 \pm 0.49 \times 10^2$	0.202 ± 0.031	0.992
	5	$2.54 \pm 1.78 \times 10^2$	0.186 ± 0.052	0.954
	6	$1.70 \pm 0.67 \times 10^2$	0.207 ± 0.038	0.987
	7	$4.24 \pm 1.60 \times 10^2$	0.0744 ± 0.0089	0.985
β	2	$2.12 \pm 1.39 \times 10^3$	1.88 ± 0.17	0.978
	3	$1.01 \pm 0.65 \times 10^3$	0.507 ± 0.116	0.942
	5a	$3.58 \pm 1.01 \times 10^2$	-3.12 ± 0.30	0.992
	5b	$9.18 \pm 3.82 \times 10^2$	4.09 ± 0.37	0.986
	6a,b	$4.66 \pm 2.70 \times 10^1$	-1.24 ± 0.51	0.991
	7	$1.77 \pm 1.04 \times 10^1$	-2.04 ± 1.02	0.998
γ	2	No significant association		
	3			
	5			
	6			
	7			

Table A19: Regression Analysis Results for PFDMMOBA and α-, β-, and γ-Cyclodextrin

CD	Fluorine	$K_{1:1}$, M^{-1}	$\Delta\delta_{cd\text{-}F}$, ppm	R^2
α	2	No significant association		
	3			
	4			
	6			
	7			
β	2	$1.07 \pm 0.57 \times 10^4$	0.878 ± 0.026	0.995
	3	$2.00 \pm 0.21 \times 10^4$	2.12 ± 0.05	0.996
	4	$1.79 \pm 1.15 \times 10^4$	1.84 ± 0.05	0.970
	6	$2.26 \pm 0.43 \times 10^2$	-1.28 ± 0.10	0.997
	7	$5.77 \pm 0.49 \times 10^4$	0.294 ± 0.028	0.999
γ	2	$7.14 \pm 1.24 \times 10^2$	0.319 ± 0.014	0.997
	3	$6.05 \pm 0.81 \times 10^2$	0.939 ± 0.033	0.998
	4	$7.34 \pm 4.68 \times 10^1$	0.344 ± 0.137	0.984
	6	$1.07 \pm 0.33 \times 10^3$	-0.937 ± 0.059	0.990
	7	$9.64 \pm 3.26 \times 10^2$	-0.184 ± 0.013	0.988

Table A20: Regression Analysis Results for PFO2HpA and α-, β-, and γ-Cyclodextrin

CD	Fluorine	$K_{1:1}$, M^{-1}	$K_{2:1}$, M^{-1}	$\Delta\delta_{cd\text{-}F}$, ppm	$\Delta\delta_{2cd\text{-}F}$, ppm	R^2
α	2	No significant association				
	4					
	5	$5.61 \pm 0.42 \times 10^1$	Not observed	0.425 ± 0.022	Not observed	0.999
	7	$5.06 \pm 0.53 \times 10^1$	Not observed	1.17 ± 0.09	Not observed	0.999
β	2	$6.51 \pm 3.29 \times 10^2$	$3.45 \pm 1.23 \times 10^2$	0.979 ± 0.264	-31.7 ± 5.5	0.992
	4	$5.46 \pm 2.16 \times 10^2$	$3.07 \pm 1.41 \times 10^2$	0.797 ± 0.357	-36.1 ± 6.3	0.988
	5	$2.26 \pm 0.68 \times 10^2$	$5.10 \pm 1.57 \times 10^2$	0.861 ± 0.127	-28.9 ± 3.9	0.989
	7	$2.02 \pm 0.59 \times 10^1$	Not observed	-2.58 ± 0.62	Not observed	0.996
γ	2	$5.26 \pm 1.16 \times 10^1$	Not observed	0.527 ± 0.080	Not observed	0.998
	4	$1.33 \pm 0.75 \times 10^2$	Not observed	0.0446 ± 0.0129	Not observed	0.977
	5	No significant association				
	7	$6.74 \pm 1.05 \times 10^1$	Not observed	0.222 ± 0.022	Not observed	0.999

Table A21: Regression Analysis Results for PFO2DA and α-, β-, and γ-Cyclodextrin

CD	Fluorine	$K_{1:1}$, M^{-1}	$K_{2:1}$, M^{-1}	$\Delta\delta_{cd\text{-}F}$, ppm	$\Delta\delta_{2cd\text{-}F}$, ppm	R^2
α	2	No significant association				
	4					
	5					
	7					
	8					
	9					
	10					
β	2	$2.85 \pm 0.40 \times 10^4$	$5.18 \pm 1.24 \times 10^3$	0.706 ± 0.028	-7.13 ± 2.23	0.993
	4	$8.83 \pm 2.33 \times 10^2$	Not observed	1.45 ± 0.08	Not observed	0.975
	5	$1.74 \pm 0.62 \times 10^4$	$9.23 \pm 2.07 \times 10^3$	2.29 ± 0.21	-15.7 ± 2.06	0.987
	7	$9.27 \pm 1.66 \times 10^3$	$1.01 \pm 0.28 \times 10^4$	2.60 ± 0.24	-18.2 ± 2.5	0.990
	8	$1.64 \pm 0.53 \times 10^4$	$1.02 \pm 0.65 \times 10^4$	1.17 ± 0.95	-9.42 ± 2.16	0.966
	9	$6.76 \pm 1.79 \times 10^3$	$5.47 \pm 0.40 \times 10^3$	0.896 ± 0.014	-13.6 ± 5.6	0.997
	10	$1.77 \pm 0.88 \times 10^4$	$6.11 \pm 1.60 \times 10^3$	0.764 ± 0.154	-7.43 ± 0.45	0.994
γ	2	$1.10 \pm 0.22 \times 10^3$	Not observed	0.631 ± 0.025	Not observed	0.996
	4	$1.83 \pm 0.37 \times 10^3$	Not observed	-0.308 ± 0.010	Not observed	0.997
	5	$1.83 \pm 0.37 \times 10^3$	Not observed	-0.308 ± 0.010	Not observed	0.997
	7	No significant association				
	8	$2.80 \pm 1.90 \times 10^1$	Not observed	0.290 ± 0.155	Not observed	0.994
	9	$3.13 \pm 1.20 \times 10^3$	Not observed	-0.295 ± 0.013	Not observed	0.992
	10	$4.05 \pm 0.74 \times 10^2$	Not observed	0.270 ± 0.016	Not observed	0.997

Table A22: Regression Analysis Results for PFO3DA and α-, β-, and γ-Cyclodextrin

CD	Fluorine	$K_{1:1}$, M^{-1}	$K_{2:1}$, M^{-1}	$\Delta\delta_{cd\text{-}F}$, ppm	$\Delta\delta_{2cd\text{-}F}$, ppm	R^2
α	2	No significant association				
	4					
	5					
	7					
	8	$1.59 \pm 0.44 \times 10^2$	Not observed	0.125 ± 0.020	Not observed	0.999
	10	$2.66 \pm 1.17 \times 10^1$	Not observed	1.34 ± 0.51	Not observed	0.999
β	2	$4.22 \pm 1.39 \times 10^3$	$3.76 \pm 1.15 \times 10^3$	0.716 ± 0.031	-8.19 ± 2.40	0.988
	4	$4.73 \pm 2.34 \times 10^3$	Not observed	0.514 ± 0.022	Not observed	0.966
	5	$6.64 \pm 1.70 \times 10^3$	$1.70 \pm 0.48 \times 10^3$	0.771 ± 0.082	-21.1 ± 5.3	0.981
	7	$2.47 \pm 1.11 \times 10^2$	$4.69 \pm 1.27 \times 10^3$	14.0 ± 5.6	-81.7 ± 33.1	0.984
	8	$1.25 \pm 0.35 \times 10^3$	$5.63 \pm 1.32 \times 10^3$	1.56 ± 0.12	-16.7 ± 4.5	0.996
	10	$1.12 \pm 0.66 \times 10^3$	$4.81 \pm 1.16 \times 10^3$	0.962 ± 0.105	-11.8 ± 5.1	0.996
γ	2	$4.28 \pm 0.58 \times 10^2$	Not observed	0.516 ± 0.022	Not observed	0.998
	4	No significant association				
	5					
	7	$6.75 \pm 1.16 \times 10^2$	Not observed	-0.356 ± 0.016	Not observed	0.997
	8	$1.52 \pm 0.33 \times 10^3$	Not observed	-0.205 ± 0.007	Not observed	0.996
	10	$4.17 \pm 3.34 \times 10^2$	Not observed	-0.0388 ± 0.0099	Not observed	0.950

Table A23: Regression Analysis Results for PFO3TDA and α-, β-, and γ-Cyclodextrin

CD	Fluorine	$K_{1:1}$, M^{-1}	$K_{2:1}$, M^{-1}	$\Delta\delta_{cd\text{-}F}$, ppm	$\Delta\delta_{2cd\text{-}F}$, ppm	R^2
α	2	No significant association				
	4					
	5					
	7					
	8					
	10					
	11					
	12					
	13					
β	2	$8.28 \pm 0.47 \times 10^5$	$3.79 \pm 1.51 \times 10^4$	0.361 ± 0.023	-3.62 ± 1.37	0.968
	4	$1.75 \pm 0.64 \times 10^6$	$6.45 \pm 0.76 \times 10^4$	0.853 ± 0.050	-6.32 ± 1.42	0.960
	5	$3.25 \pm 0.21 \times 10^5$	$1.94 \pm 0.99 \times 10^5$	0.113 ± 0.032	2.77 ± 0.33	0.936
	7	No significant association				
	8	$3.68 \pm 0.97 \times 10^3$	$1.78 \pm 0.36 \times 10^5$	0.147 ± 0.068	4.50 ± 0.97	0.951
	10	$4.88 \pm 0.39 \times 10^5$	$3.62 \pm 0.29 \times 10^5$	0.152 ± 0.090	1.04 ± 0.70	0.920
	11	$5.72 \pm 0.30 \times 10^4$	$1.57 \pm 0.23 \times 10^5$	-0.335 ± 0.257	5.26 ± 1.33	0.967
	12	$6.93 \pm 1.20 \times 10^5$	$7.27 \pm 0.73 \times 10^4$	0.442 ± 0.059	-5.89 ± 1.22	0.976
	13	$6.03 \pm 0.86 \times 10^5$	$2.21 \pm 1.01 \times 10^4$	0.263 ± 0.019	-4.47 ± 0.83	0.975
γ	2	$9.16 \pm 1.18 \times 10^2$	Not observed	0.817 ± 0.026	Not observed	0.996
	4	No significant association				
	5					
	7					
	8					
	10					
	11					
	12	$1.95 \pm 0.93 \times 10^3$	Not observed	0.921 ± 0.075	Not observed	0.955
	13	$7.58 \pm 3.46 \times 10^3$	Not observed	1.03 ± 0.04	Not observed	0.971

Appendix 3: Chapter 4

Structures

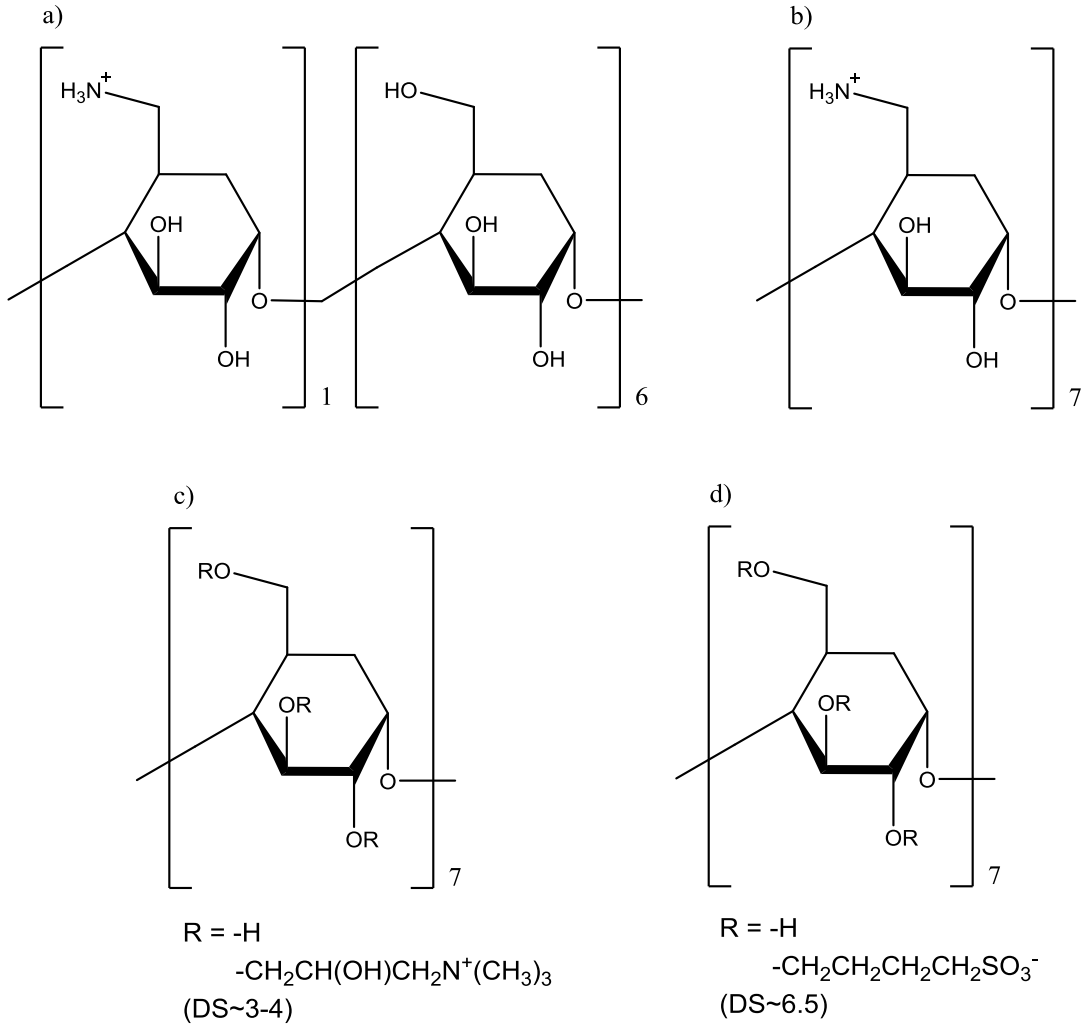

Figure A26: Structures of β-CD derivatives: a) mono-am-β-CD; b) hepta-am-β-CD; c) QACD; d) SBECD. "DS" refers to the degree of substitution.

^{19}F NMR Spectra of β-CD Derivative:PFAS Interactions

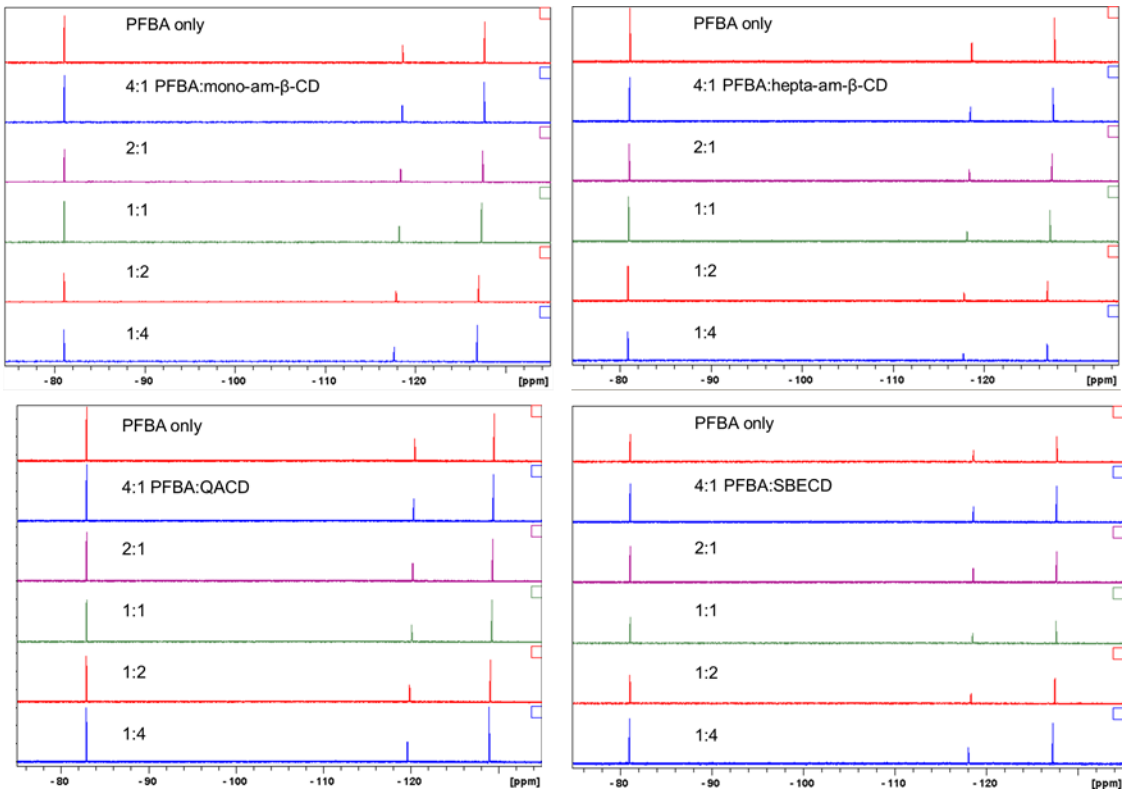

Figure A27: ^{19}F NMR spectra of perfluorobutanoic acid with (clockwise, from top left): mono-am-β-CD; hepta-am-β-CD; QACD; and SBECD. [PFBA] = 0.00242 M, pH 7, 50% D_2O/50% H_2O, 400 MHz NMR.

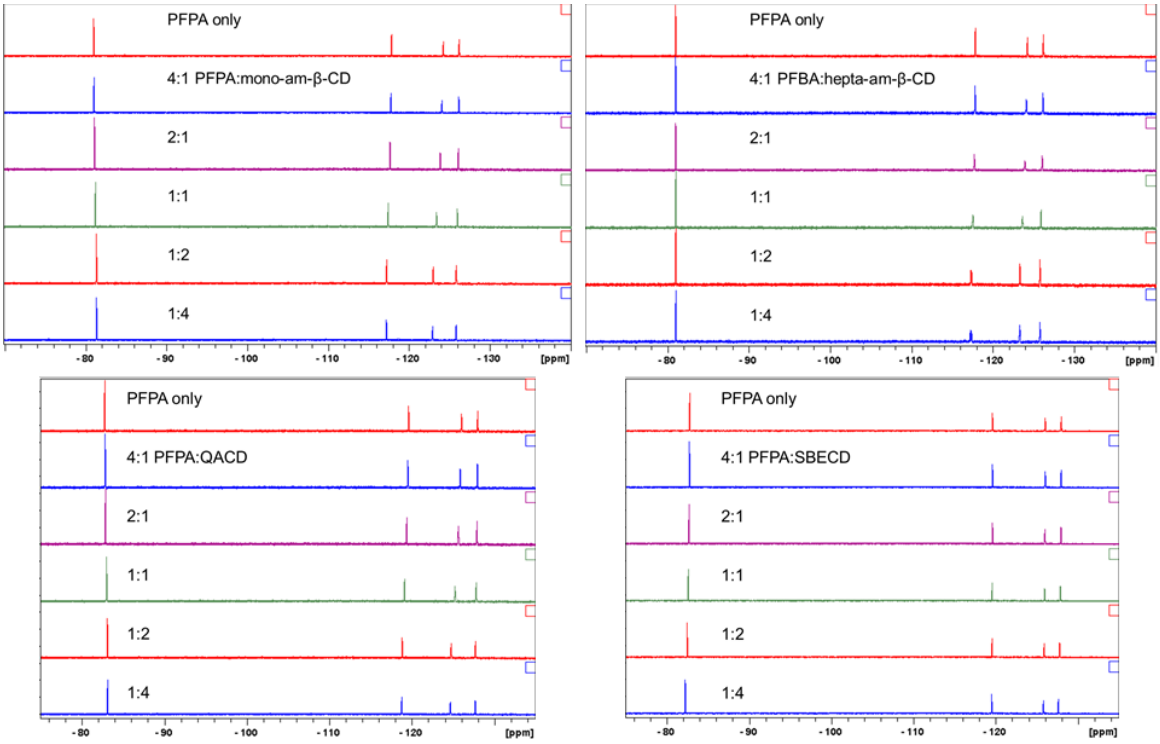

Figure A28: ^{19}F NMR spectra of perfluoropentanoic acid with (clockwise, from top left): mono-am-β-CD; hepta-am-β-CD; QACD; and SBECD. [PFPA] = 0.00242 M, pH 7, 50% D_2O/50% H_2O, 400 MHz NMR.

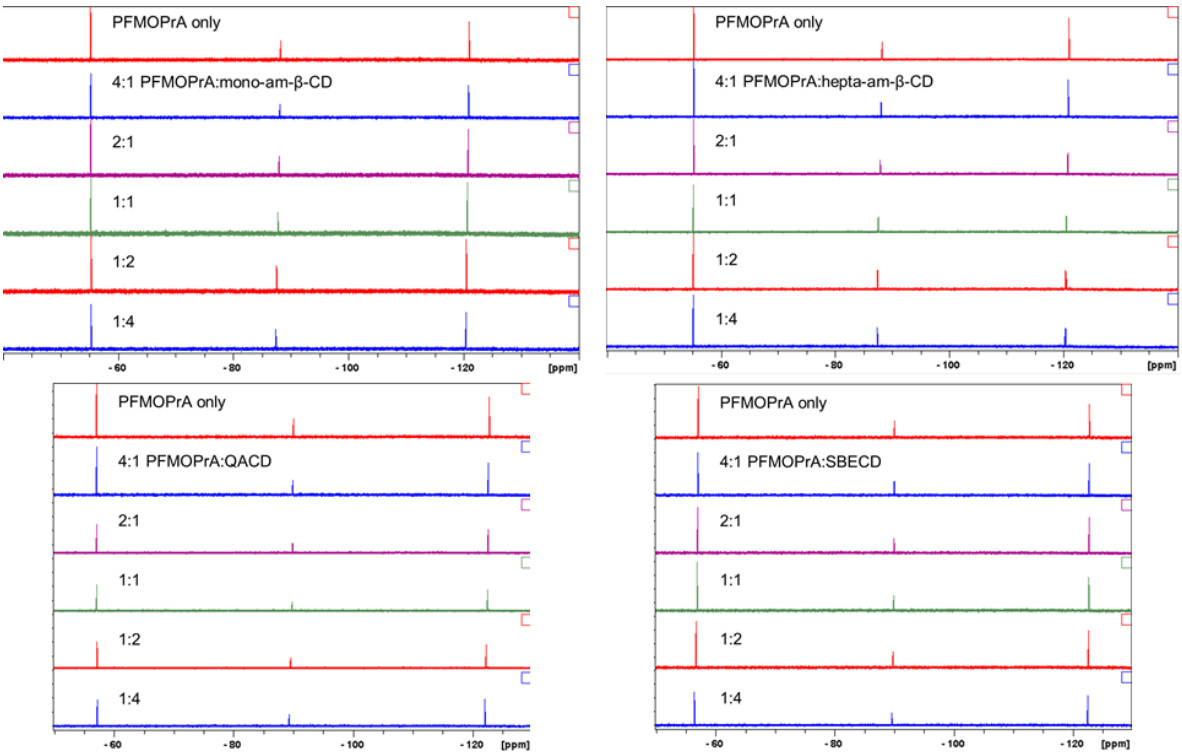

Figure A29: ^{19}F NMR spectra of perfluoro(3-oxabutanoic) acid with (clockwise, from top left): mono-am-β-CD; hepta-am-β-CD; QACD; and SBECD. [PFMOPrA] = 0.00242 M, pH 7, 50% D_2O/50% H_2O, 400 MHz NMR.

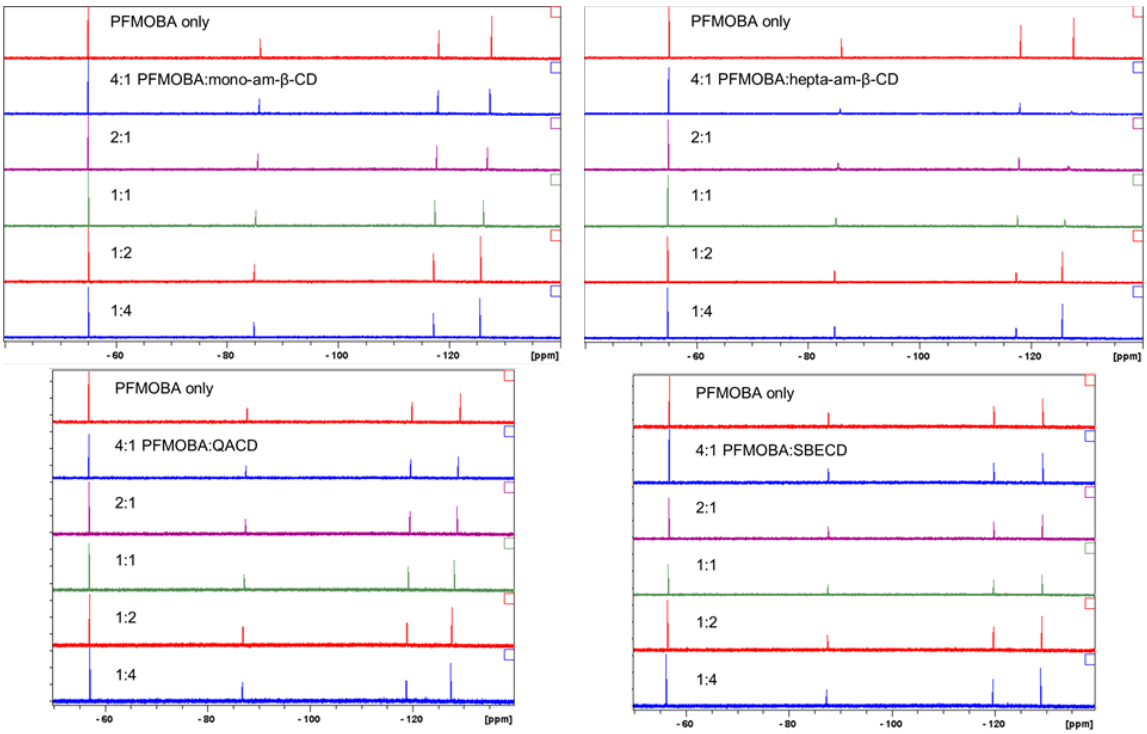

Figure A30: ^{19}F NMR spectra of perfluoro(4-oxapentanoic) acid with (clockwise, from top left): mono-am-β-CD; hepta-am-β-CD; QACD; and SBECD. [PFMOBA] = 0.00242 M, pH 7, 50% D_2O/50% H_2O, 400 MHz NMR.

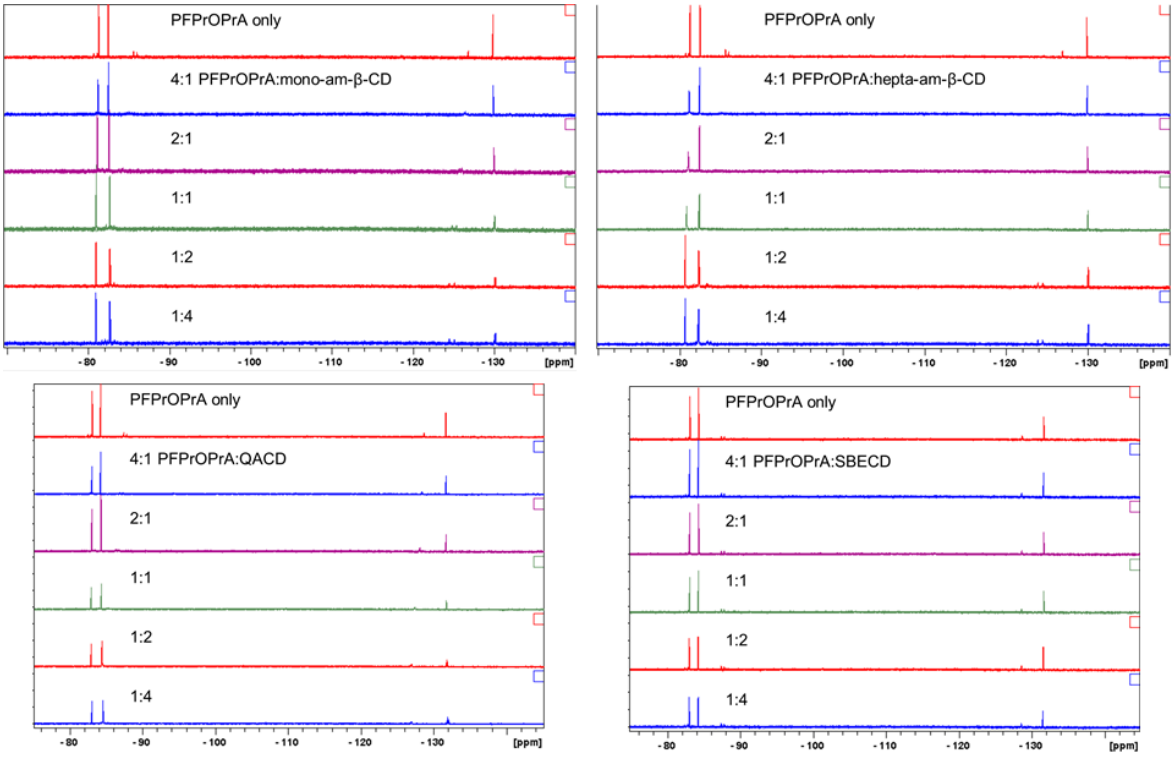

Figure A31: ^{19}F NMR spectra of perfluoro(2-methyl-3-oxahexanoic) acid with (clockwise, from top left): mono-am-β-CD; hepta-am-β-CD; QACD; and SBECD. [PFPrOPrA] = 0.00242 M, pH 7, 50% D_2O/50% H_2O, 400 MHz NMR.

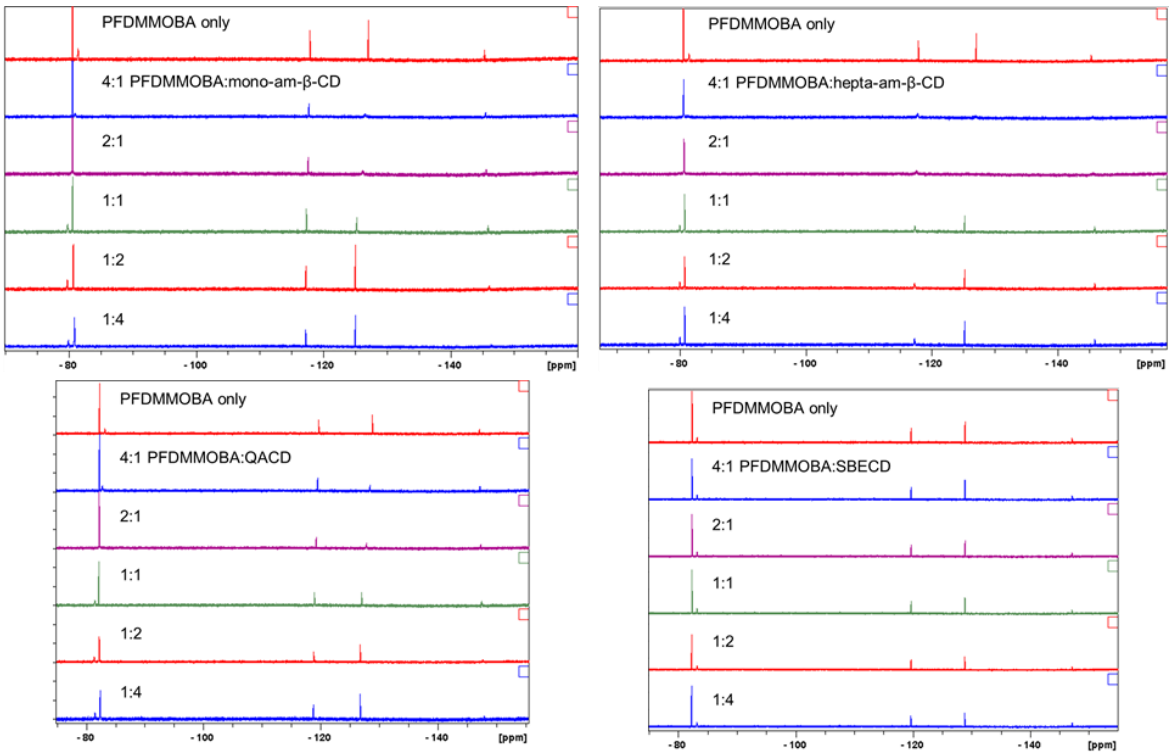

Figure A32: ^{19}F NMR spectra of perfluoro(5-oxa-6-dimethylhexanoic) acid with (clockwise, from top left): mono-am-β-CD; hepta-am-β-CD; QACD; and SBECD. [PFDMMOBA] = 0.00242 M, pH 7, 50% D_2O/50% H_2O, 400 MHz NMR.

Individual Association Constants of Emerging PFASs with CD Derivatives

Table A24: Regression analysis results for PFBA with Mono-am-β-CD, Hepta-am-β-CD, QACD, and SBECD

CD	Fluorine	$K_{1:1}$, M^{-1}	$\Delta\delta_{cd\text{-}F}$, ppm	R^2
Mono-am-β-CD	2	$2.10 \pm 1.02 \times 10^2$	1.51 ± 0.31	0.982
	3	$2.04 \pm 1.00 \times 10^2$	1.36 ± 0.29	0.982
	4	$2.33 \pm 1.10 \times 10^2$	0.0803 ± 0.0156	0.982
Hepta-am-β-CD	2	$7.05 \pm 3.26 \times 10^2$	1.11 ± 0.13	0.981
	3	$1.28 \pm 0.51 \times 10^3$	0.897 ± 0.065	0.988
	4	$1.09 \pm 0.35 \times 10^3$	0.265 ± 0.017	0.991
QACD	2	$1.93 \pm 0.37 \times 10^2$	2.20 ± 0.19	0.997
	3	$1.17 \pm 0.27 \times 10^2$	1.76 ± 0.22	0.997
	4	$1.28 \pm 0.28 \times 10^2$	0.319 ± 0.036	0.997
SBECD	2	No significant association		
	3			
	4			

Table A25: Regression Analysis Results for PFPA with Mono-am-β-CD, Hepta-am-β-CD, QACD, and SBECD

CD	Fluorine	$K_{1:1}$, M^{-1}	$\Delta\delta_{cd\text{-}F}$, ppm	R^2
Mono-am-β-CD	2	$1.04 \pm 0.61 \times 10^3$	0.731 ± 0.087	0.975
	3	$1.01 \pm 0.59 \times 10^3$	1.54 ± 0.19	0.974
	4	$9.66 \pm 5.68 \times 10^2$	0.445 ± 0.055	0.974
	5	$1.02 \pm 0.65 \times 10^3$	-0.402 ± 0.052	0.971
Hepta-am-β-CD	2	$5.69 \pm 4.23 \times 10^2$	0.703 ± 0.144	0.956
	3	$1.22 \pm 0.70 \times 10^3$	1.10 ± 0.12	0.977
	4	$1.72 \pm 1.03 \times 10^3$	0.488 ± 0.045	0.978
	5	$6.98 \pm 1.02 \times 10^3$	-0.0269 ± 0.0028	0.945
QACD	2	$6.70 \pm 3.09 \times 10^2$	1.60 ± 0.19	0.981
	3	$6.11 \pm 3.02 \times 10^2$	1.96 ± 0.26	0.978
	4	$5.34 \pm 2.82 \times 10^2$	0.637 ± 0.095	0.975
	5	$8.57 \pm 4.72 \times 10^2$	-0.203 ± 0.025	0.976
SBECD	2	$1.06 \pm 0.18 \times 10^2$	2.29 ± 0.22	0.998
	3	$1.06 \pm 0.17 \times 10^2$	3.01 ± 0.27	0.999
	4	$9.96 \pm 1.48 \times 10^1$	0.859 ± 0.072	0.999
	5	$1.17 \pm 0.21 \times 10^2$	-0.302 ± 0.029	0.998

Table A26: Regression Analysis Results for PFMOPrA with Mono-am-β-CD, Hepta-am-β-CD, QACD, and SBECD

CD	Fluorine	$K_{1:1}$, M^{-1}	$\Delta\delta_{cd\text{-}F}$, ppm	R^2
Mono-am-β-CD	2	$7.16 \pm 0.83 \times 10^2$	0.670 ± 0.019	0.999
	3	$6.64 \pm 0.90 \times 10^2$	1.00 ± 0.03	0.998
	5	$5.37 \pm 1.45 \times 10^2$	-0.107 ± 0.008	0.993
Hepta-am-β-CD	2	$1.53 \pm 0.69 \times 10^3$	0.675 ± 0.051	0.986
	3	$5.32 \pm 2.28 \times 10^3$	0.851 ± 0.030	0.994
	5	$2.34 \pm 1.03 \times 10^3$	0.112 ± 0.006	0.990
QACD	2	$8.37 \pm 1.33 \times 10^2$	1.65 ± 0.06	0.998
	3	$6.76 \pm 0.86 \times 10^2$	1.46 ± 0.05	0.998
	5	$5.62 \pm 2.49 \times 10^2$	0.0271 ± 0.0033	0.979
SBECD	2	No significant association		
	3			
	5			

Table A27: Regression Analysis Results for PFMOBA with Mono-am-β-CD, Hepta-am-β-CD, QACD, and SBECD

CD	Fluorine	$K_{1:1}$, M^{-1}	$\Delta\delta_{cd\text{-}F}$, ppm	R^2
Mono-am-β-CD	2	$1.97 \pm 1.07 \times 10^3$	1.08 ± 0.08	0.984
	3	$1.97 \pm 1.06 \times 10^3$	2.23 ± 0.17	0.984
	4	$1.82 \pm 0.99 \times 10^3$	1.20 ± 0.10	0.983
	6	$1.30 \pm 0.96 \times 10^3$	-0.0155 ± 0.0008	0.966
Hepta-am-β-CD	2	$2.99 \pm 0.67 \times 10^3$	0.835 ± 0.054	0.986
	3	$4.94 \pm 1.20 \times 10^3$	2.11 ± 0.08	0.994
	4	$6.97 \pm 1.24 \times 10^3$	1.24 ± 0.04	0.994
	6	$3.36 \pm 1.77 \times 10^3$	0.227 ± 0.013	0.989
QACD	2	$2.72 \pm 0.61 \times 10^3$	1.61 ± 0.11	0.984
	3	$2.59 \pm 0.58 \times 10^3$	2.37 ± 0.18	0.983
	4	$2.51 \pm 0.58 \times 10^3$	1.21 ± 0.10	0.981
	6	$5.35 \pm 0.74 \times 10^3$	-0.0638 ± 0.0021	0.990
SBECD	2	$1.15 \pm 0.24 \times 10^2$	2.49 ± 0.29	0.997
	3	$1.19 \pm 0.25 \times 10^2$	3.71 ± 0.42	0.997
	4	$1.13 \pm 0.24 \times 10^2$	1.82 ± 0.21	0.997
	6	$3.98 \pm 1.81 \times 10^1$	0.0876 ± 0.0293	0.995

Table A28: Regression Analysis Results for PFPrOPrA with Mono-am-β-CD, Hepta-am-β-CD, QACD, and SBECD

CD	Fluorine	$K_{1:1}$, M^{-1}	$\Delta\delta_{cd\text{-}F}$, ppm	R^2
Mono-am-β-CD	2	$1.20 \pm 0.49 \times 10^4$	2.08 ± 0.04	0.997
	3	$1.09 \pm 0.42 \times 10^4$	0.340 ± 0.007	0.997
	5a	$1.13 \pm 0.50 \times 10^4$	-1.35 ± 0.57	0.993
	5b	$3.56 \pm 1.22 \times 10^4$	2.89 ± 0.16	0.956
	6a,b	$8.58 \pm 0.51 \times 10^3$	-0.282 ± 0.010	0.992
	7	$1.47 \pm 1.02 \times 10^4$	-0.217 ± 0.007	0.993
Hepta-am-β-CD	2	$1.94 \pm 1.37 \times 10^3$	2.97 ± 0.31	0.973
	3	$2.34 \pm 0.96 \times 10^3$	0.660 ± 0.036	0.991
	5a	$1.42 \pm 1.03 \times 10^3$	-1.27 ± 0.16	0.967
	5b	$1.94 \pm 1.49 \times 10^3$	3.21 ± 0.24	0.969
	6a,b	$3.28 \pm 1.82 \times 10^3$	-0.154 ± 0.009	0.983
	7	$2.52 \pm 1.02 \times 10^2$	0.244 ± 0.039	0.986
QACD	2	$4.94 \pm 1.71 \times 10^2$	2.53 ± 0.25	0.990
	3	$5.88 \pm 2.14 \times 10^2$	0.511 ± 0.049	0.989
	5a	$4.38 \pm 1.68 \times 10^2$	-1.96 ± 0.23	0.987
	5b	$4.44 \pm 1.67 \times 10^2$	4.49 ± 0.51	0.988
	6a,b	$1.61 \pm 0.56 \times 10^2$	0.351 ± 0.160	0.994
	7	$5.36 \pm 2.22 \times 10^2$	0.289 ± 0.033	0.986
SBECD	2	$1.23 \pm 0.31 \times 10^2$	3.56 ± 0.47	0.996
	3	$1.13 \pm 0.33 \times 10^2$	0.649 ± 0.104	0.995
	5a	$2.84 \pm 1.13 \times 10^2$	-2.09 ± 0.59	0.951
	5b	$2.41 \pm 1.10 \times 10^2$	4.98 ± 0.92	0.983
	6a,b	$9.08 \pm 3.43 \times 10^1$	0.274 ± 0.061	0.993
	7	$1.37 \pm 1.07 \times 10^3$	-0.0126 ± 0.0017	0.942

Table A29: Regression Analysis Results for PFDMMOBA with Mono-am-β-CD, Hepta-am-β-CD, QACD, and SBECD

CD	Fluorine	$K_{1:1}$, M^{-1}	$\Delta\delta_{cd\text{-}F}$, ppm	R^2
Mono-am-β-CD	2	$1.18 \pm 0.72 \times 10^4$	0.669 ± 0.021	0.993
	3	$2.63 \pm 0.40 \times 10^4$	2.09 ± 0.04	0.997
	4	$9.29 \pm 0.63 \times 10^4$	1.64 ± 0.05	0.974
	6	$4.51 \pm 1.22 \times 10^2$	-1.31 ± 0.11	0.993
	7	$5.87 \pm 1.99 \times 10^3$	0.154 ± 0.029	0.999
Hepta-am-β-CD	2	$1.67 \pm 0.32 \times 10^5$	0.614 ± 0.016	0.992
	3	$3.70 \pm 0.97 \times 10^5$	1.81 ± 0.13	0.931
	4	$3.68 \pm 0.84 \times 10^5$	1.45 ± 0.057	0.972
	6	$6.91 \pm 1.79 \times 10^4$	-0.591 ± 0.050	0.962
	7	$8.52 \pm 1.59 \times 10^4$	-0.217 ± 0.008	0.984
QACD	2	$1.33 \pm 0.21 \times 10^5$	1.15 ± 0.03	0.994
	3	$2.74 \pm 0.60 \times 10^5$	2.29 ± 0.05	0.994
	4	$2.17 \pm 0.36 \times 10^5$	2.03 ± 0.05	0.994
	6	$6.57 \pm 0.39 \times 10^4$	-0.220 ± 0.009	0.991
	7	$3.21 \pm 1.63 \times 10^5$	0.345 ± 0.005	0.997
SBECD	2	$7.35 \pm 1.62 \times 10^3$	1.11 ± 0.05	0.989
	3	$5.88 \pm 1.67 \times 10^3$	2.42 ± 0.17	0.978
	4	$6.38 \pm 1.40 \times 10^3$	2.10 ± 0.10	0.989
	6	$1.93 \pm 0.56 \times 10^3$	-0.163 ± 0.014	0.978
	7	$1.09 \pm 0.87 \times 10^4$	0.380 ± 0.017	0.986

Appendix 4: Chapter 5

Representative Absorbance Spectra of HSA in the Presence and Absence of PFOA and β-CD and Equation for Correcting Fluorescence Emission Spectra

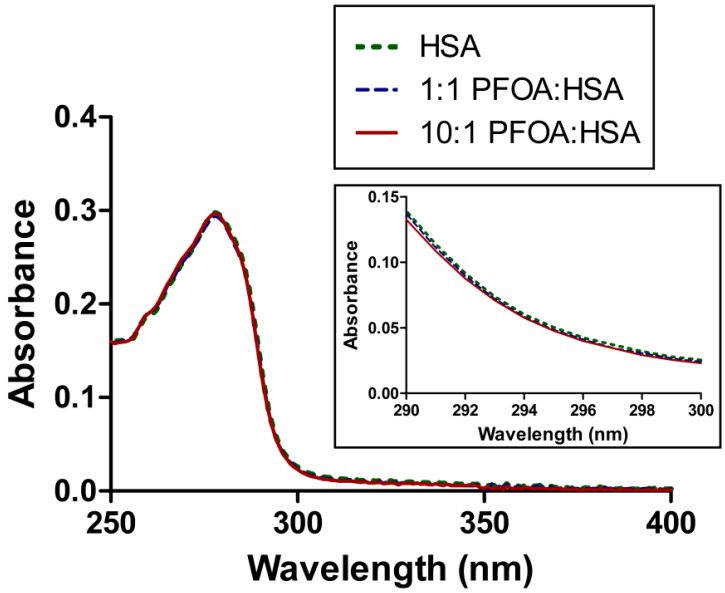

Figure A33: Representative absorbance spectra of 10 μM HSA with no PFOA, 10 μM PFOA, and 100 μM PFOA.

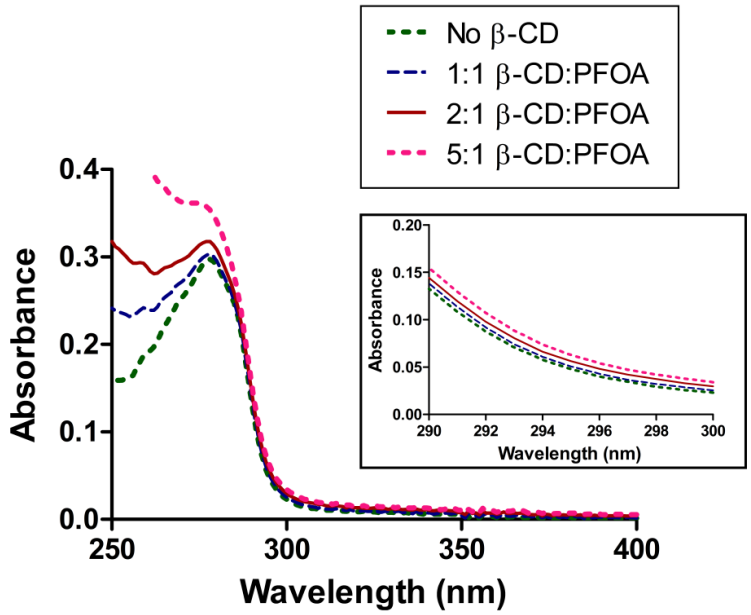

Figure A34: Representative absorbance spectra of 10 μM HSA and 100 μM PFOA with no β-CD, 100 μM β-CD, 200 μM β-CD, and 500 μM β-CD.

To correct for the inner filter effect, the following equation (Bolattin et al. 2016) is used:

$$F_{corr} = F_{obs} e^{(A_{ex}+A_{em})/2} \quad \text{(S16)}$$

where F_{corr} is the corrected fluorescence intensity, F_{obs} is the observed fluorescence intensity, A_{ex} is the absorbance at the excitation wavelength (295 nm), and A_{em} is the absorbance at the emission wavelength (335 nm). The absorbance at 295 nm and 335 nm was low; although the fluorescence data was corrected, this correction did not significantly alter the results and did not affect the trends observed in the fluorescence data.

^{19}F NMR Spectra of β-CD:PFOA Interactions in the Presence and Absence of HSA

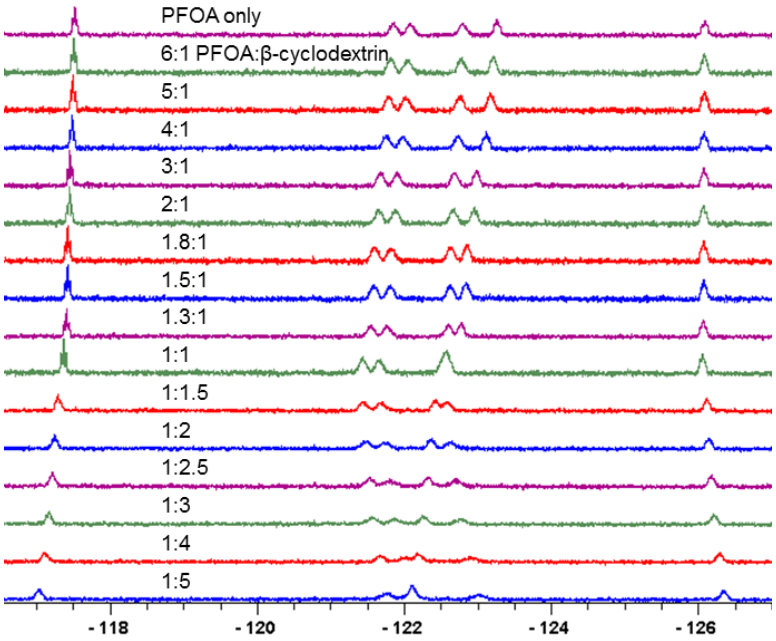

Figure A35: ^{19}F NMR spectra of 2.42 mM PFOA with β-CD in 50% D_2O/50% 100 mM phosphate buffer in H_2O, 400 MHz NMR (F8 peak not pictured).

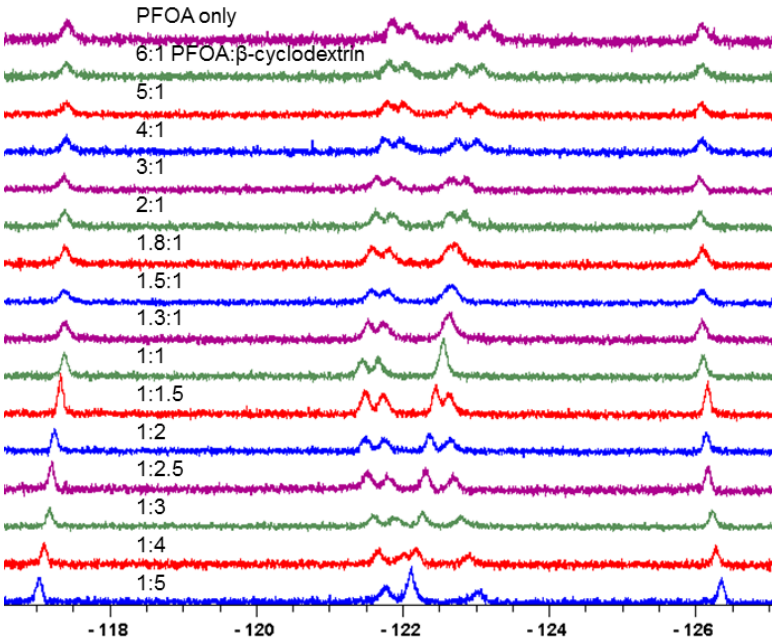

Figure A36: ^{19}F NMR spectra of 2.42 mM PFOA with β-CD in the presence of 35 μM HSA in 50% D_2O/50% 100 mM phosphate buffer in H_2O, 400 MHz NMR (F8 peak not pictured).

NMR Individual Association Constants of β-CD:PFOA Interactions

Table A30: Regression Analysis Results for Perfluorooctanoic Acid and β-Cyclodextrin in 50 mM Phosphate Buffer

Fluorine	$K_{1:1}$, M^{-1}	$K_{2:1}$, M^{-1}	$\Delta\delta_{cd\text{-}F}$, ppm	$\Delta\delta_{2cd\text{-}F}$, ppm	R^2
2	$1.29 \pm 0.24 \times 10^3$	Not observed	0.244 ± 0.008	Not observed	0.990
3	$7.57 \pm 1.29 \times 10^2$	Not observed	0.493 ± 0.020	Not observed	0.990
4	$5.91 \pm 1.88 \times 10^5$	$4.35 \pm 1.13 \times 10^2$	0.592 ± 0.023	-31.9 ± 12.4	0.983
5	$8.55 \pm 0.91 \times 10^5$	$5.91 \pm 2.74 \times 10^2$	0.644 ± 0.027	-30.0 ± 7.5	0.990
6	$8.55 \pm 2.17 \times 10^5$	$4.56 \pm 2.58 \times 10^2$	0.898 ± 0.037	-37.1 ± 2.8	0.974
7	$2.82 \pm 0.79 \times 10^5$	$9.15 \pm 1.01 \times 10^2$	0.201 ± 0.095	-16.3 ± 2.1	0.998
8	$3.23 \pm 0.42 \times 10^5$	$8.14 \pm 1.44 \times 10^2$	0.218 ± 0.009	-18.6 ± 4.4	0.998

Table A31: Regression Analysis Results for Perfluorooctanoic Acid and β-Cyclodextrin in 50 mM Phosphate Buffer in the Presence of 35 μM HSA

Fluorine	$K_{1:1}$, M^{-1}	$K_{2:1}$, M^{-1}	$\Delta\delta_{cd\text{-}F}$, ppm	$\Delta\delta_{2cd\text{-}F}$, ppm	R^2
2	$2.60 \pm 1.13 \times 10^2$	Not observed	0.182 ± 0.031	Not observed	0.925
3	$8.59 \pm 1.29 \times 10^2$	Not observed	0.498 ± 0.017	Not observed	0.992
4	$4.58 \pm 0.84 \times 10^4$	$1.34 \pm 0.50 \times 10^2$	0.599 ± 0.052	-99.6 ± 45.8	0.985
5	$3.43 \pm 0.46 \times 10^4$	$7.47 \pm 2.05 \times 10^2$	0.731 ± 0.076	-27.3 ± 7.4	0.988
6	$3.58 \pm 1.61 \times 10^4$	$1.17 \pm 0.11 \times 10^3$	0.979 ± 0.133	-20.3 ± 13.3	0.973
7	$5.28 \pm 0.31 \times 10^5$	$1.24 \pm 0.21 \times 10^3$	0.174 ± 0.159	-12.2 ± 1.9	0.986
8	$5.28 \pm 1.67 \times 10^5$	$1.26 \pm 0.17 \times 10^3$	0.234 ± 0.038	-12.9 ± 2.2	0.991

Representative Steady State Fluorescence Emission Spectra of HSA in the Presence and Absence of PFOA

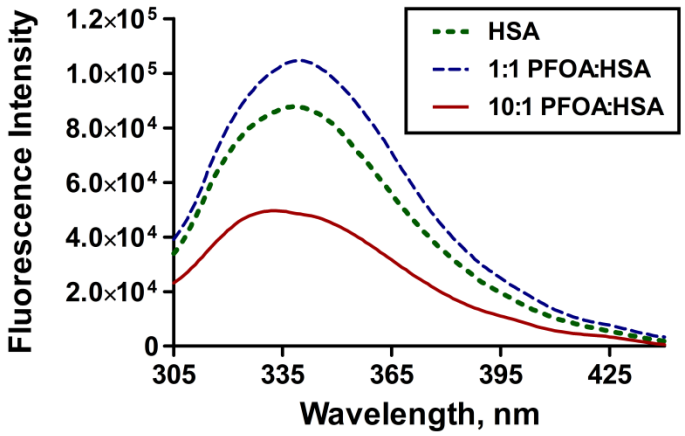

Figure A37: Representative fluorescence emission spectra of 10 μM HSA: with no PFOA, 10 μM PFOA, and 100 μM PFOA.

Representative Circular Dichroism Spectra of HSA in the Presence and Absence of PFOA

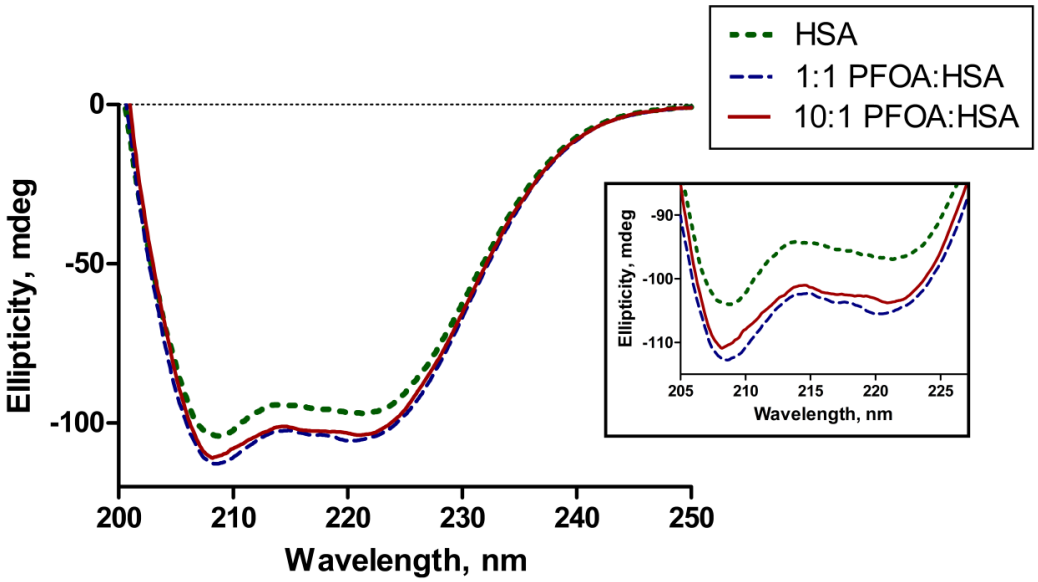

Figure A38: Representative circular dichroism spectra of 10 μM HSA: with no PFOA, 10 μM PFOA, and 100 μM PFOA.

Change in α-Helical Content of HSA with Increasing PFOA Concentration and Equation to Calculate α-Helical Content from Circular Dichroism Data

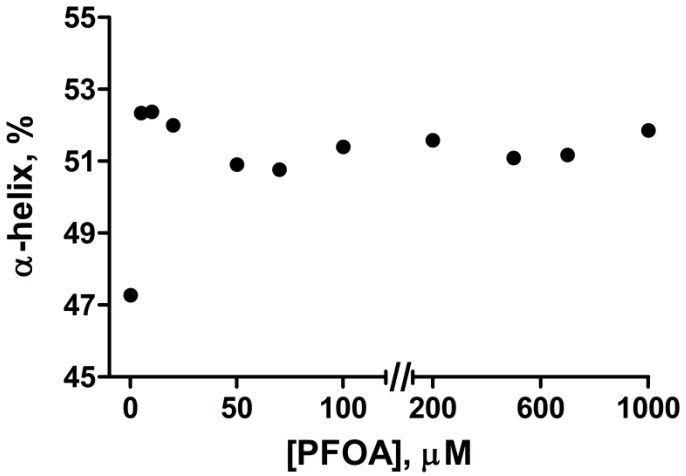

Figure A39: Change in α-helical content of 10 μM HSA upon addition of PFOA calculated from the circular dichroism ellipticity measured at 208 nm.

To calculate the α-helical content of the protein, first the ellipticity at 208 nm measured in the circular dichroism spectra is converted to the mean residue ellipticity (MRE) by using the following equation:

$$MRE = \frac{Ellipticity\ measured\ at\ 208\ nm}{C_p n l} \quad \text{(S17)}$$

where C_p is the molar concentration of the protein, n is the number of amino acid residues in the protein (585 for HSA), and *l* is the path length in mm. The MRE is then converted to the α-helical content by the following equation:

$$\alpha - helix\ content\ (\%) = \frac{-MRE-4000}{33000-4000}\ x\ 100\ \% \quad \text{(S18)}$$

where 4000 is the MRE of the β-form or random coil conformations at 208 nm, and 33000 is the MRE of a pure α-helical conformation at 208 nm (Bolattin et al. 2016).

Double Logarithm Plot and Equation to Calculate the Binding Constant

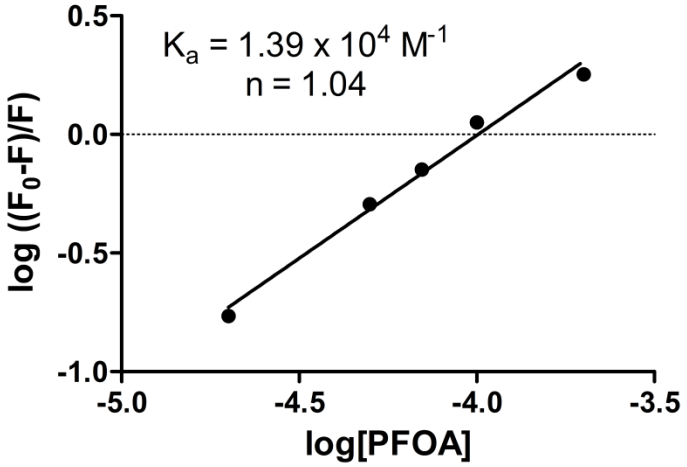

Figure A40: Double logarithm plot of fluorescence emission intensity of HSA with PFOA to calculate the binding constant ($K_{a,2}$) of PFOA to the low affinity binding site on HSA. R^2 = 0.987.

The binding constant (K_a) and number of binding sites (n) can be calculated from the double logarithm plot (Wei et al. 2010) of the quencher concentration and fluorescence emission intensities:

$$log\,\frac{(F_0-F)}{F} = logK_a + nlog[Q] \quad \text{(S19)}$$

where F_0 is the fluorescence intensity in the absence of the quencher.

Modified Scatchard Plot and Equation to Calculate the Number of Binding Sites

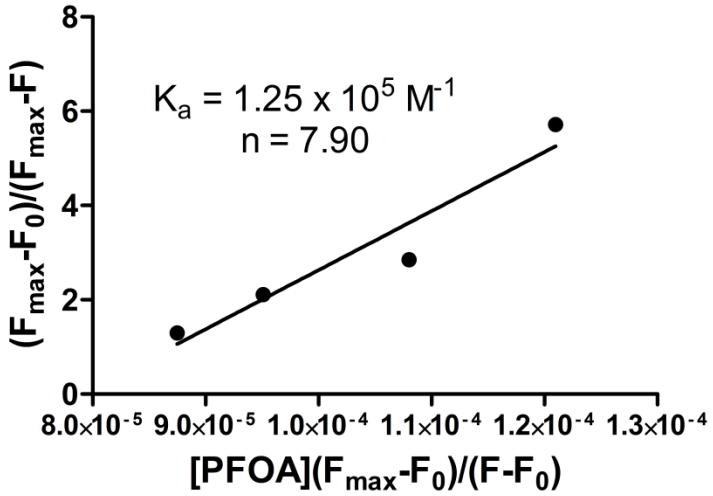

Figure A41: Modified Scatchard plot of fluorescence emission intensity of HSA with PFOA to calculate the number of low affinity binding sites on HSA for PFOA. R^2 = 0.920.

The binding constant (K_a) and number of binding sites (n) can be calculated from the modified Scatchard plot (Wei et al. 2010) of the quencher concentration and fluorescence emission intensities:

$$\frac{(F_{max}-F_0)}{(F_{max}-F)} = K_a[Q]\frac{(F_{max}-F_0)}{(F-F_0)} - nK_a[P] \quad \text{(S20)}$$

where F_0 is the fluorescence intensity at the 1:1 PFOA:HSA ratio, F_{max} is the fluorescence intensity at the 20:1 PFOA:HSA ratio, and [P] is the concentration of HSA.

Average Lifetime of Trp Residue in HSA with PFOA and β-CD

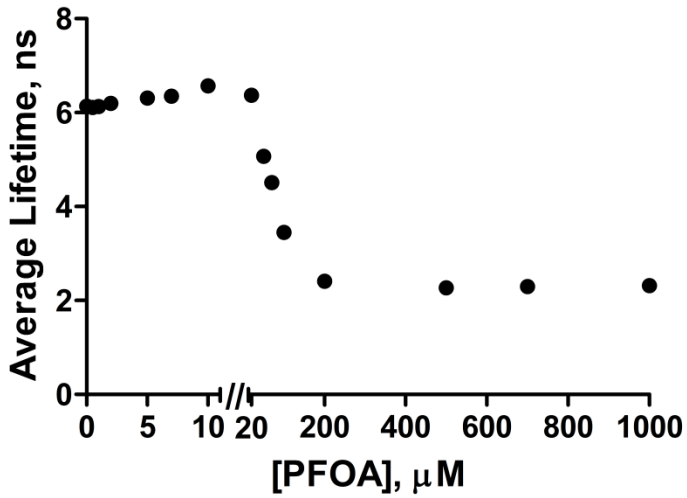

Figure A42: Average fluorescent lifetime of 10 μM HSA titrated with increasing concentrations of PFOA.

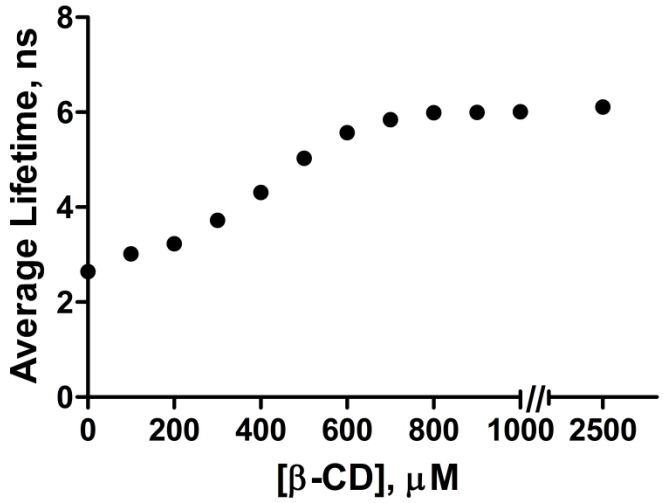

Figure A43: Average fluorescent lifetime of 10 μM HSA with 500 μM PFOA titrated with increasing concentrations of β-CD.

VITA

MARY JOELLE ERRICO

2010-2014	Bachelor of Science in Honors Chemistry Georgetown University Washington, District of Columbia
2013	Research Experience for Undergraduates (REU) Intern University of North Carolina-Chapel Hill, Institute of Marine Sciences Morehead City, North Carolina
2014-2017	Master of Science in Chemistry Florida International University Miami, Florida
2014-2018	Doctoral Candidate Florida International University Miami, Florida

PUBLICATIONS AND PRESENTATIONS

Froelich, B.A.; Weiss, M.J.; Noble, R.T. The evaluation of four recent culture-based methods for the isolation and enumeration of *Vibrio vulnificus* bacteria from oyster meat. J. Microbiol. Methods 2014, 97, 1-5.

Bentley, K.W.; de los Santos, Z.A.; Weiss, M.J.; Wolf, C. Chirality sensing with stereodynamic biphenolate zinc complexes. Chirality 2015, 27, 700-707.

Weiss-Errico, M.J.; O'Shea, K.E. Detailed NMR investigation of cyclodextrin-perfluorinated surfactant interactions in aqueous media. J. Hazard. Mater. 2017, 329, 57-65.

Weiss-Errico, M.J.; Ghiviriga, I.; O'Shea, K.E. ^{19}F NMR characterization of the encapsulation of emerging perfluoroethercarboxylic acids by cyclodextrins. J. Phys. Chem. B 2017, 121, 8359-8366.

Weiss-Errico, M.J.; Berry, J.P.; O'Shea, K.E. β-Cyclodextrin attenuates perfluorooctanoic acid toxicity in the zebrafish embryo model. Toxics 2017, 5, 31.

Weiss-Errico, M.J.; Miksovska, J.; O'Shea, K.E. β-Cyclodextrin reverses binding of perfluorooctanoic acid to human serum albumin. Chem. Res. Toxicol. 2018, 31, 277-284.

Weiss, M.J.; O'Shea, K.E. NMR evaluation of cyclodextrin-perfluorinated surfactant host-guest interactions. Book of Abstracts, 250th ACS National Meeting, Boston, MA, August 16-20, 2015; American Chemical Society, Washington, DC, 2015; ENVR-235.

Weiss, M.J.; O'Shea, K.E. Effects of environmental factors on β-cyclodextrin-perfluorinated surfactant host-guest interactions. Books of Abstracts, 251st ACS National Meeting, San Diego, CA, March 13-17, 2016; American Chemical Society, Washington, DC, 2016; ENVR-85.

Weiss-Errico, M.J.; Hopkins, Z.; Knappe, D.; O'Shea, K.E. Encapsulation of legacy and emerging perfluoroalkyl substances by cyclodextrins. Book of Abstracts, 253rd ACS National Meeting, San Francisco, CA, April 2-6, 2017; American Chemical Society, Washington, DC, 2017; ENVR-614.

Weiss-Errico, M.J.; O'Shea, K.E. Protective effects of β-cyclodextrin in biological systems contaminated with perfluoroalkyl substances. Book of Abstracts, 253rd ACS National Meeting, San Francisco, CA, April 2-6, 2017; American Chemical Society, Washington, DC, 2017; ENVR-615.

Weiss-Errico, M.J.; Ghiviriga, I.; O'Shea, K.E. Tailored cyclodextrins for environmental remediation of emerging perfluoroalkyl substances. Book of Abstracts, 255th ACS National Meeting, New Orleans, LA, March 18-22, 2018; American Chemical Society, Washington, DC, 2018; ENVR-147.

Weiss-Errico, M.J.; Miksovska, J.; O'Shea, K.E. Can β-cyclodextrin attenuate the negative health effects of perfluorooctanoic acid? Book of Abstracts, 255th ACS National Meeting, New Orleans, LA, March 18-22, 2018; American Chemical Society, Washington, DC, 2018; ENVR-385.

Hopkins, Z.; Weiss-Errico, M.J.; O'Shea, K.; McCord, J.; Lindstrom, A.; Strynar, M.; Knappe, D. Detection and treatment of per- and polyfluorinated compounds in Cape Fear River Basin, North Carolina surface water. Book of Abstracts, 255th ACS National Meeting, New Orleans, LA, March 18-22, 2018; American Chemical Society, Washington, DC, 2018; ENVR-231.